Aalto University
School of Chemical
Engineering

Ariane Victoria Mader

FABRICATION OF POROUS HIERARCHICAL MULTILEVEL COMPOSITE THIN FILMS BY COMBINING DIFFERENT SELF-ASSEMBLY PROCESSES

Master´s Programme in Chemical, Biochemical and Materials Engineering
Major in Functional Materials

Master's thesis for the degree of Master of Science in Technology
submitted for inspection, Espoo, 15 July, 2020.

Supervisor Professor Jaana Vapaavuori

Instructor M.Sc. Hoang Nguyen

Aalto University
School of Chemical
Engineering

Aalto University, P.O. BOX 11000, 00076 AALTO
www.aalto.fi

Abstract of master's thesis

Author Ariane Victoria Mader

Title of thesis Fabrication of Porous Hierarchical Multilevel Composite Thin Films by Combining Different Self-Assembly Processes

Degree Programme Chemical, Biochemical and Materials Engineering

Major Functional Materials

Thesis supervisor Jaana Vapaavuori

Thesis advisor(s) / Thesis examiner(s) Hoang Nguyen, Maarit Karppinen

Date 15.07.2020 **Number of pages** 113 **Language** English

Abstract

In nature, directed self-assembly on multiple length scales is commonly used to create superior structural and functional materials. Such control over different levels of patterning would also be of great interest for many advanced devices. By now, it remains challenging to fabricate such hierarchical structures. The spontaneous self-organization of block copolymers can further be used as a bottom-up self-assembly technique creating patterns with a 10-100 nm period. The formed pattern can be used to organize nanoparticles. Another self-assembly technique is the condensation of water onto drying polymer films, which can lead to highly ordered honeycomb like patterns, called breath figures, with pores of up to 20 μm in diameter. The pores can be utilized to selectively incorporate nanoparticles into the film. The combination of block copolymer (BCP) assembly and breath figure formation with the incorporation of different nanoparticles into the respective patterns should lead to a multi-hierarchical composite material allowing for unique property combinations and the independent tunability of each level of hierarchy. Using dip-coating for film formation will also allow to create such patterns on an industrial scale.

In this thesis, an extensive literature review of the relevant mechanisms is presented. Polymer thin films were created *via* dip-coating and the complexity of the system increased stepwise. Poly(styrene) was chosen as preliminary cheap model polymer. Breath figures were induced by dispersing water droplets containing sucrose in the solution. Solution and synthesis parameters were optimized, and small ordered pores were mainly found at the bottom of the substrates, among some bigger ones. TiO_2 nanoparticles were successfully introduced to assemble at the pores. Replacing poly(styrene) with poly(styrene)-*block*-poly(4-vinylpyridine) lead to multi-level polymer patterns, with breath figure induced micropores of 1-50 μm diameter, and BCP induced nanopores of 10-80 nm between. The nanoparticles presumably dissolved in the poly(4-vinylpyridine) block. Future directions of this research are discussed, including the continuation with a second type of nanoparticle to reach the desired organisation of different nanoparticles at different length scales.

Keywords Self-assembly, thin film, dip-coating, block copolymer, breath figure, nanoparticles, hierarchy

Preface

The basis of this thesis is the literature work and laboratory research conducted to begin the investigation of multi-hierarchical thin films incorporating two levels of nanoparticles in the Multifunctional Materials Design group at Aalto University. The thesis has been written to fulfil the graduation requirements of the Functional Materials Program at Aalto University. The work already began with finding a suitable topic in December 2019. The research was conducted from January to June 2020 and the writing, revising, and presentation proceeded until August 2020.

The specific research question was suggested by me after intensive literature research into a topic of interest suggested by my supervisor Jaana Vapaavuori. I chose this work and research group due to my keen interest in complex dynamic processes, such as self-assembly and crystallization, and because of a good match of expectations with my supervisor. The research itself was challenging, as no one had dealt with breath figures at this university before, and a lot of time was spent on optimizing the system rather than the actual research question. The research was further complicated by the corona crisis, which caused the practical part of this thesis to be less than otherwise.

I would like to thank my two supervisors, Hoang Nguyen and Jaana Vapaavuori, who guided me when I need help, but also gave me a lot of independence, and were always understanding and supporting. My thanks also go to the whole Multifunctional Materials Design group for their input during the group meetings, and especially my office mate Duck Lee, who made my workdays more enjoyable. Finally, I would like to thank Luca A. Mader and Juho A. Savola for supporting me during those difficult times and control skyping with me during quarantine.

This work made use of Aalto University Bioeconomy and RawMatters infrastructure.

Contents

List of Acronyms

AFM, atomic force microscopy

BCP(s), block copolymer(s)

BF(s), breath figure(s)

DCM, dichloromethane

EDX, energy-dispersive X-ray spectroscopy

NPs, nanoparticles

PMMA, poly(methyl methacrylate)

PS, poly(styrene)

PVP, poly(vinylpyridine)

P2VP, poly(2-vinylpyridine)

P4VP, poly(4-vinylpyridine)

rH, relative humidity

SEM, scanning electron microscope/microscopy

THF, tetrahydrofuran

WS, withdrawal speed

1 Introduction

In nature, most materials for any structural or functional application are made of polymers and polymer composites.[1] The key to using these classes of materials for a wide variety of applications lies in the precise control of hierarchical levels. Organisms naturally obtain this control of multiple length scales by utilizing the principles of directed self-assembly.[1] Such a hierarchical structure is also very interesting for synthetic materials, as it can enable the independent control of multiple different properties or lead to novel ones by the synergistic interplay of different components and their structuring.[2] This enormous diversity that can be introduced by the different levels of patterning is of great interest for many advanced applications in sectors such as biomedicine, aerospace, photonics, electronics, as well as energy harvesting and storage.[3] While there are many reports on synthetically mimicking hierarchical structures, it remains a challenge to prepare them in a well-controlled manner and on a larger scale.[3–5]

Top-down approaches, such as lithographic techniques, are ultimately not sufficient to achieve this, since they are usually complex, time consuming, expensive, not scalable, or suffer from a resolution limit.[2,6–9] Bottom-up self-assembly methods seem more promising, since they can ideally provide a versatile and fast one-step method of pattern fabrication, mimicking processes in nature.[6] However, most self-assembly techniques possess certain length scale constraints and usually only allow for the control of one level of hierarchy. Therefore, in order to achieve a more complex material structure, the combination of compatible self-assembly techniques will be crucial.

The spontaneous organization of block copolymers (BCPs) into periodic nanoscale structures has played a significant role for progress in the field of synthetic self-organization.[10] In the simplest form, these BCPs consist of a linear chain with two

covalently bonded blocks of thermodynamically incompatible polymers.[11] These blocks will aim to organize in a way that contact between dissimilar blocks is minimized during annealing, leading to their periodic morphologies. Common stable morphologies in the bulk are body centred cubic spheres or hexagonally packed cylinders of the minority block in a matrix of the other, and lamellae.[11] The morphology can be easily influenced by changing the BCP composition, molecular weights, ratios, or synthesis related parameters, allowing for a great control over the final morphology.[9] In thin films, this is further complicated by the confinement and increased relevance of surface energetics.[11–13]

The domains formed by BCP assembly into thin films can be used as a prime template to guide nanoparticles by either adsorbing them to or directly synthesizing them within one of the domains.[11] This enables the organization of nanoparticles into well-ordered arrays, giving the final material an additional level of hierarchy and an opportunity to attain additional functionality. By further controlling the type, shape, size, and spatial distribution of the nanoparticles, mechanical,[14] chemical,[15,16] optical,[17–19] magnetic,[18] and electrical[18–20] properties can be tailored and new collective ones obtained. However, the overall periodic length scales of the BCP patterns tend to be limited to 10-100 nm.[10,21–23]

The process of breath figure (BF) formation is a phenomenon that can be utilized for the creation of microporous films. Such micropores in the order of 0.2 to 20 μm[24] diameter give the film additional functionalities, allowing for it to be used for biomedical devices and tissue engineering scaffolds, for example.[25–31] BFs are formed from the condensation of water droplets onto a solution surface.[31–34] A similar effect can be obtained by directly introducing the water droplets into the solution and creating an emulsion.[35–39] Under the right circumstances, monodisperse water droplets will spontaneously organize into a periodic hexagonally close-packed pattern.[31–34] Various external or synthesis related parameters can be adapted to obtain the desired pore size and distance.[31,34,40–49] Nanoparticles may also be

introduced into such a system, acting as emulsifiers and arranging at the interface of the two liquids, forming a so-called Pickering emulsion.[50] In the case of a polymer solution, the pores that form in the drying polymer film will then be coated with the introduced particles.[51] This may further be controlled by the surface chemistry of the nanoparticles and their concentration within the solution, allowing for not only pores but also rings to form on the outside or within a film at the pores.[51,52]

Both the BCP and the BF self-assembly methods are highly time and cost effective, and comparatively simple once the set-up is optimized.[9,11,14,31,53] They are also governed by different forces and lead to patterns at different length scales, which should allow for the combination of these techniques to create a multi-hierarchical film, leading to new functionality combinations. For example, one could coat a fabric with a polymer film, which has an ordered array of pores that are decorated with nanoparticles, in addition to another shorter length scale nanoparticle array in the polymer phase between the pores. Then, one could control the optical properties with the pore order and spacing, use the nanoparticles between the pores to photocatalytically degrade pollutants, and the nanoparticles in the pores to sense for toxins. By just a simple coating process, any fabric would have gained several functionalities. One might also introduce magnetic properties in the block copolymer matrix that can be controlled by the exact pattern formation and tuned independently of other properties, which may be tuned just as easily. Once the necessary synthetic skills have been developed, it seems like only our imagination limits the countless possibilities that a multi-hierarchical structure offers.

There are numerous successful reports of ordering nanoparticles with the BCP[54–65] and the BF[15,66–72] approach, respectively. Block copolymers are also commonly used for the breath figure method, so these two approaches are inherently compatible.[31,73] However, no literature on the combination of all of these techniques with the organization of two different types of NPs at the respective different length scales of pattern formation was found. Moreover, research has barely been conducted on the

spontaneous organization of different nanoparticles into a polymer film at different length scales. The closest found research is the creation of binary nanoparticle arrays with the purpose of using them as lithography templates, therefore using two different self-assembly sequences and removing the polymer layers.[2,74] Otherwise, the first type of nanoparticles would have stayed covered with the polymer layer of the second round. In one case, the pattern formed by BCP self-assembly was used to deposit different nanoparticles in the different domains *via* a multi-step procedure.[2] In another, BCPs were used to form micelles around the different nanoparticles, using an emulsion with a non-solvent in the first round to leave pores to deposit micelles with the second type of nanoparticle into during the second round.[74] While both methods have successfully yielded binary nanoparticle arrays, they are still rather complex including several steps, and the different orders of hierarchy cannot be tuned independently. Moreover, the stepwise nature leads to a loss of the polymer functionality during the etching step necessary to bring the first assembly product to the surface again. Therefore, the combination of the BCP and BF method with controlled decoration of their respective features with nanoparticles would be superior to what was found in literature in several ways.

The overall aim of this work is to create a thin film with a multi-hierarchical order of both polymer and nanoparticles at different length scales. This is predicted to allow for unique property combinations and potentially synergistic properties of the final material. To achieve this, it will be attempted to take advantage of several self-assembly processes and effects, including breath figure formation, block copolymer assembly, and Pickering emulsions. Preferably, the pattern induced by the block copolymer assembly will also be circular, like the one of the breath figures (Figure 1). The main challenge will be to find the optimum range for the relevant processing parameters, while increasing the complexity of the system stepwise. Once that has been achieved, the synthesis of such a complex multi-level film should be comparatively facile to accomplish.

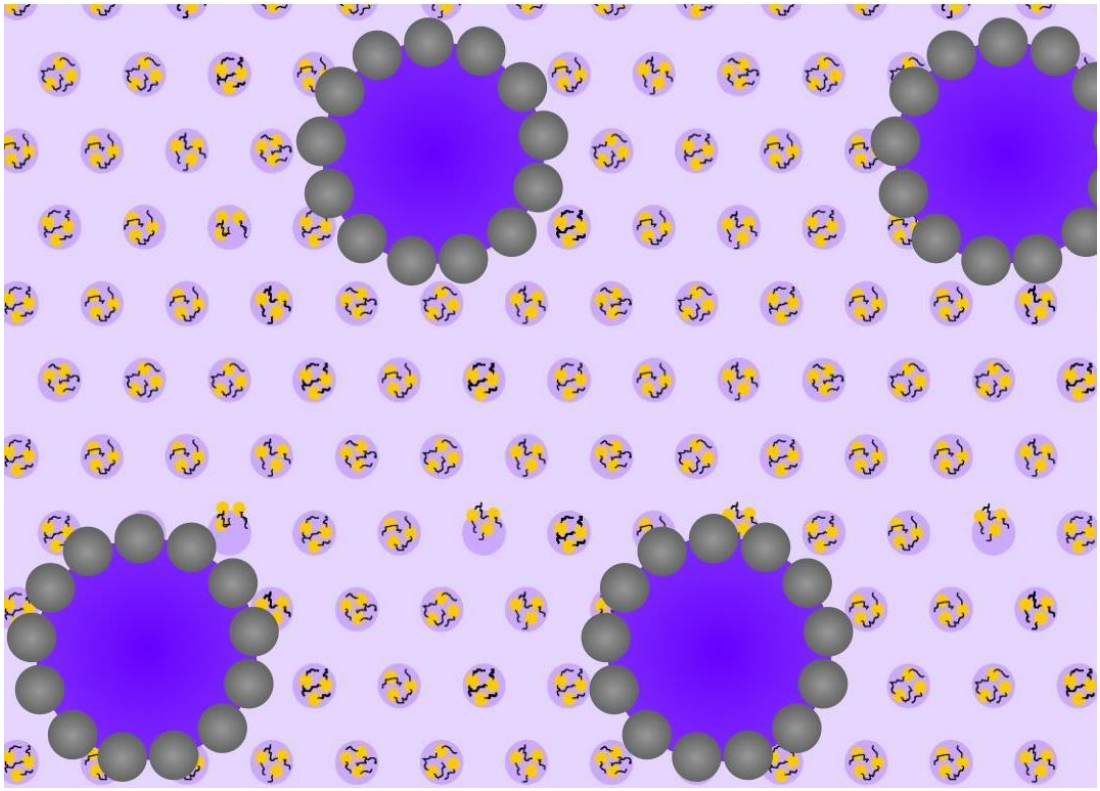

Figure 1. Schematic illustration of the desired patterned film. The big dark purple circles represent the pores formed from breath figures, the grey circles around it represent the TiO_2 NPs. The light purple background represents the polymer film with a spherical surface pattern from microphase separation. In the minority phase, ligand stabilized gold particles organized, which are represented by the yellow circles with black lines. The drawing is not representative of actual size scales and is merely meant as an orientation to give an idea about the several levels of pattern formation that are aimed for.

There are different techniques to create polymer films with these self-assembly methods, however, among those dip-coating is superior in terms of cost, simplicity, scalability, and wide applicability.[53,75,76] Moreover, it allows for the coating of any arbitrarily shaped surface,[53] thus enriching another material with the newly created surface functionalities.[76] Since the focus of this work will be on the proof of concept and not on designing a functional device, the materials are chosen with regard to already proven compatibility and feasibility rather than function. Poly(styrene)-*block*-Poly(4-vinylpyridine) (PS-*b*-P4VP) was chosen as very commonly used BCP, 20 nm TiO_2 nanoparticles were picked to assemble at the pores, and 4 nm Au nanoparticles stabilized with dodecanethiol ligands to interact with the BCP matrix. These choices will be justified more thoroughly in the discussion.

The novelty of this work lies in the ambitious combination of the mentioned methods, leading to a higher degree of hierarchy in a fully self-assembled thin film than reported before. Moreover, the combination of some of the techniques is only poorly understood by now. This is especially true for obtaining breath figure patterns *via* the dip-coating procedure. Therefore, another goal of this study is to further the knowledge about the involved processes by conducting more systematic experiments to devise a theoretical framework and unbind the full potential of these methods for future applications. Due to the unexpected laboratory work restrictions imposed by the pandemic, these ambitious goals could not be met fully, however, a lot of optimization has been done to pave the way for the continuation of this project, and future adaptations will be suggested.

2 Literature Review

This section is aimed to give the reader a scientific background for this thesis. The research of this work utilizes various self-assembly processes dependent on different phenomena. Therefore, it will be attempted to explain these processes individually, linking them where appropriate.

2.1 Dip-Coating

Dip-coating was the first wet chemical thin film deposition technique to be commercially applied, with its first patent for the creation of silica films from sol-gels in 1939.[77,78] Single layer films from 20 nm to 1 μm thickness have been obtained for various sol-gel materials.[75] With dilute polymer solutions the thickness can be much less, a film of 3.0 ± 0.1 nm thickness has been reported for example.[79] Since the late 1950s, this dip-coating is used in mirror production for cars and for optical coatings.[75] Its industrial applicability stems from the many advantages of the technique, of which some are the simplicity of the technique, the speed with which it can be applied, and the relatively low cost.[53]

2.1.1 Dip-Coating Fundamentals

Dip-coating is a complex process and for a thorough understanding, a detailed discussion of fluid dynamics and evaporation would be necessary. This is beyond the scope of this thesis, therefore, a more intuitive and conceptual understanding will be aspired.

The dip-coating process at moderate to high speeds can be summarized as follows: First, a substrate is immersed into a solution at a constant speed, usually vertically, and allowed to dwell there to facilitate complete wetting of the substrate.[75,78] Then, the substrate is withdrawn from the solution at a constant speed and some of the coating fluid is entrained (Figure 2). The solvent will now evaporate, and excess solution will drain, leading to the consolidation of the solute into a film. The film formation can also be aided by post-treatments such as heating to induce curing, sintering, patterning, or simply facilitate drying. This whole film formation may only take few seconds, depending on the volatility of the solvent and the environmental parameters.[75,78]

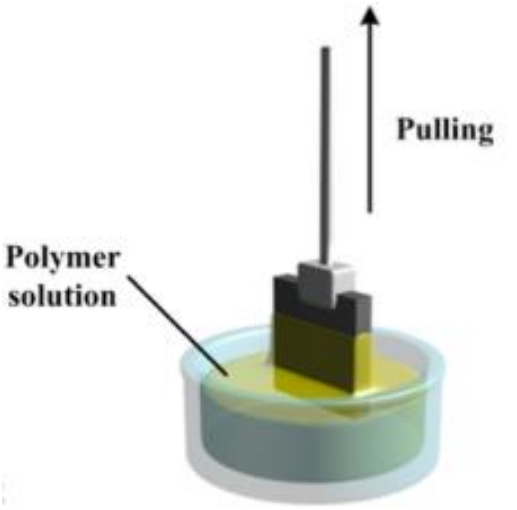

Figure 2. Illustration of the dip-coating process from a polymer solution. Figure from *Escale et al.*[69]

One quality of the dip-coating process is that the thickness of the final thin film can be controlled well by controlling the evaporation rate and withdrawal speed,[80] which can even be used to program topography profiles.[81] The first theoretical model to determine the final film thickness was developed by Landau and Levich for Newtonian fluids.[82] Processes such as evaporation or gelation are not considered in it, but the basic dependence of thickness on withdrawal speed became clear, as the thickness was estimated to increase when increasing the withdrawal speed.[75] There have been several refinements on this first model, however, most of the theoretical predictions do not match practical results well.[75] The many time-dependent gradients of concentration, viscosity, and temperature are complex to model and dependent on many environmental factors.[80] Therefore, it has been proven more valuable to create calibration curves for each system and its respective conditions.[75]

A semi-experimental model for sol-gels in great agreement with experimental data showed that the relations of the Landau-Levich equation only roughly applies to a specific regime of withdrawal speed.[76,80] At higher speeds (approximately > 60 mm/min for sol-gels), the thickness indeed increases with withdrawal speed and the governing force is the viscous drag from the gravity-induced draining. At lower withdrawal speeds (approximately < 12 mm/min for sol-gels), however, the capillary force dominates, and here the thickness increases with decreasing withdrawal speed. These two regimes combine at intermediate speeds, leading to a thickness minimum when the viscous drag and capillary force approximately cancel each other out. Thinner films than the ones at this critical speed can only be created by changing the experimental conditions, for example by diluting the solution.[76,80]

Understanding the presence of these different regimes is crucial for deliberately altering the process for desired results. Since the capillary force is governed by the evaporation rate, increasing the temperature leads to a greater film thickness.[76,80] In the higher withdrawal speed draining regime, however, a temperature change does not affect the dominant forces, and therefore not the final film thickness. Moreover, wetting the substrate can be difficult with high surface tension liquids, such as water, in the draining regime. The capillary regime, on the other hand, is barely affected by this, as it only needs a concave meniscus to form by a wetting solvent. For the formation of silica sol-gels, the intermediate regime was found around speeds of 12 to 60 mm/s, but these regimes have to be determined for each respective system before intentional thickness optimizations can be made.[76,80]

The simple method of dip-coating also lends itself to some more complex methodologies. For example, multiple depositions on the same substrate can be used to layer different materials, provided the previous film does not dissolve in the subsequent solution.[75] Another modification is to conduct the dipping at an angle, which leads to a thicker coating on the upper side.[75] Moreover, topography profiles

can be programmed for thickness gradients and likely more complex surface patterns by controlling the withdrawal rate.[81]

2.1.2 Dip-Coating Procedure

Due to the intricate interplays relevant to the dip-coating process, the smallest atmospheric variation can lead to inhomogeneities in the obtained film.[75] Therefore, ensuring reproducibility and high quality in film formation requires great caution and cleanliness. Temperature and humidity should be kept as even as possible and the dip-coating should be conducted within an enclosure to protect from dust. Furthermore, the set-up must be damped against vibrations.[75]

The most common solvents are short-chained aliphatic alcohols, due to their comparatively low surface tension and moderate volatility, allowing for homogeneous liquid film distribution while keeping the drying time short.[75] A boiling point between 50 and 120 °C seems to be beneficial for this. Solvents can be mixed to obtain desired properties, but they may not evaporate separately. Solute concentrations are commonly in the range of 10 to 80 g/L.[75] It is crucial for the solute to remain dispersed in the fluid, and the dilution must also be high enough to not yield cracking from high tensile stresses caused by excessive shrinking.[78]

The substrate should be cleaned and smooth to prevent soaking of the coating liquid.[75] Moreover, a dwell time of 30 s is commonly used for heat equilibration with the solution and for turbulences from immersion to settle. It also should be taken into account that transitions zones during immersion lead to irregularities. Such irregularities accumulate at the edges of a substrate for up to 20 mm at all margins, which is called edge effect.[75]

2.2 Block Copolymer Assembly

Block copolymers (BCPs) are composed of at least two polymer blocks that are chemically distinct, usually immiscible, and covalently bound.[11,22,23] One of the

simplest and most studied types is an A-B diblock copolymer, with a linear chain of A type monomers connected to a linear chain of B type monomers, which will also be the focus of this work.[11] The thermodynamic incompatibility between the different constituent blocks, while being bound to each other, leads to the spontaneous organization into a nanoscale structure of microphase separated domains with a periodicity of 10-100 nm.[11,21–23] In the bulk, this leads to the common patterns of body centred cubic spheres, hexagonally packed cylinders, bicontinuous gyroids, and lamellae that can be either parallel or perpendicular to the substrate.[11,22,83,84] Depending on the synthesis conditions, these patterns can be thermodynamically or kinetically stable. The morphology is affected by many parameters, some of the most important ones are the chemical nature of the blocks, the relative volume fractions, the degree of polymerization, and the free energy cost from contact between the constituent blocks (Flory-Huggins interaction parameter).[11,23,84–87]

When it comes to creating thin films, the pattern formation is further complicated by the confinement and greatly increased importance of the interface energetics.[11–13] In general, there can be symmetric or asymmetric wetting.[12] Symmetric wetting means that the same block is preferred at both interfaces, while asymmetric wetting means that a different block is preferred at each interface, and both blocks are wetting equally well at a neutral surface.[88,89] Preferential wetting at a surface usually leads to a parallel[1] orientation of the microdomains with respect to the substrate.[87] The surface effect is felt up to distances of six times the dimension of the micropattern normal to the substrate, also called interlamellar spacing, and the film may transform into the bulk morphology afterwards.[12] The wetting preferentiality partly depends on the surface tension of the individual blocks.[12] In the case of a ‘‘soft’’ confinement,

[1] The words ‘‘parallel’’ and ‘‘perpendicular’’ when describing the orientation of the microdomains will be used to describe their orientation respective to the plane of the substrate.

meaning that one of the interfaces is with air, the block with the lower surface tension is commonly preferred to assemble at the air interface.[12]

The parallel orientation of microdomains with respect to the substrate can lead to a patterned surface, because the thickness of thin films is comparable to the interlamellar spacing.[12] When this spacing is incommensurable with the thickness of the film, the self-assembly process accommodates for this difference.[12,90] The mismatch can be lessened in one of two ways. One is to form morphologies as islands, holes, or a bicontinuous pattern at the surface to reach the optimum thickness for the respective interlamellar spacing at least in part (Figure 3).[90] The interlamellar spacing can then be derived from the height of these surface features.[90] The other way is for the pattern to adapt a perpendicular orientation, rendering the film thickness trivial for the perpendicular interlamellar spacing.[12] Since preferential wetting leads to a parallel microphase morphology, it hence leads to holes, islands, or bicontinuous patterns at the surface for many film thickness ranges.[88,89] One exception is when the films is thinner than the interlamellar spacing, which usually leads to the perpendicular orientation of microdomains in the film in case of symmetric wetting and to a range of morphologies, also hybrid ones, for asymmetric wetting.[88,91,92] Lastly, neutral surfaces also lead to a perpendicular microphase orientation in case of incommensurability of the film thickness with the interlamellar spacing.[88,89]

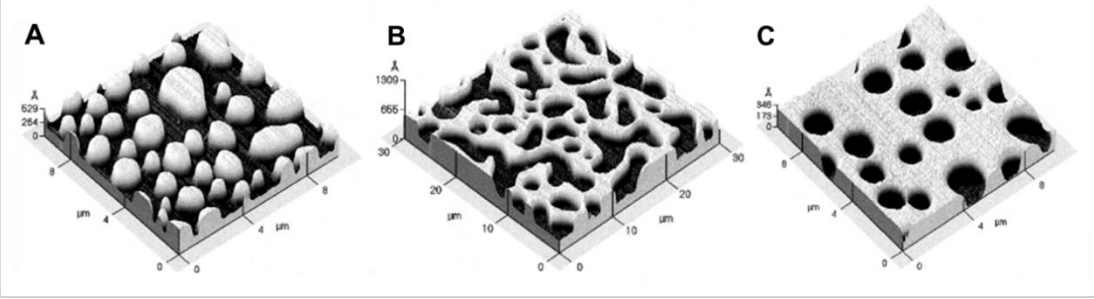

Figure 3. Different surface morphologies occurring from the BCP adapting to the incommensurability of the film thickness and the interlamellar spacing (L). A) "Islands" formed for film thicknesses between nL and (n + 1/3)L, B) bicontinuous pattern formed for film thicknesses between (n + 1/3)L and (n +

1/2)L, C) "holes" formed for film thicknesses between (n + 1/2)L and nL. n is an integer value. Figure adapted from Green *et al*.[90]

2.2.1 Microdomain Manipulation

For many applications, a certain microdomain morphology and orientation is desired. When cylindrical or lamellar microdomains are created, they are commonly preferred to be oriented perpendicular to the substrate, so the pattern is visible at the film surface. For this, one needs to pick a matching surface or modify it for the desired wetting.[12,87] However, true surface neutrality can be difficult to achieve.[12] There are several other ways to create a perpendicular pattern: If the surface tension of the different blocks is somewhat close, then the temperature can be adapted to a degree where they are close to equal. This thermal treatment method can only be used for limited systems, as many block copolymers have blocks that are too dissimilar or would decompose at the necessary temperatures.[12] Another way to change the microphase orientation is vapor annealing, during which the polymer film is exposed to a solvent vapor or a mixture thereof that will induce the desired surface preferentiality.[13,93–96] Instead of such annealing techniques, external fields like electricity may also be applied to ensure the desired ordering and orientation.[9,87]

Apart from applying an external field, the controlled evaporation of a solvent from a cast film can also align the formed microdomains.[87] The evaporation typically proceeds normal to the surface.[87] During fast evaporation, the perpendicular microdomain orientation is favoured.[97] For 4 μm thick films from the same solution, evaporation within 5 min lead to a perpendicular alignment of the domains, whereas elongated evaporation for 2 hours induced by increased solvent vapor lead to a parallel alignment.[97] The use of a selective solvent can also swell one of the blocks, increasing its volume fraction and thereby affecting the final micropattern.[13,98] Using a solvent system also has other advantages, as the chain mobility is increased and the difference in surface tension of the blocks can be mediated.[87] For these reasons, spin-coating and dip-coating have been found to create perpendicular patterns rapidly over a wide thickness range.[87]

Solvent swelling has also been found to lead to the generation of perpendicular nanopores by "morphology reconstruction".[99] For this to happen, a solvent selective to the minority phase of the BCP must be used as post-annealing step.[99] This is commonly applied to micellar cylindrical domains, but can in principle work for any domain morphology.[100] The solvent will then diffuse into the preferred block domain and expand it.[99,101] This expansion puts pressure on the matrix of the other block, which will undergo a permanent plastic deformation. If the pressure is high enough, the expanding polymer domain will flow out of its initial confinement and shield the surface of the domains of the other blocks from the solvent. Once the solvent is removed and the sample dried, the swollen polymer block will shrink again and collapse onto the walls of the matrix it is chemically bound to. Due to this, pores covered with the former swollen block and a film up to completely coated with the same are formed (Figure 4A,B).[99,101]

Nanopores are commonly created when annealing PS-*block*-poly(vinylpyridine) (PVP) BCPs with ethanol.[99,101–103] Yin *et al*.[101] found that PS_{50k}-*b*-poly(2-vinylpyridine)$_{16.5k}$ can first be annealed with a non-selective solvent vapour, such as chloroform, to obtain a perpendicular cylinder orientation for films of up to 600 nm thickness within only 40 s.[101] This produced hexagonally ordered pores in the film from the perpendicular alignment of cylinders, with the PS matrix being about 2 nm higher than the poly(2-vinylpyridine) (P2VP) cylinders (Figure 4C1).[101] Then, the film was immersed in ethanol at 50°C for 3 h and dried in air.[101] This lead to the collapse of the swollen P2VP domains and the formation of straight and highly ordered nanopores penetrating the entire film (Figure 4C2).[101]

The diameter of the pores can also be altered with the swelling temperature, with a higher temperature leading to larger pores.[101] The pore diameter increased from 18 nm at 40°C to 52 nm at 70°C, with a constant interpore distance, indicating that there was more pressure on the PS phase, which was alleviated by the matrix increasing in thickness. The molecular weight also greatly affects the pore sizes

formed. Moreover, using PS_{23k}-*b*-$P4VP_{4.5k}$ instead of the P2VP BCP lead to parallel cylinders after annealing with chloroform. This was explained with chloroform dissolving P4VP less well than P2VP, making it a less neutral solvent for PS-*b*-P4VP. When ethanol was mixed with chloroform to restore the neutrality of the solvent, perpendicular domains were obtained again, confirming that a neutral solvent leads to a perpendicular orientation.[101]

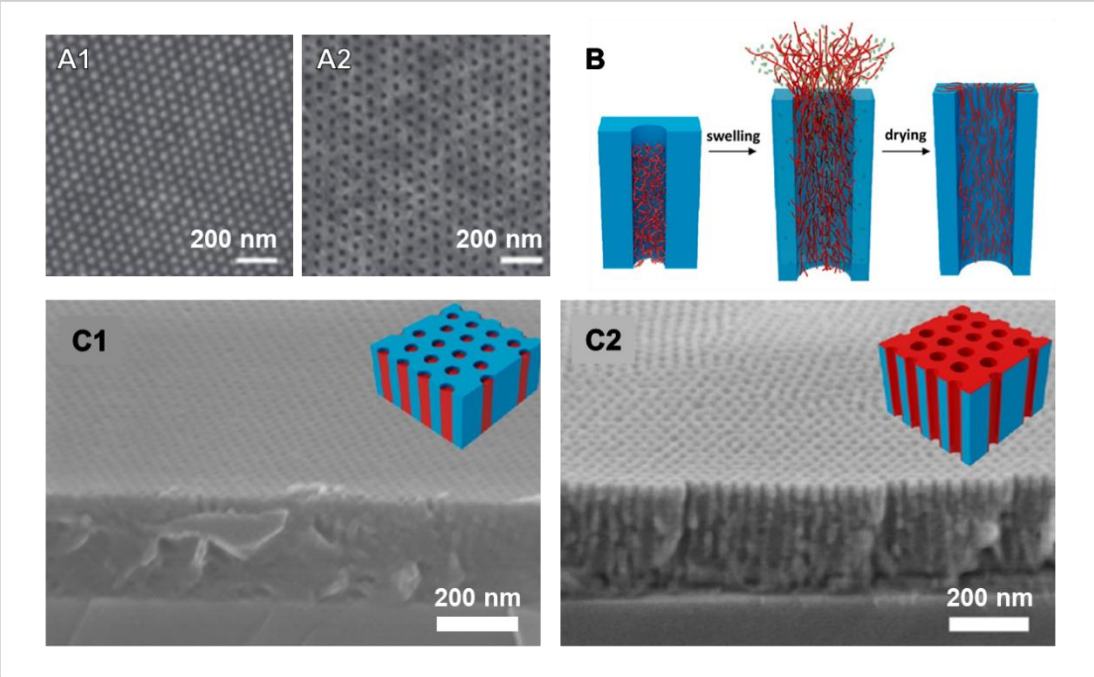

Figure 4. A) AFM images taken from micellar films of PS-*b*-P4VP cast and solvent-annealed in toluene before (1) and after (2) immersion in ethanol for 30 min, showing hexagonally packed micelle protrusions and pores on the BCP films respectively. Figure adapted from Cho et al.[104] B) Schematic of the pore formation mechanism for PS-*b*-P2VP films treated with hot ethanol: The P2VP chains are embedded in the PS matrix as perpendicular cylinders and swell in ethanol, deforming the PS matrix and overflowing. When dried, the P2VP phase collapses onto the surface and pore walls. Figure adapted from Yin et al.[101] C) SEM images taken of a 45° tilted PS-*b*-P2VP films annealed in chloroform for 40 min (1) and subsequently swollen in ethanol at 50°C for 3 h (2). PS is highlighted in blue and P2VP in red. Figure adapted from Yin et al.[101]

2.2.2 Dip-Coating Block Copolymer Films

In this work, dip-coating will be used to induce perpendicular BCP patterns. Despite the advantages of dip-coating and its great industrial applicability, most BCP thin films are still created by spin-coating, electrospray deposition, or zone casting. Therefore, the research on how dip-coating affects the film formation is still limited. Most

experiments combining BCPs and dip-coating were conducted with poly(styrene-*block*-vinylpyridine) (PS-*b*-PVP), often using the pyridine functional group to create a supramolecular comb copolymer by forming hydrogen bonds to another molecule.[21] The dip-coating speeds for PS-*b*-PVP thin films ranged from 1 to 360 mm/min and mostly lead to spherical or cylindrical domains, depending on the experimental conditions.[13,93,105,106]

Meiners *et al*.[105] investigated spherical patterns formed by dip-coating from PS-*b*-P2VP solutions in toluene, which is a selective solvent for the PS block. They proved that the spherical pattern stems from entire micelles being adsorbed from the solution onto the substrate. In addition, a lower speed limit to observe such micellar patterns was found to increase with decreasing polymer concentration,[105] indicating that it is related to the film thickness. It was assumed that a higher withdrawal speed is needed to trap the micelles in the film, whereas at lower speeds the micelles have more time to be "squeezed out",[105] which might also come from an insufficient film thickness.

Roland *et al*.[106] found that the dip-coating regimes observed for sol-gels also apply to polymers and strongly influence the final morphologies of the films formed from a solution of a supramolecular polymer. The film thickness of samples varied with dip-coating speed in the predicted V shape manner, with a minimum of 10 nm around 10 mm/min for a 5 mg/mL polymer and 5 mg/mL 1-naphthol solution in tetrahydrofuran (THF). The addition of 1-napthol was found to have no influence on the thickness progression of the formed film. An increase in the solution concentration lead to a thicker film, analogous to sol-gels. The morphology of the films was dots in the capillarity regime, featureless in the intermediate regime, and dots and stripes or only dots in the draining regime (Figure 5A). With a higher concentration of the small molecule (10 mg/mL), the film in the intermediate regime was 20 nm thick and exhibited a mixed dots and stripes pattern, and the dots and stripes in the draining regime consisted of thicker domains in general (Figure 5B).

Using another small molecule, morphologies stemming from incommensurability of interlamellar spacing and film thickness could be observed at higher withdrawal speeds (Figure 5C). The dot patterns created were associated with spherical micelles in the capillarity regime and with perpendicular cylinders in the draining regime, the stripes corresponding to parallel cylinders. The featureless film was confirmed to be a single brush polymer layer on the substrate, which developed due to the film being thinner than the critical thickness to form domains, determined as 13 nm for this particular system.[106]

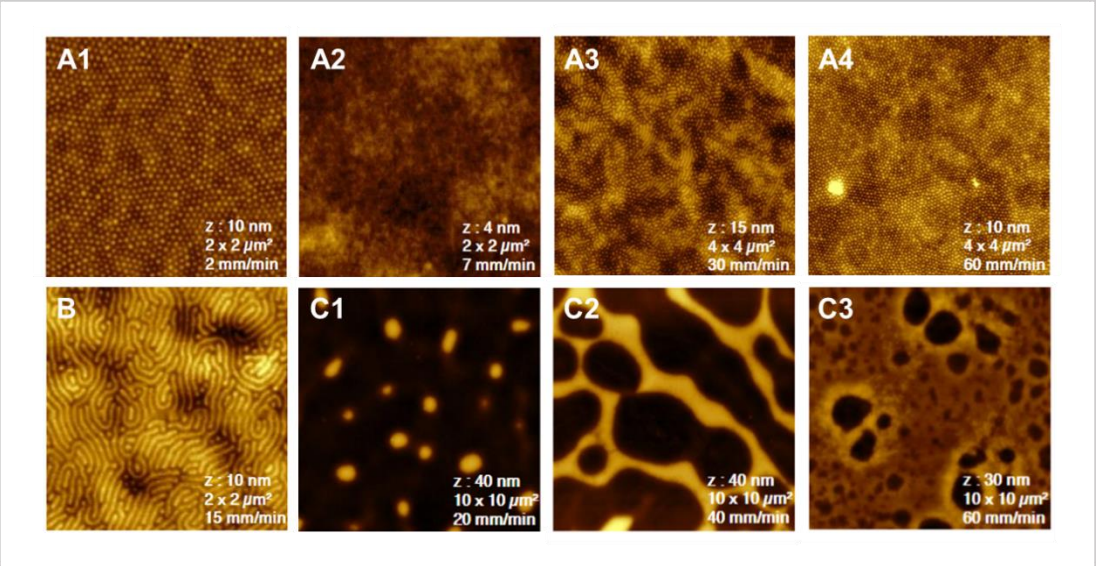

Figure 5. AFM images of representative thin film morphologies observed for various dip-coating rates. A) Created from a solution of 5 mg/mL PS-*b*-P4VP and 5 mg/mL 1-naphtho, leading to dots from spheres (1), featureless brush films (2), mixed dots and stripes from mixed cylinder orientations (3), and dots from perpendicular cylinders (4). B) Created from a solution of 5 mg/mL PS-*b*-P4VP and 10 mg/mL 1-naphthol, the selected pattern displays cylinders oriented parallel to the substrate. C) Created from a solution of 5 mg/mL PS-*b*-P4VP and 5 mg/mL 1-naphthoic acid, morphologies displayed are islands (1), bicontinuous pattern (2), and holes (3). Figure adapted from the supporting information of Roland *et al*.[106]

These experiments showed that the withdrawal speed and corresponding film thickness greatly affected the final film morphologies.[106] Such a morphology change can be induced by the different withdrawal speeds and corresponding film thickness alone, however, in this case, films from solutions without 1-naphthol formed only dot patterns for the entire range of 2 to 40 mm/min withdrawal speed. The dot patterns

likely stem from spherical micelles, while cylinders perpendicular to the substrate could not be excluded. Therefore, 1-naphthol was assumed to induce the morphology change. The uptake ratio of the molecule was found to increase from 20% at 1 mm/min to 90% from 20 mm/min onwards. Since 1-naphthol selectively swells the P4VP phase, this effectively means that the volume ratio of the P4VP block increased with dip-coating speed,[106] which is known to influence the morphology of the created films.[23,85–87] The change in volume ratio explains the change in morphology from spherical to cylindrical,[106] while the evaporation rate and film thickness likely determined the orientation.[97] It was assumed that 1-naphthol diffused back into the solution through the prolonged meniscus to the drying film at slower dip-coating rates, whereas higher withdrawal rates did not allow for the molecule to diffuse out of the entrained film,[106] similarly to what was found for the micelles.[105]

2.2.3 Introducing Nanoparticles into Block Co-Polymer Films

The microphase separation of BCPs can also be utilized to aid the ordered spatial distribution of NPs.[107] The introduction of nanoparticles into a block copolymer film can be either during or after the thin film formation. When introducing NPs during the film formation, these NPs may affect the orientation and morphology of the microphases.[58,108–110] The parameters of the NPs that play an especially crucial role are the size and surface chemistry.

In order for the NPs to be distributed well, they need to favourably interact with the polymer matrix, which is often achieved by selecting a compatible ligand.[107] The NPs are found in different domains depending on how favourably their surface chemistry matches the respective polymer blocks.[60,111] Particles can even be coated with the homopolymer of the desired domain they should go into.[111] For mixed preferences, which can be induced by either having neutral NPs or a mix of ligands preferring different domains, the NPs organize at the interfaces of the domains.[111]

The size of the NPs also plays a crucial role, as the polymer chains must stretch around them.[107] Therefore, without any specific interactions with the polymer, smaller particles may end up in the domains, and larger particles are likely expelled from the bulk. In the case that the particles interact with one of the blocks, then smaller particles are more likely to be dispersed throughout the domain, whereas larger particles are often found in the middle so the polymer chains need to stretch less.[107]

The incorporation of the NPs during film formation can even change the domain morphology.[58,108–110] The addition of NPs has been found to orient the domains normal to the surface,[58] or change the domain morphology completely above a critical NP volume fraction.[109,110] Interestingly, the change in volume fraction for the domains when the NPs are incorporated in one of them does not explain this change, since the bound NPs change the morphology phase diagram.[108,109] Purely the size of the NPs added can also change the morphology of the domains formed.[108]

Some of the most common materials used to organize NPs in BCP patterns will be listed in the following. The PVP polymer blocks are commonly used to guide NPs,[55,58,64,65,109–111] because the nitrogen group allows for the formation of bonds or other positive interactions with ligands or metals.[21,55,65,109] Sizes of NPs used range from 2[55] to 45[65] nm in diameter. In most cases, the BCP thin film was created first from solutions of 0.1[64] to 3[60] wt% of polymer (mostly onto Si wafers[58–61,63,64]) and subse(quently dipped into a NP solution[54,56,59–65] for 10 s[60] to 16 h[59]. The NPs that have been used to be incorporated into BCP patterns are manifold, including Pd complexes,[54,65] ligand stabilized Au,[55,56,59,60,64,111] ligand stabilized CdSe,[58,63,64] ligand stabilized CdS,[109] titanium tetraisopropoxide based sol-gel precursor,[61] fullerene,[62] Au reduced from $HAuCl_4$,[65] and Ag reduced from $AgNO_3$.[57]

2.3 Breath Figures

The first report of using breath figures to pattern a polymer film was in 1994.[73] François *et al*.[73] accidentally created the first known breath figure polymer film using

polystyrene-*b*-polyparaphenylene dissolved in carbon disulphide, dried under a flow of moist gas. The pattern of the film was immediately visible due to the iridescent interference colours it creates. The film was found to exhibit "empty spherical cells" or pores, arranged in a hexagonal pattern, which was so even it could also be identified from its diffraction pattern. Those first experiments yielded films of 10-30 μm thickness with pores of 0.2-10 μm diameters and walls of 0.1-0.2 μm separating them. Closer investigation showed that the films created sometimes consisted of multiple layers of empty spheres (Figure 6A), and removing the surface with tape revealed that the diameter of the sphere was often greater than it appeared (Figure 6B). The same structure was found for star-shaped polystyrene, but not for the linear polymer or copolymers not containing polystyrene. Furthermore, the structure could not be created with dry or methanol saturated gas. Of all the solvents tested, only carbon disulphide lead to the pores.[73] Hence, François *et al*.[73] proposed that humidity and the cooling of the solution surface by fast evaporation were crucial to create the micro-porous films. They also assumed the architecture of the polymer to be essential to control viscosity and favour phase separation, as well as aid the gelation process believed to be involved.[73]

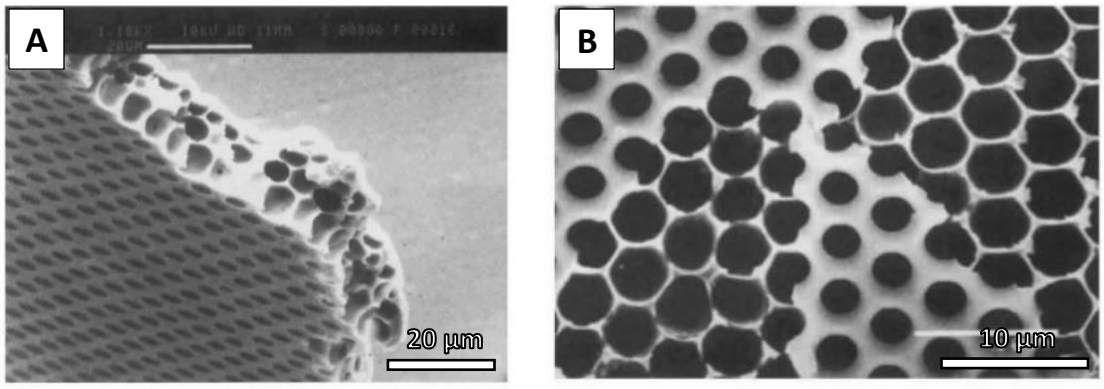

Figure 6. A) SEM image of polystyrene-*block*-polyparaphenylene (30K-*block*-7K) breath figure film displaying multiple empty sphere layers. B) SEM image of a seven-branched (each 10K) star polystyrene breath figure film with part of the surface removed. Figure adapted from François *et al*.[73]

2.3.1 Proposed Mechanisms of Breath Figure Formation

After the breath figure (BF) structure was observed for polymers in solvents they cannot gel in, the gelation process was excluded as possible mechanism.[32] The subsequent explanation that water droplets are responsible for the observed pattern is still widely accepted and will therefore be the main focus of the current work. In addition, some other theories for pattern formation and less popular theories for general pore formation will be introduced at the end.

An indication for the humidity theory was that micron-sized water droplets were observed to be trapped at the surface of the reaction solution, and the droplet shape fits the pore shape (Figure 7). The formation of the droplet pattern can be difficult to observe, as the ordered structure appears rapidly within 10 seconds.[32,34]

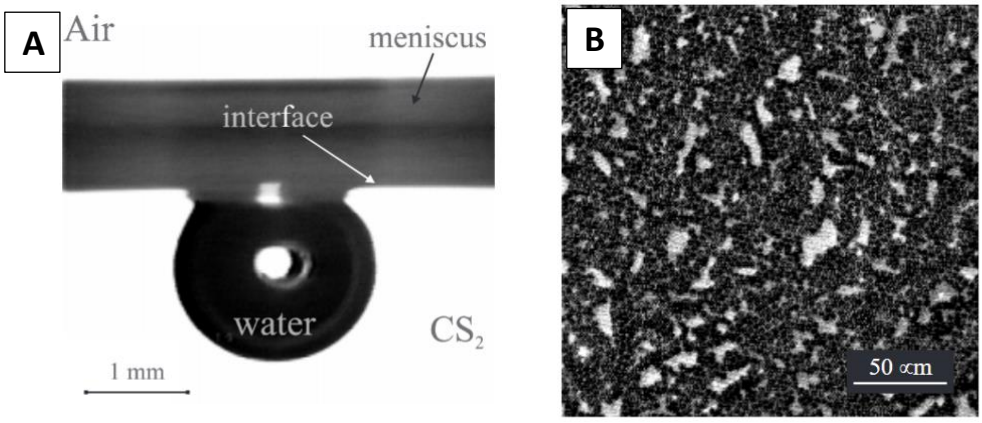

Figure 7. A) Photograph of a drop of water floating underneath the carbon disulphide surface. The meniscus on the cell wall masks the top of the water droplet. B) Photograph of the monodisperse water droplets floating on the surface of the solution during condensation. The solution was cooled to 5°C in order to observe the pattern formation. Both figures are taken from François *et al*.[32]

What is known of the mechanism can be summarized as follows: The solvent of the solution evaporates, thereby cooling the surface of the solution.[31–34] With a high enough humidity, this will lead to the condensation of water vapour from the surrounding air, forming spherical droplets floating underneath the surface. There are different theories for which forces are mainly responsible for the ordering of the droplets. One of them is that the mobile water droplets assemble into a hexagonal

order due to Brownian motion and attraction and repulsion to other droplets. The attraction comes from capillary forces induced by the curvature of the solution surface close to the water droplets. Driven by this, droplets aggregate and form islands which in turn aggregate with others. Different areas of the pattern can be separated by grain boundaries, and with enough time, may reorganize into a monocrystalline layer.[31–34]

Without the polymer in the solution, the droplets would coalesce and form bigger and very polydisperse droplets on the surface.[31,32,34] The polymer, however, precipitates at the water/solvent interface, and this envelope prevents the coalescence. This layer also is the reason for the repulsion among the droplets, since internal pressure of the water droplets is created from the compression when they touch. The polymer in the solution (or amphiphilic stabilizers) acts as thermodynamic coalescence control, while the high volatility of the solvent acts as kinetic control. Therefore, the ability of the polymer to precipitate at the water/solvent interface together with a volatile solvent are crucial for a regular and stable BF pattern and subsequent film.[31,32,34]

The polymer solution was also found to spread on top of the water droplets. When the water evaporates, it will therefore have to burst this layer.[32] In some cases, the layer stays intact and the water escapes through a neighbouring pore.[32] It is also important to note that the polymer layer does not hinder the growth of the water droplets, which has been tested by injection.[33] Instead, it is assumed that the precipitated polymer layer is easily stretched to accommodate for additional volume and create more interface area.[33] How the condensing water reaches the existing water droplet with a potential polymer layer shielding it from the atmosphere was not elaborated, and the idea of this additional polymer layer has not gained much popularity in the field by now.

The monodispersity of the final pores can be achieved through very rapid water droplet nucleation and comparatively slow growth thereafter.[31,32,34] The nucleation occurs simultaneously all over the uniform solution surface. If the humidity is removed before complete evaporation of the solvent in the solution, the pattern disappears due to the evaporation of the water droplets. On the other hand, water condenses until all of the solvent evaporated. Like this, multilayers with usually less ordered lower layers can be created if the solvent density is less than that of water, so the water droplets can sink. Once the solvent completely evaporates, the pattern is permanently fixed in the polymer film.[31,32,34]

2.3.1.1 Other Theories for Breath Figure Formation

While capillary forces are widely believed to lead to the hexagonal arrangement of the condensed droplets, there is another popular and more complex theory for how the droplets sink and arrange in a more macroscopic manner, which is based on Marangoni instabilities.[48,112–115] These Marangoni instabilities describe movement in a solution due to local variations of surface tension. Such variations in surface tension are caused by temperature or composition gradients.[116] Both variations are present in the formation of a polymer film, since the evaporation cools and simultaneously increases the polymer concentration in the top layer. The exchange of warmer and colder fluid from the different layers for example can lead to cellular convection patterns, with warm fluid rising in the centre and cold returning at the outside of the cell.[116] These Marangoni currents can order and compact the water droplets into the well-ordered hexagonal breath figure pattern.

Marangoni currents can also serve as an explanation for more breath figure related observations.[48,113,117] For example, the breath figure pattern is often concentrated in the middle of a cast film. Due to the middle of an evaporating drop-cast film being colder than the edges, the fluid would be moved inwards from the edges to minimize the overall surface energy, dragging any condensed water droplets with it. Moreover, this motion could also be responsible for how the water droplets sink into the

solution,[48,113,117] if buoyancy and viscous force are smaller.[117] Lastly, such currents within the droplets can be a reason why they do not coalesce, since fluid interfaces resist deformation.[53,116]

Bormashenko *et al*.[118] reported mesoscopic cells of 30-50 μm (Figure 8) for several polymers on different substrates. The cell domains were separated by highly porous areas, with pores of about 1 μm size. Concentration and temperature gradient induced Marangoni instabilities were assumed to have caused cell vorticity, leading to the observed mesoscopic pattern in addition to the smaller pores. They also observed that the substrate thickness was crucial for this pattern formation, metal substrates had to be less than 100 μm thick.[118] The formed mesoscopic pattern seems like a clear indication that Marangoni instabilities played a role in the ordering in this specific case.

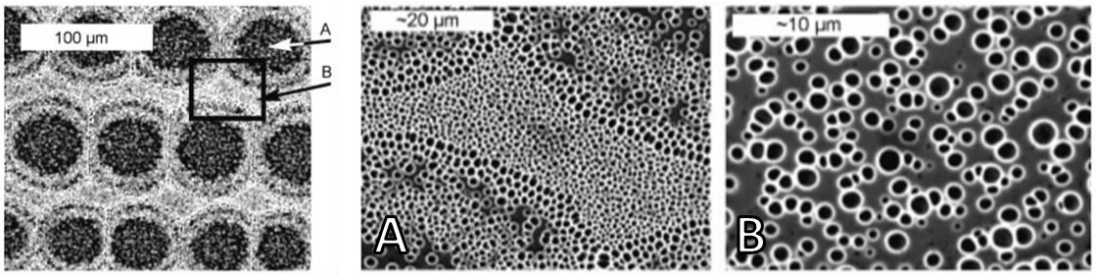

Figure 8. SEM image of self-organized mesoscopic structures obtained *via* dip-coating of polycarbonate in dichloromethane on a chrome steel substrate. A) Magnification of the interior area of the cell, B) magnification of the boundary area of the cells. Figure adapted from Bormashenko *et al*.[118]

The research by Bormashenko *et al*.[118] yielding the mesoscopic pattern was different to the other research mentioned by now in another way. The mesoscopic pattern was found in films produced *via* dip-coating with around 480 mm/min withdrawal speed.[118] The general breath figure mechanism for dip-coating likely is different, as gravity cannot be responsible for the droplets sinking, but the morphology of the created films is almost the same as for casting.[47] Bormashenko *et al*.[118,119] actually did not find humidity to play a role for their film formation and since their drying was

conducted at temperatures close or above the boiling point of the solvent, deduced that the pores must come from bubbles initially filled with solvent vapor.

This so-called "boiling process"[119] seems to be the only theory competing with the humidity theory. Other researchers using dip-coating while inducing breath figures used humidity for this and found it to play a clear role.[14,47,120,121] One thing that seems suspicious about the methodology to obtain patterns claimed to stem from vapor bubbles is that the substrates were cleaned with a "big amount of distilled water".[118] However, assuming that these patterns really arise from solvent boiling, this does not rule out that a similar pattern can be created with water droplets. Unlike for other systems, the choice of solvent, polymer and substrate was also reported to barely have an influence on the boiling process,[118] indicating that the patterns might really stem from a different mechanism entirely. As the formation of water droplets has literally been observed for some systems,[32,34] and for many others a clear dependence on humidity was reported, there also is no reason to believe something else to be responsible for the pores. It is possible, however, that the differences in methodology have indeed led to different causes for the pores in different systems. After all, the ordering forces for water droplets and vapor bubbles would likely be the same, so should lead to similar patterns.

It should be noted that the term "breath figure" is only used to describe the ordered microporous patterns in the frame of the humidity theory. In the following, the porous patterns will still be called breath figures for ease of readability and because the humidity theory seems most plausible for most systems.

2.3.2 Parameters Affecting the Breath Figure Formation

There are many factors affecting the order and intrinsic sizes, as well as pore size distribution, of the porous films created. To ease fast readability of relevant information, these are listed in Table 1.

Table 1. Some critical parameters affecting the final breath figure films, mainly collected from the drop-casting technique.

Parameter	Effect on film structure
Polymer	- Needs to precipitate around water droplet or coalescence occurs, which would lead to disordered droplets[31,32,34] - Higher segment density (star of comb-like > linear) leads to better precipitation around water[46] - Most polymers reported have a polystyrene component[122]
Molecular weight of polymer	- Best: relative molecular mass from 1 500 to 50 000, above and below less homogeneous pattern[73] - A greater molecular weight leads to larger pores[42,43]
Polymer concentration	- Higher concentration leads to lower surface tension of water droplets,[32] increases polymer density and solution viscosity, leading to a better monodispersity[46] - A greater concentration leads to a faster precipitation at the water droplets[121] - A greater concentration leads to smaller pores and thicker walls[34,44,45]
Humidity	- Increasing humidity leads to larger pore diameters[45–48] - Higher relative humidity enhances the regularity[46] until it decreases, in many cases, around 90%[47]
Gas flow velocity	- Increased velocity can lead to the formation of larger ordered areas[33] - Increased velocity leads to smaller pores[40,49]
Evaporation rate	- A higher rate leads to a smaller pore size and distance between the pores[41] - Too high leads to random pore distribution[31]
Solvent	- Should be immiscible with water, have a high vapor pressure and low boiling point[53,123] - If the volatility is too high, the solvent evaporates before condensation can occur[48] - The higher the volatility, the smaller the pores[43,44] - The thermodynamic affinity between polymer and solvent must be good for the polymer to move freely[43,123] - Most often used solvents (due to fitting parameters) are chloroform and CS_2[53]
Substrate	- Needs to be below a certain thickness threshold for breath figures to occur, thick substrates stabilize the temperature of the solution too much for condensation to occur[24] - Affects size and shape of pores[47] - Better wetting of the solution makes the pattern more regular[45] - Substrate to be coated does not need to be flat[53] - Mainly glass and silicone used by now[31]
Temperature	- Lower temperature increases condensation and viscosity of solution, which leads to wider pore walls and more ordered patterns[40,43] - Lower drying temperature leads to greater pores[119] - Appropriate cooling can induce breath figures for all organic solvents[24]

It is important to note that these parameters cannot be optimized independently from each other. Systems for breath figure creation are very intricate. The conflicting findings reported on inducing BFs from linear polystyrene (PS) solutions showcase this well.

Several authors reported that no regular breath figure patterns could be obtained when using linear polystyrene.[51,73,124,125] Others with similar experimental procedures, however, reported well-ordered polymer films.[48,123,126] Due to the controversial results, a more thorough study testing the effect of different substrates and solvents on linear polystyrene without polar end groups has been conducted.[123] Linear PS dissolved in eight different solvents was drop-casted onto nine different substrates in a static humid environment. The goal was to find a link between the final films and different substrate and solvent properties like solubility in water, surface tension or vapor pressure. One of the key findings was that the match of the solvent and the substrate is crucial.[123]

The performance of all solutions was highly dependent on the substrate (Figure 9).[123] Carbon disulphide, for example, was the only solvent with which well-ordered porous films could be created on untreated glass, but this could not be reproduced on any other inorganic substrates tested. Several solvents did not yield an ordered pattern on any substrate, while the patterns induced by chloroform seemed least affected by the substrate used and induced regular patterns on silicon wafers. After reviewing all parameters likely to be relevant, it was concluded that the choice of the substrate must presumably only match the solvent to allow for good wetting (Figure 10).[123]

The solvent must not only match the substrate, but also fulfil the previously listed criteria in addition (Table 1). Toluene, for example, evaporated too slowly for the surface to be cooled sufficiently for water condensation.[123] One could of course counter this by external cooling of the solution.[24] The solvent must additionally fit the polymer to allow for sufficient migration of the chains within the solution.[123]

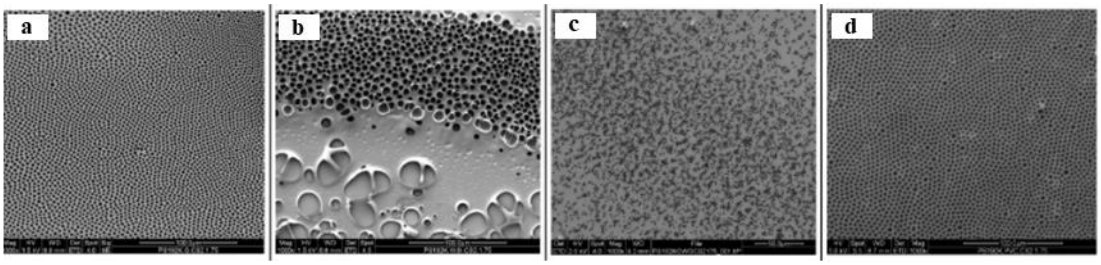

Figure 9. Scanning electron microscopy images of breath figure patterns formed from the same 1 wt%/vol PS solution in carbon disulphide cast on different substrates at 75% rH and 23 °C. a) glass, b) RCA1 washed silicon wafer, c) piranha washed glass silanized with 3-glycidoxypropyltrimethoxysilane, d) polyvinyl chloride. Figure adapted from Ferrari *et al*.[122]

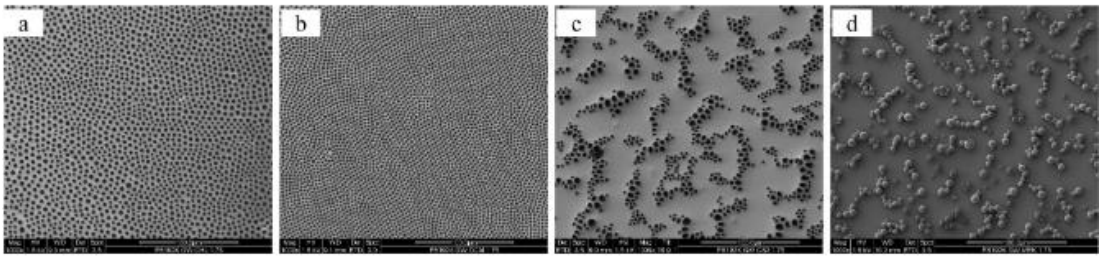

Figure 10 Scanning electron microscopy images of breath figure patterns formed on piranha cleaned glass from a 1 wt%/vol PS solution at 75% rH and 23 °C using different solvents: a) chloroform, b) dichloromethane, c) carbon disulphide, d) methyl ethyl ketone. Figure taken from Ferrari *et al*.[122]

Ultimately, it was not possible to determine one key factor for creating a successful porous film, thus highlighting the interdependence of the different processes involved.[123] No clear quantitative correlations to the order of the final patterns were found. However, the qualitative roles of solvent and substrate became much clearer, as well as the complexity of the interplay.[123] These experiments show how crucial it is for the whole experimental system to be well-matched, while each part must fulfil own criteria.

Another curious finding of this research was that while a humid airflow generally should facilitate pattern formation due to the increased evaporation rate, Ferrari *et al*.[123] were unable to create any well-ordered patterns *via* this method.[123] This showcases another important cause of confusion among different researches conducted, as there are no standard procedures, the equipment is often homemade, and details on experimental procedure are scarce.[53] Therefore, it is no surprise that

a process heavily reliant on complex mass and heat transfers, which both depend on numerous parameters, yields very different results with even slight variation.[53] Keeping in mind that only two parameters of the many were varied in the presented research and that each researcher will introduce subtle differences to the procedure, even if it is documented well, it is predictable that results from different authors can appear controversial.

2.3.3 Methods to Induce Breath Figures

Breath figure patterns can be induced using various techniques. Classically, a drop of the polymer solution is cast on a substrate in a humid environment. The humidity can be dynamic with a humid airflow, or static as enclosed environment, both usually creating well-ordered patterns. A humid airflow is commonly achieved using saturated nitrogen gas by bubbling it through distilled water[32,33,68,73] and a humidity chamber needs to be of a relative humidity (rH) of at least 50%.[31,40] The optimum relative humidity for ordered films was reported as 70-80%[68] and even 80-95%[45] for different systems. The BF method can be further combined with other techniques like dip-coating and spin-coating.[53,127] Combined with the aforementioned variety in parameters to alter, this yields a plethora of opportunities to create breath figures.

Using electrostatic repulsion among the droplets to increase the distance between one another has also been reported for drop-casting.[113] This method can lead to the creation of non-close-packed patterns of distances up to 16.5 times the average pore diameter between individual pores. This could be achieved by introducing hydrogen bromide, which charged forming water droplets positively. The solvent system should be adapted towards a high ion mobility for best results.[113]

The modifications of the breath figure method include the so-called “generalized” BF methods.[53] Those methods do not need a humid atmosphere, because they are not BF methods in the strictest sense, and the water droplet array is not generated from

water vapor. An example of this is the water-in-oil emulsion technique, for which the water is directly introduced into a non-solvent system.[53]

In this research, the breath figure pattern will be combined with the self-assembly of block copolymers, using dip-coating to create the polymer film. The previously mentioned advantages of dip-coating are especially obvious when comparing the technique to the more common drop-casting, which clearly is not a feasible method to scale up. The crucial parameters of cast volume and solvent evaporation rate for casting films, the most common method to create BF films, are approximately equivalent to the concentration of the solution and the withdrawal speed for dip-coating in the draining regime.[47] Interestingly, a breath figure pattern could be obtained *via* dip-coating for a polymer for which this was not possible using the casting method.[47] Therefore, dip-coating in a humid environment to induce BFs might even open up new opportunities. In addition, the gradual film creation allows for other gradual experimental changes. Tian *et al*.[128] for example decreased the humidity from 85 to 35% during dip-coating, which lead to gradual decrease in pore size from 1.2 to 0.59 μm, allowing for the direction of droplet motion on the created surface.

In some cases where breath figure patterns were obtained by dip-coating, the dip-coating speed or more exact method was not reported.[15,120,128] Some specific withdrawal speeds for creating ordered BFs ranged from 12, 150, and 300 mm/min,[121] over the 400 mm/min[35] of the "fast dip-coating process", and up to 5000 mm/min[129]. An increase in dip-coating withdrawal speed from a poly(sulfone) solution from 150 to 300 mm/min led to an increase in the diameter of the obtained pores.[121] However, there was no explanation or investigation about whether this might be linked to the thickness obtained at certain speeds and the different deposition regimes. Despite the regimes being at different speeds depending on the system, the reported work combining breath figures and dip-coating was likely conducted in the viscous drag and maybe intermediate, but not the capillary regime.

Therefore, it would be of interest to study how the different dip-coating regimes affect the formation of breath figures. It is also unclear if different dwell times before withdrawal affect the breath figure pattern, as this was even proven and disproven for different systems within the same paper.[121]

As elucidated earlier, each parameter of the system is linked to many others, and research concerning this type of optimization is well-justified and even necessary for each system and laboratory set-up. The following ranges can therefore only serve as rough indication for likely orders of magnitude to work with. The polymer content in solutions successfully yielding ordered patterns *via* various methods ranges from 0.25 g/L[45] to 100 g/L[73]. Drop-casting volumes range from at least 20 µL[124] to 200 µL[130]. Silicon wafers and glass have mainly been used as substrates to create breath figure films on,[31] and chloroform and carbon disulphide are the most common solvents.[53] However, due to the complex interdependence, using a new polymer or even creating an own set-up might require a lot of testing and variation of parameters and procedure before successful BF pattern creation.

2.3.4 Generalized BF Method: Emulsions

As mentioned before, there are other ways to induce a breath figure like pattern from water droplets than the humidity approach. One of these other methods is the water-in-oil emulsion technique. It allows for the creation of breath figure like patterns[2] with a very similar dependence on the listed parameters, while the high relative humidity is not needed. Such a high humidity should be avoided in technology heavy laboratories[38] and might be difficult to precisely control in combination with other techniques, such as dip-coating. In addition to the common drop-casting technique,

[2] from now on simply referred to as breath figure patterns

the emulsion breath figure formation has also been combined successfully with spin-coating[38,39] and dip-coating.[35,37]

The breath figure patterns formed with the emulsion technique generally looked very similar to patterns created with the humidity method, which might support the water condensation theory for breath figure formation. In one case, the pores created from an emulsion were reported to be interconnected at the lateral walls,[36] and in another they penetrated through the entire film (Figure 11).[35] These slightly different results are likely caused by their specific experimental procedures.

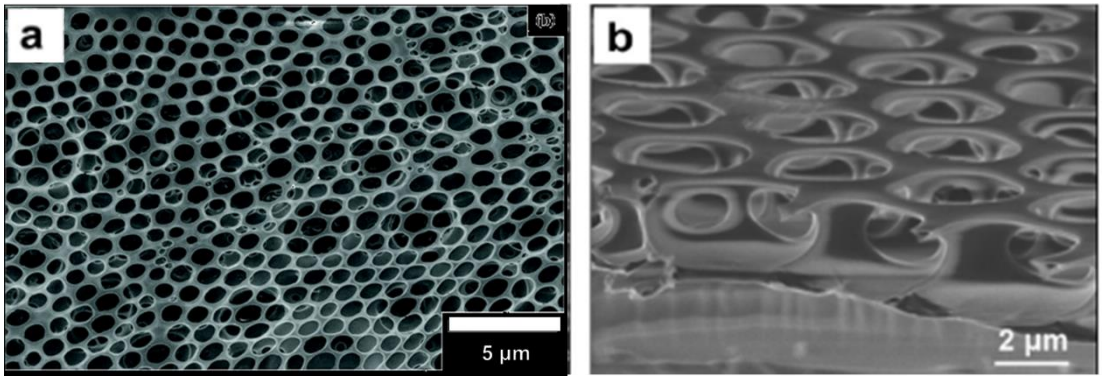

Figure 11. SEM images of different polymer films. a) A PS film created *via* dip-coating from a benzene emulsion with 2 wt% of water. The pores penetrate through the film. Figure taken from Ham *et al*.[35] b) Cross section of a $EuSiW_{11}$/poly(methyl methacrylate) (PMMA) hybrid film cast from an emulsion of 6 mg/mL PMMA and 0.5 mg/mL pluronic P123 in DCM and 8 mg/mL of $EuSiW_{11}$ in water, with 5 v% of the aqueous phase. Some of the pores were interconnected. Figure taken from Lian *et al*.[36]

Generally, these breath figure mimicking emulsion techniques can be roughly divided into using solvents that are fully immiscible or partly miscible with water. In several cases, THF, which is miscible with water, has been used as solvent to create hexagonally ordered porous films.[38,39,131–133] As the volatility of THF is much greater than that of water, this will over time lead to a phase separation in the final stage of film evaporation.[39,133] This comes from the polymer and water concentrations increasing greatly, leading to the formation of distinct water droplets due to the insolubility of the polymer in water. Like in the proposed breath figure mechanism, polymer molecules can then precipitate at the water droplet interface, protecting the

water droplets from coalescing.[39,133] The coalescence is additionally hindered by the fast evaporation of the solvent.[35] This mechanism is assumed to be similar for solvents that are not miscible with water and the final patterns are thought to be formed by ordering in the same manner as for conventional breath figure formation.[36] Using THF as solvent additionally stabilizes the water droplets with the "solvent surfactant",[51,134] and the system may also be stabilized by using ordinary surfactants, which will become embedded in the pore walls of the final film.[36,133]

For such emulsions, the role of humidity was tested by creating films in different atmospheres.[36,133] It was found that the pores are also present after film creation in dry atmosphere, which lead to the conclusion that water condensation from the atmosphere does not play the primary role in pore formation.[36,133] An increase in water in the emulsion also lead to an increase in final pore size,[38,39,131–133] and when the water amount is increased too greatly, this leads to squeezed, non-spherical pores, and finally to them merging.[131] Even with up to 80% rH, it was concluded that the effect of the water already mixed into the emulsion is significantly greater than the ambient moisture.[38] This was linked to the water in the solution contributing greater to the humidity at the air boundary layer than the more distant ambient humidity, causing only minor condensation from the atmosphere.[38] However, while the ambient humidity does not contribute greatly, a relative humidity of 30-40% may be most suitable to form breath figure patterns to restrict the water evaporation and enhance phase separation by different evaporation rates in the emulsion.[36,135] Another study found that while the ambient humidity does not seem to affect the surface of the film much, it increases the number of pore layers that are formed.[132] At greater water contents or higher humidity, particles, or so-called "reverse breath figures", were found underneath the surface film, and at even greater concentrations only such particles were found (Figure 12).[132]

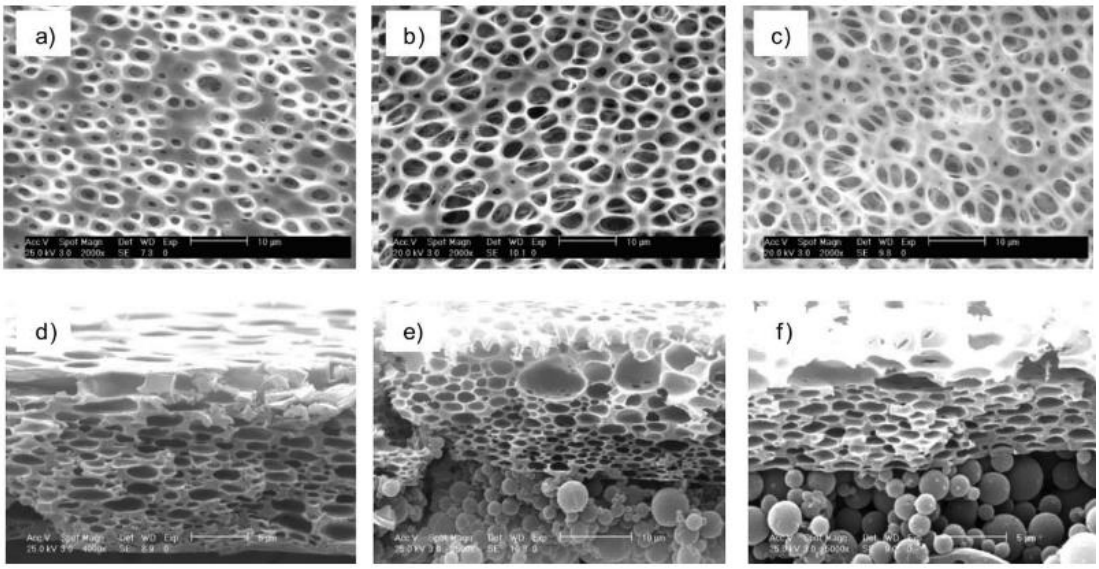

Figure 12. SEM images of films formed from 30 mg/mL polymer (PMMA matrix with 10 wt% glycopolymer) in THF with 50 uL water/mL of THF. a)-c) are surface images and d)-f) the corresponding cross sections of films cast onto glass under different relative humidity: a),d) 28%; b),e) 60%; c),f) 76%. Figure taken from de Léon *et al*.[132]

The final pore size in the film was found to be up to 20 times greater than the water globules measured in the emulsion before film creation.[35–37,124,135] This was attributed to several effects: the large volume reduction of a solution with low polymer concentration during drying,[35] slight droplet growth due to water condensation from the atmosphere,[36,37] and the fusion of water droplets during evaporation.[36,37,124,135] It is also very important to maintain the droplets in the emulsion at a suitable size.[36] The demarcation of an opaque emulsion is easy to see when it becomes clear,[50] but the slightly different colours of an emulsion also indicate different droplet sizes. Liang *et al*.[36] found that for an emulsion of water in dichloromethane (with poly(methyl methacrylate) and stabilizer), a translucent grey colour indicates a droplet size of 30-300 nm and yields ordered patterns, whereas a more milky colour indicates that the droplets are in the order of micrometres and more disordered patterns will be obtained. Therefore, the stability of the emulsion and the mixing method is crucial for the quality of the final film. Interestingly, the reported mixing methods vary wildly from sonication for 30 s[124] to 4 h.[35] Emulsions are also reported to be sonicated and then shaken again before casting.[130] In some

instances, the solution is solely shaken, because the high shearing force of sonication is thought to generate unstable droplets.[135]

For a method as dip-coating, where the film only starts to evaporate after the substrate is immersed, held in the solution, and withdrawn at a certain speed, the stability of the emulsion is even more important than for faster methods as drop-casting. A water in dichloromethane (DCM) emulsion with poly(methyl methacrylate) (PMMA) has been successfully stabilized by pluronic P123[36] and with didodecyldimethylammonium bromide when using PS,[36,135] but many tested stabilizers have not been successful.[36] Using amphiphilic block copolymers does not only stabilize the water droplets by forming micelles, but also yields great control over the droplet sizes by controlling the block lengths.[124] Another way to stabilize such an emulsion instead of adding surfactants is to dissolve another solute that is selectively soluble in the water phase and may later be washed out.[35] Unlike with amphiphilic surfactants, solutes not soluble in the organic solvent are expected to accumulate at the bottom of the film pores.[135] Sucrose has been tested as such a solute, as it is essential non soluble in nonpolar solvents,[136] and by adding 3 wt% into the water solution, the stability of emulsions for which water immediately recombined after mixing (PMMA in benzene) was greatly increased.[35] The size of the water globules in the emulsion did not even double and still were of diameters less than 300 nm after 40 h. The sucrose in the film was later removed by soaking it in water for 24 h. Interestingly, the sucrose should also hinder the water droplet growth by collision and coalescence. Therefore, the Ostwald ripening mechanism was proposed as an alternative for droplet growth.[35]

The governing forces of creating breath figure patterns *via* emulsions must be very similar to the ones created *via* the humidity approach, as changing certain parameters lead to very similar changes in the patterns formed. This includes that the diameter of the pores decreases when the vaporization temperature is increased.[131] This is in line with the evaporation rate playing an important role, and

also fits that an organic solvent with a higher boiling point leads to the formation of bigger pores, as the droplets will have more time to grow.[135] When the surfactant concentration is greater, the pores formed are smaller,[135] similarly to increasing the concentration of the polymer, which both decreases viscosity and stabilization of the water droplets.[135] Moreover, a higher polymer concentration also leads to more regular patterns.[37] All of this supports the suggested mechanism of breath figure formation with the emulsion technique, which essentially is governed by the same parameters as the humidity technique.

Other volatile solvents that have been used to successfully obtain breath figure patterns from an emulsion with water include benzene,[35,135] DCM,[36,37,135,137] CS2,[37,137] and chloroform.[51,52,135,138] The matrix solutes used by now include PMMA,[35,36,38,131–133,135] PS,[35–37,131,135] cellulose acetate butyrate,[39] cellulose triacetate,[138] amphiphilic diblock copolymer,[137] PS-*b*-P4VP,[74,135] even metal oxides from sol-gels.[139] Polymer amounts ranged from 0.5[138] to 100 mg/mL[38,39] in the organic solvent and water amounts from 18.5[35] to 100[130] µL/mL organic solvent. Somewhat stable patterns were even reported for 50 vol% emulsions,[124] whereas in other cases a water content greater than the previously mentioned range lead to the formation of reverse breath figures.[132] It was also pointed out that a smaller water content can be beneficial, as it reduces the number of collisions that can occur in the specific experimental time scale.[35]

In most cases, glass has been used as substrate. Silicon wafers with[38] and without protective oxide layer[74] have also been reported. Here it is important again to match the substrate with the solution used, as good wetting is crucial. In some cases, it was generalized that hydrophilic substrates are needed for good spreading of the solution.[36,37] On the other hand, it was reported that using nonpolar PS as polymer makes the use of a hydrophobic substrate necessary, and coating silanized glass with PS dissolved in benzene worked well.[35] Additionally, no regular patterns could be obtained with PS dissolved in THF in combination with a SiO_x substrate.[38] This shows

that such generalized statements are often not appropriate or accurate for such a complex system.

PS is thought to not be polar enough to stabilize water droplets sufficiently on its own.[135] In comparison with PMMA as polymer and otherwise using the same experimental conditions, no ordered patterns could be obtained for PS when they were for PMMA.[38] Using a blend of PMMA and PS, breath figures were only observed in the PMMA domains, where water preferably accumulated.[38] In another research, where a stabilizer was used in addition, the pores created with PS were less ordered and larger than for PMMA, which is thought to be caused by the stronger phase separation of PS with water.[131] However, as has been proven for the humidity induced breath figures, the special case of PS likely just has to be accommodated for with a more sophisticated experimental design adapted specifically for it.

2.3.5 Introducing Nanoparticles

In 1907, Pickering[50] reported that "insoluble emulsifiers" can be used to stabilize the mix of two insoluble liquids. These so-called "Pickering emulsions" are not only more stable than using common surfactants as emulsifiers but can also add the properties of the employed particles to the mixture.[50,140] The colloid particles were observed to coat the globules of one liquid dispersed in the other by microscopy. This protective layer consists of a hexagonal monolayer of particles and prevents the coalescence of the globules, thereby stabilizing the emulsion.[50,140]

It was further found that the size of the particles is crucial for the stability of the emulsion.[50] Once a spherical particle dispersed in the emulsion reaches the fluid-fluid interface by Brownian motion, its adsorption to the interface may result in a reduction of the total surface energy.[51,140,141] The amount of energy needed to remove the particle again, also called energy of attachment, depends on the square of the particle radius.[51,140,141] Particles of sizes less than 0.5 nm are very easily detached from the interface, as their energy of attachment is close to the thermal

energy (k_BT) causing spatial fluctuations in particles.[140] Therefore, if the particle is so big that the energy of attachment is high in relation to k_BT, it will effectively be irreversibly confined to the interface. This effect increases with particle sizes. The permanent confinement to the interface also is why particles stabilize emulsions better than surfactant emulsifiers, which are typically smaller and constantly desorb and re-adsorb onto the interface.[51,140,141]

The interfacial energy of attachment also depends on the contact angle the particle forms with the different fluids, so the wettability.[140,141] This is especially important for smaller nanoparticles, as the thermal energy will be comparable to their interfacial attachment energy.[140–142] While micrometre sized colloids are trapped at the interface, nanoparticles may reach their equilibrium state distribution in the solution.[140,141]

A particle is held strongest at the interface for a contact angle of 90°, which indicates that the particle is approximately equally immersed in both liquid phases.[140] If the angle with water is greater, then the particle is more hydrophobic and the layer of nanoparticles will curve in a way that most of the particles stay in the non-aqueous liquid. However, if the interaction with one liquid is greatly preferred over the other, the particles will re-disperse in that phase and not stabilize the emulsion.[140]

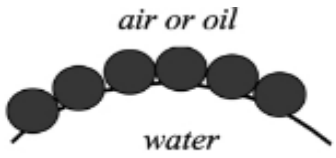

Figure 13. Position of small spherical particles at a fluid-water interface for a contact angle greater than 90°. Figure taken from Binks.[140]

In order to obtain the desired surface properties, particles may be coated or stabilized with ligands.[140,142] This allows to control the interactions with the surrounding independently from the other properties of the particles. It is also possible to only partly coat particles, which then are called "Janus" particles. Like this, the particle can possess different surface chemistry and wetting characteristics on different sides,

which offers a straightforward solution to obtain a contact angle of 90° with both liquids.[140,142]

The other important parameters for the effectiveness with which a particle stabilizes an emulsion are its shape, concentration, and interparticle interactions.[140] Moreover, there are definite limits for the amount of emulsifier that can be added to obtain a stable emulsion. Lastly, the particle size also seems to influence the globule size in the emulsion.[50]

2.3.5.1 Pickering Emulsions and Breath Figures

The formation of breath figures by condensation of water droplets onto an immiscible solvent basically creates a water-in-oil emulsions. Therefore, this allows for the one-step creation of breath figures decorated with nanoparticles such as metals by simply mixing nanoparticles into the polymer solution and creating Pickering emulsions.[31] The pores formed by the breath figure mechanism will be selectively decorated with the particles once the water evaporated.[51] This has been observed for many different materials and the following nanoparticles, some of which were stabilized using ligands: Ag,[66,67] Au,[66,71,72] Fe_2O_3,[67,72] CdSe,[68] Al_2O_3,[70] ZnO,[70] TiO_2,[15,70] SiO_2,[51,69,70,126] zeolites,[143] PS particles,[52] microgels,[52] and clay[14].

One of the first reported studies on this was with 4 nm CdSe particles self-assembling into the pores of a polystyrene film as a 5-7 nm thick layer *via* the breath figure method.[68] The nanoparticles were stabilized with tri-n-octylphosphine oxide ligands, which further allowed to functionalize the holes after film formation *via* ligand exchange. The addition of the nanoparticles did not affect the characteristic sizes of the final pattern (Figure 14). This indicates that the optimal nanoparticle content may be investigated after the optimization of the system for the desired order without particles.[68]

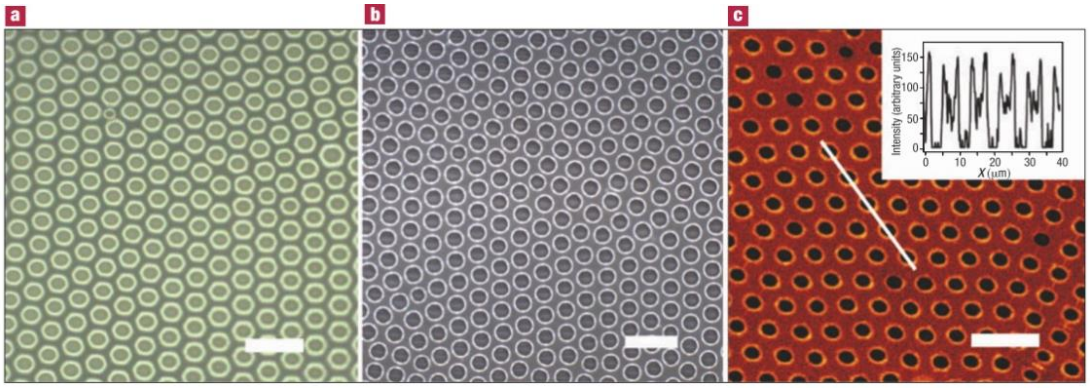

Figure 14. Images of breath figures obtained with optical and confocal fluorescence microscopy and scale bars of 16 μm. a) Breath figure pattern obtained with pure polystyrene, b) optical and c) confocal fluorescence microscopy images of a film obtained from a polystyrene solution containing CdSe nanoparticles, inset shows the fluorescence intensity along the line drawn in the image. Figure taken from Böker *et al*.[68]

It was found using drop-casting that the additional stabilization of the system with SiO_2 particles can lead to the formation of ordered breath figures under conditions for which none were obtained without the particles.[51,52] As colloidal science predicts, the use of larger SiO_2 particles also increased the stability of the system, thereby creating more regular breath figure patterns. The particle sizes used to show this were 100 nm, 200 nm, and 1 μm. Moreover, the area of the pores that will be covered with the particles can also be controlled by the particle concentration (Figure 15): First, the particles will spontaneously assemble at the liquid-liquid interface, which reduces the interfacial energy and prevents the water droplets from coalescing. Then, due to capillary flow and contact line pinning effects when the polymer solvent evaporates faster than the water droplets, the particles are carried to the three-phase contact line. The meniscus further compresses these particles, and their position is fixed during solidification of the polymer film. This leads to a ring-like pattern at the edge of the final pore at low particle concentrations, while the whole inside of the pore is covered when more particles are dispersed in the solution (Figure 15e,f).[51,52] It was later found that hydrophilic particles are well visible in the pore walls, whereas hydrophobic particles mainly reside in the polymer matrix at the interface, so are much harder to observe.[52] This shows that a combination of the self-

assembly processes in Pickering emulsions and breath figures, and capillary flow can be utilized to direct particle deposition within a microporous substrate.[51,52]

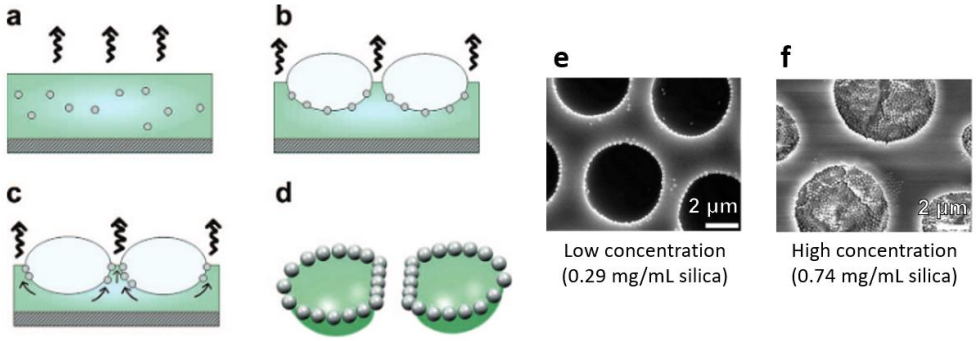

Figure 15. a)-d): Proposed mechanism of directed nanoparticle deposition during breath figure formation. e-f: SEM images of structures formed from solutions of 10 g/L PS in 1 mL chloroform, with 30 µL (e) or 80 µL (f) of a 10 mg/mL alcoholic silica particle (200 nm) alcoholic suspension added. Figure adapted from Sun *et al*.[51]

Zeolite crystals of different polarities and 40 nm size were tested for their ability to stabilize and create coated pores using the breath figure process.[143] When hydrophilic crystals were used, the formed pattern was irregular. Ambipolar crystals, however, stabilized the water droplets and lead to highly ordered patterns.[143] This shows how the surface chemistry of the particles added is very relevant, especially for particles of the nanometre size range.

Some nanoparticles have also been created *in situ*. Ag and Au nanoparticles were directed to the surface of the pores by reducing $AgNO_3$ and $HAuCl_4$ with $NaBH_4$ in the solution as one-step process.[66,67] There also is a remarkable example of TiO_2 microparticles being created *in situ*.[144] These microparticles lie in the pores of the final film, which was called the "bead-in-pore" morphology (Figure 16). The water droplets functioned as microreactors in which the hydrolysis of $TiCl_4$ took place, while a polymer matrix organized around them. Like this, particles only slightly smaller than the holes were created, with one particle in each hole. Due to the non-spherical water droplet shape in the breath figure method, the obtained TiO_2 particles confined by the droplets were hemispherical. The shape of the particles can be tuned by varying

the $TiCl_4$ concentration and humidity. When the relative humidity is increased, the bigger water droplets lead to the formation of bigger particles. However, when it is increased too much, the obtained particles are tablet like due to the lower concentration of the hydrolysis product in the pores. Overall, a relative humidity of only 20-50% was sufficient only when the Ti salt was part of the solution, which was linked to its hygroscopic character. By increasing the $TiCl_4$ concentration, mushroom like particles were obtained. This shows that the breath figure method can yield controlled and ordered asymmetrical particles, which can be very difficult to be obtained otherwise.[144]

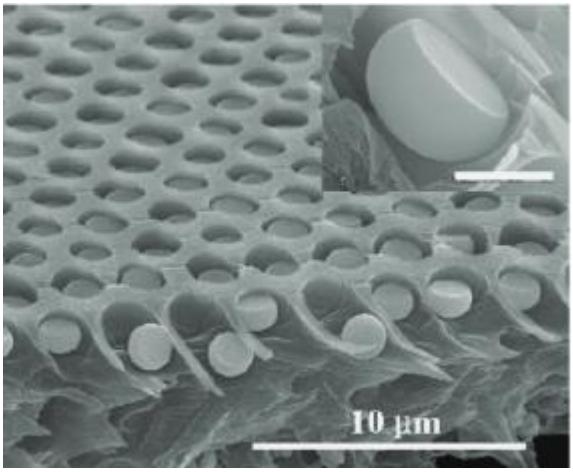

Figure 16. Cross section of a polystyrene film with TiO2 particles in its pores created by the breath figure method. Scale bar of the inset is 1 µm. Figure taken from Li *et al*.[144]

In many cases where nanoparticles were incorporated into the breath figure pattern, polystyrene dissolved in chloroform was used as polymer solution.[51,67,68,71,72] The nanoparticle content, when reported, was often close to 1 mg/mL,[67,72] with NP:polymer ratios of 1:9 to 3:5 by weight.[67,68,71,72,145] The nanoparticle location was proven using confocal microscopy,[143] confocal fluorescence microscopy,[68] transmission electron microscopy,[68] and in case of big particles even scanning electron microscopy.[51]

3 Materials and Methods

3.1 Materials

All chemicals were used as purchased unless noted otherwise. Chloroform (≥ 99.8%, Honeywell Riedel-de Haën) and acetone (≥ 99%, Honeywell Riedel-de Haën) were purchased from Fisher Scientific. Hydrogen peroxide (30% w/w H_2O, grade puriss p. a.), polystyrene (avg. M_w ~280 000), 2-propanol (≥ 99.8%), sulfuric acid (95-97%, ISO grade), tetrahydrofuran (≥ 99.0%), and toluene (≥ 99.9%, LiChrosolv) were purchased from Sigma-Aldrich. Poly(styrene)-*block*-poly(4-vinyl pyridine) (ID P780-P4VP, M_n(PS) = 3.3 kg/mol, M_n(P4VP) = 18.7 kg/mol, 1.14 M_w/M_n) and poly(styrene)-*block*-poly(4-vinyl pyridine) (ID P9289-S4VP, M_n(PS) = 32 kg/mol, M_n(P4VP) = 4.5 kg/mol, 1.15 M_w/M_n) were purchased from Polymer Source. Silicon substrates (525 ± 25 μm, (100) orientation, p-type, light B doping, > 1 Ω cm^{-1}) were provided by Ville Jokinen from Micronova. 20 nm diameter TiO_2 nanoparticles (99.9%, rutile:anatase 85:15) were purchased from Nanoshel. All water used was deionized Milli-Q (18.2 MΩ.cm) water. Sucrose "kidesokeri" was obtained from the supermarket (Rainbow).

Substrates were prepared by cutting silicon wafers into 1 x 1.5 cm rectangles and cleaned in a piranha solution (70:30 vol% H_2SO_4:H_2O_2) for 10 min. Subsequently, the substrates were rinsed off with Milli-Q water and dried with a nitrogen gun. The samples were stored for at least a day before use.

3.2 Dip-Coating

In order to find the right parameter ranges, dip-coating was conducted from various polymer and nanoparticle solutions, mainly in chloroform. Pure polymer solutions were stirred for at least one day and solutions containing nanoparticles, and later also emulsions, were sonicated for 40 min before use and cooled with ice. After testing the effect of shaking just before the experiment, the solutions were also shaken again for at least 10 s before the experiment.

The SiO_x substrate was immersed at 8.4 mm/min and the dwell time for the initial experiments was 10 s, which was later increased to 30 s. The dip-coating speed of the Miniature Langmuir-Blodgett Mini Trough 2 (KSV Instruments Ltd) dip coater could be adapted from around 8.4 to 84 mm/min in 8.4 mm/min intervals. Different withdrawal speeds were tested.

3.2.1 Humidity Control

Two different humidity controls were tried, the static and the dynamic one (Figure 17). For the dynamic control, N_2 gas (later also referred to as air) was blown through Milli-Q water to fully saturate it and then directed at the substrate. Different blow positions, distances and flow speeds were tested. For the static control, a small humidity chamber was constructed. Due to the arm of the dip-coater moving in and out, a silicone tent was used to seal the environment more. Humid N_2 gas was flowing into the chamber and a humidity meter measured the relative humidity reached, which could be up to 86% with this set-up.

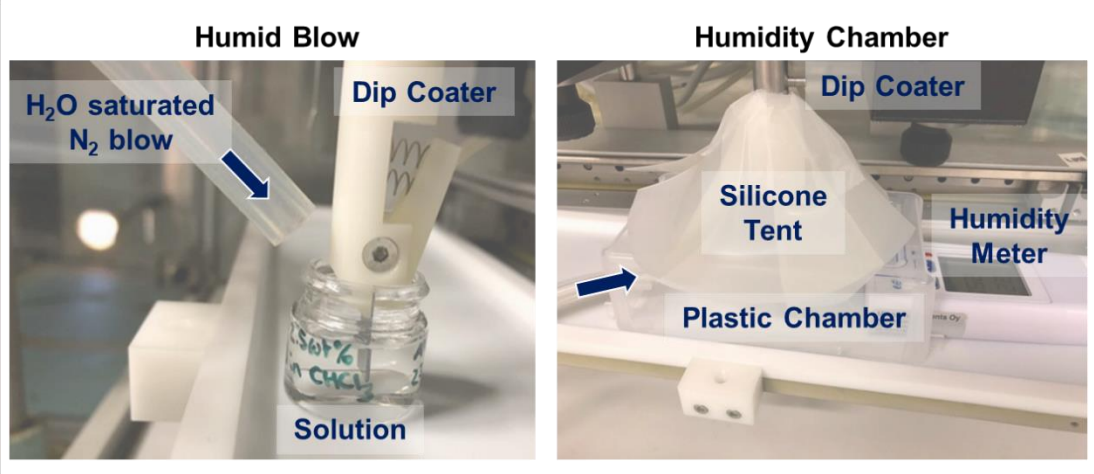

Figure 17. Different humidity set-ups tested for dip-coating.

3.2.2 Optimized Conditions

The optimized conditions used for the final experiment were the following: The final emulsion contained 10 mg PS_{32k}-*b*-$P4VP_{4.5k}$/mL and 0.1 mg TiO_2/mL in chloroform, which were both dissolved the day prior to the experiments. The TiO_2 NPs were

dispersed in chloroform in order to transfer smaller weights than would be possible with the scale. The aqueous phase contained 30 mg sucrose per mL and 32 µL of the aqueous phase were added per mL of chloroform solution. Both the NP and the aqueous solution were sonicated for 40 min and cooled with ice to not overheat before their respective amounts were transferred to the polymer solution. Then, the entire emulsion was sonicated for another 40 min and cooled with ice.

The SiO_x substrates were still cut to 1 x 1.5 cm size. Then, they were cleaned by first sonicating them in acetone and subsequently in 2-propanol for 10 min respectively. Lastly, they were rinsed off with Milli-Q water and blown dry with N_2.

Before conducting the dip-coating experiments, the solution was shaken by hand for 30 s and again for 15 s between each experiment with the same solution. The SiO_x substrate was immersed at 8.4 mm/min and the dwell time in the solution was 30 s. The substrate was then withdrawn at withdrawal speeds of 8.4, 16.8, and 67.2 mm/min and left to air dry. Before AFM measurements, the samples were immersed in Milli-Q water for around 24 h to re-dissolve the sugar.

3.3 Sample Analysis

An Olympus BH2-UMA optical microscope was used to examine the regularity of the breath figure patterns. Overview and zoom in pictures were taken.

To have a closer look at the breath figures, the samples were coated by sputtering 10 nm of Au/Pd (80/20) on them using a Quorum Q150T ES. Then, the samples were imaged using either a Hitachi S-4700 or a Tescan Mira3 SEM with 5 kV and 20 µA.

A Bruker MultiMode 8 AFM was used for even higher magnifications, which are necessary to identify the block copolymer patterns and depth profiles. NCHV-A tips from Bruker were used and measuring was conducted in tapping mode. Usually, different 5 μm^2 areas were recorded for an overview of the sample and 1 μm^2 areas

for close-ups. For this, 256 lines and 2 Hz were used. Results were corrected and analysed using Nanoscope Analysis 1.5.

4 Results and Discussion

4.1 Material Choices

The polymer PS-*b*-P4VP was selected to create thin films because, together with the closely related PS-*b*-P2VP, various types of this polymer have been proven to work for creating ordered breath figures, even with the emulsion technique.[74,135] Moreover, the PS-*b*-PVP BCPs are very commonly used to induce ordered BCP patterns, even in combination with dip-coating,[21] leading to spherical or cylindrical domains.[13,93,105,106] This BCP type has also been frequently used to organize NPs, [55,58,64,65,109–111] mostly due to the ability to form supramolecular bonds with the nitrogen of the pyridine. Therefore, this block copolymer is expected to work well for the purpose of combining its nanoscale self-organized domain formation with NP organization and BF formation. The volume fractions of $PS_{3.3k}$-*b*-$P4VP_{18.7k}$ and PS_{32k}-*b*-$P4VP_{4.5k}$ were chosen to induce a spherical morphology in the film, with the predominant block as matrix. In the initial experiments, however, PS was used as model system in order to optimize the system before using the more expensive block copolymers, which also contains a PS block.

For the choice of nanoparticles, it was important to ensure that they would assemble at the right place – either at the liquid-liquid interface to end up in the pores or at one of the polymer blocks to create a pattern between the pores. Therefore, the particles for the polymer pattern should preferably be hydrophobic and compatible with one of the polymer blocks, so they would be less preferred to assemble at the solvent-water interface. For this, it is also essential that they are small, which allows them to reach their equilibrium state in the solution rather than being trapped at the solvent-water interface due to their size.[140,141] Therefore, 4 nm dodecanethiol stabilized gold nanoparticles were chosen to assemble in the polymer phase in an ordered fashion.

Au NPs with different chemical stabilizing groups have been used to create ordered NP arrays on a BCP film and the NPs selectively assembled at either the interface of the two polymer blocks or one of the block domains only.[55,56,64,65] Pure Au formed complexes with the nitrogen in the P4VP block of PS-*b*-P4VP,[65] and dodecanethiol stabilized Au assembled at the PS domains of PS-*b*-PMMA.[56] 4 nm dodecanethiol stabilized Au NPs are also comparatively easy to synthesize with a very narrow size distribution using the well-established two-phase reduction method.[66,146,147] However, this step could not be tested anymore, due to time constraints.

TiO_2 of 20 nm diameter was chosen to assemble at the solvent-water interface, which it also did in some previous literature,[15,70] where it aided the photocatalytic degradation of pollutants.[15] No report of using TiO_2 NPs with PS-*b*-P4VP were found, only an oleic acid coated rod-like nanocrystal that preferred the PS phase[148] and the $Ti(OH)_2^{2+}$ precursor selectively binding to the P4VP block.[149] However, TiO_2 can generally interact with a pyridine functional group, for example by forming hydrogen bonds to surface hydroxyl groups or coordination bonding to acid sites,[150] so it is unclear whether the NPs would prefer this interaction over assembling at the water/solvent interface. Choosing bigger NPs should increase the likelihood that TiO_2 prefers the interface, however, 20 nm might not be enough for that.

Chloroform was chosen as solvent, because the picked polymers are soluble in it and it has been proven to be an excellent solvent for evaporative cooling to induce breath figures. Moreover, its boiling point also fits the desired range for solvents used in the dip-coating technique.[75] In the previous work employing similar materials chloroform was also mainly used as solvent, which makes it likely that all the material choices will match. Due to the slight selectivity of chloroform for PS[101] and the low volume fraction of P4VP, micelle formation would be expected in solution. Unless other parameters affect the domain morphology and/or orientation greatly, this should lead to a spherical morphology in the film, which is a desirable pattern for the aim of this research.

Herein, silicon wafers will be used as substrates, because their composition is more controlled than that of most glass types. Moreover, it has already been reported that RCA-1 (H_2O_2-NH_4OH-H_2O) washed silicon wafer, which possesses a thin oxide layer, was a good match with PS dissolved in chloroform to create the desired patterns.[123] Therefore, it is fair to assume that piranha cleaned silicon wafers will also work well with a chloroform solution.

Silicon is generally hydrophobic, but the native oxide layer that forms on it effectively makes it more hydrophilic, with a layer thicker than 30 Å decreasing the contact angle to close to 0° with water.[151] This comes from silanol groups (Si-OH) linking to the native oxide layer, leading to the adsorption of up to two water layers from washing or ambient moisture.[152] The interaction of a silica substrate with water depends greatly on the treatment before use.[153,154] If the treatment leaves OH groups at the surface, it will be hydrophilic, while CH_x and F groups make the substrate hydrophobic.[152,154] HF etching is the most common method to remove the native oxide layer and make the substrate hydrophobic, whereas piranha and RCA-1 cleaning both oxidize the silicon wafer, linking hydroxyl groups to the native oxide and making the substrate highly hydrophilic.[153,154] However, the contact angle of the hydrophilic surface does increase back to the one of the stable native oxide state before treatment after a few hours.[153–155] This has been linked to the gradual formation of the less hydrophilic oxide in air,[154] evaporation of water molecules from the surface, and recontamination of the surface by organics.[152]

Herein, the piranha cleaning will be used to remove organic residues from the surface and the Milli-Q water wash to remove other elements and minerals. The substrates will be used at least a day after washing, so the native oxide layer (SiOx) should be restored. This should make the surface more hydrophobic than directly after the washing. Later, the experiments will be conducted on freshly piranha cleaned wafers to compare the results.

4.2 Establishing Stable Conditions for Breath Figures in Model System

A selection of experiments that guided the optimization of the parameters will be presented. The complexity of the system was increased stepwise. In general, the concentrations will be given per mL of solvent instead of the common wt%. This was decided because wt% will become increasingly difficult to compare among solutions when more components are added to the system, as is the case here.

4.2.1 Testing Different Humidity Set-Ups

The first goal was to find suitable parameters to induce breath figures for a PS film. Inducing the necessary humidity for breath figure formation was attempted with a humid airflow and a self-built humidity chamber. The tested concentrations of PS in chloroform were 12.4 (<1 wt%), 37.4 (2.5 wt%), 74.6 (5 wt%), and 149 mg/mL (10 wt%), which are all well within the reported working range for inducing breath figures. The withdrawal speeds tested were 8.4, 16.8, 42, and 84 mm/min. The speeds reachable with the dip-coater fit the lowest of 12 mm/min reported in one paper.[121] However, all other dip-coating speeds of the ones reported were significantly greater with 150 to 5000 mm/min.[35,47,121] It is unclear whether this comparatively low accessible speed range will pose a problem, as there are not many reports of combining dip-coating with breath figures and out of those many do not disclose the withdrawal speed. In addition, it appears like there have been no studies investigating the effect of the dip-coating regime on the formation of these patterns.

The films created with a humid airflow were generally very inhomogeneous. The angle and distance of the airflow, as well as its pressure, were varied to find the best conditions. While a clear variation in thickness could be observed by the variation in colour of the thin film when magnified, the wells appeared rather shallow and did not reach through the film for the lower polymer concentrations (Figure 18A).

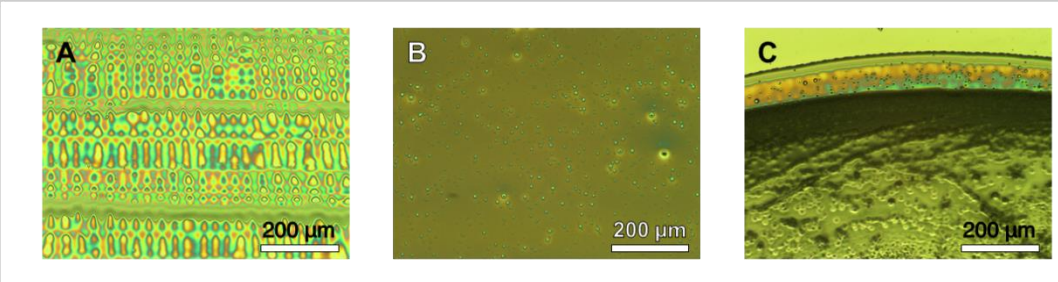

Figure 18. Optical microscopy images of different films created from a solution of 37.4 mg/mL PS in chloroform onto SiO_x. For the humid blow (A) and the humidity chamber (B) experiment, the substrates were withdrawn at 16.8 mm/min. For the drop-casted (C) film, a few drops of the solution were put onto the substrate, which was left to dry in the humidity chamber. The humidity of the chamber was between 80% and 86% rH.

At 74.6 (5 wt%) and especially 149 mg/mL (10 wt%) of PS in the solution, the precipitation of the polymer in response to the humid blow could be observed well. For 149 mg/mL, a thick film formed even on the surface of the solution and was dragged along by the substrate. Microscopy images revealed that a very porous structure formed, but it appeared very inhomogeneous and the film was much thicker than aimed for (Figure 19).

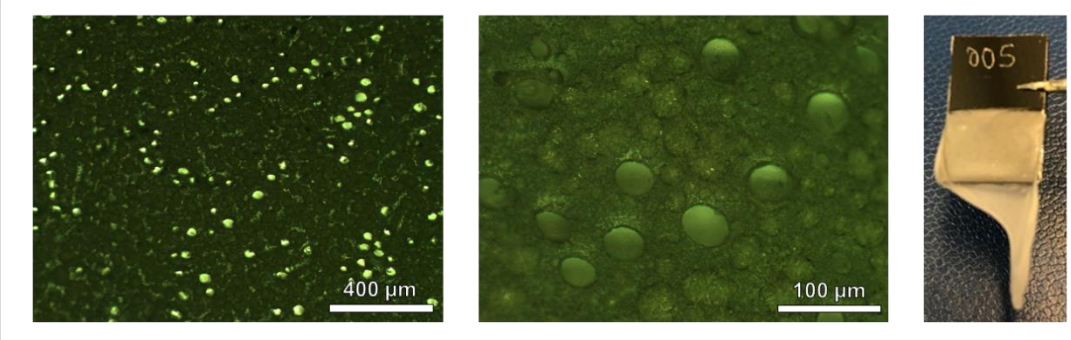

Figure 19. Optical images of a PS film formed *via* dip-coating from a chloroform solution with 149 mg/mL PS onto SiO_x under a humid airflow.

The results when using the humidity chamber seemed more promising (Figure 18B). The humidity was generally kept above 80% rH and the room temperature close to 25 °C. Pores were created on the films, but they still were relatively far apart from each other, not ordered, and comparatively large. According to the previously

introduced breath figure mechanism and research, this might indicate a high degree of coalescence or too low humidity for sufficient water droplet nucleation.

In order to rule out too low humidity, a drop-casting experiment was conducted. For this, about three drops of the solution were cast on a substrate in the same chamber. This led to a film covered with many pores (Figure 18C), so the humidity in the chamber should in principle be great enough. However, the thicker film formed with drop-casting likely leads to greater cooling and time to equilibrate in comparison to dip-coating. Due to these findings, it was concluded that this initial dip-coating system likely was not stable enough to hinder the condensed droplets from coalescing. A solution for this could be to increase the polymer concentration, however, the overall aim was to keep the concentration low for economic reasons. Linear polystyrene has also been proven to be a rather challenging polymer to induce regular breath figures with, so it was decided to continue the optimization by adding the nanoparticles to the system in hope of stabilizing it.

Since particles can stabilize an emulsion like system by assembling at interfaces, the addition of nanoparticles to a solution for breath figure creation should also allow for obtaining regular patterns with lower polymer concentrations. Initially, a 1:6 ratio of NPs:polymer by weight leading to 2 mg NPs/mL was chosen (Figure 20A), as this was close to some literature values presented earlier. This concentration appeared to be too high and led to NP agglomerations. Therefore, the ratio was changed to 1:40 of NPs:polymer, for which a good dispersion of the NPs could be obtained without additional humidity (Figure 20B).

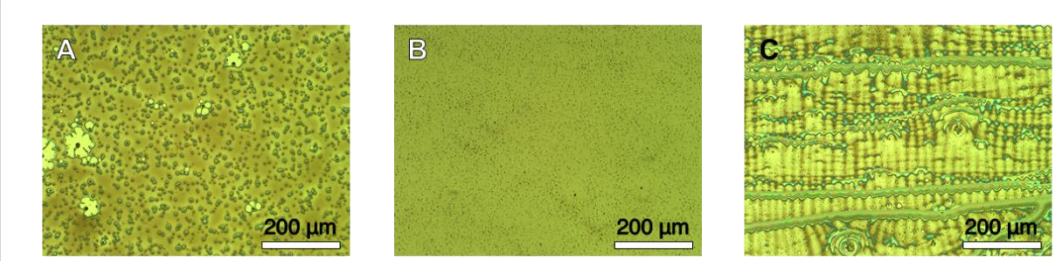

Figure 20. Optical microscopy images of different films created from 12.8 mg/mL PS and different TiO_2 NP concentrations in chloroform *via* dip-coating onto SiO_x with a withdrawal speed of 16.8 mm/min. A) The experiment was conducted in the humidity chamber with rH < 80% and from a solution containing 2 mg/mL NPs. B) The experiment was conducted at room humidity and from a solution containing 0.3 mg/mL NPs. C) The experiment was conducted under a blow of humid air and from a solution containing 0.3 mg/mL NPs.

In general, the humidity inside the partly open chamber could not be controlled precisely. Creating an air-tight humidity chamber with a moving mechanical arm is challenging and there were several openings left. As the formed breath figures greatly depend on humidity, this means that this set-up could not ensure a high enough repeatability. The humid air blow seemed even less controllable and repeatable, the pattern varied greatly throughout the substrate and among substrates (Figure 20C). The blow was difficult to aim at the moving substrate, which was partly blocked by the container of the solution. Moreover, the solvent evaporated rapidly and significantly faster than without the blow, which makes it even less repeatable, as the concentration changed drastically. This would also require creating a new solution for each experiment, which is very unsustainable. It was also attempted to first manually dip the substrate into the solution and then start the blow onto the vertically laying substrate, but this also did not yield better results. Therefore, these initial methods were concluded to be unfit to produce repeatable results and well-ordered breath figures with the current dip-coating set-up.

The initial experiments already showed a great agreement with literature. The pores did not form at ambient humidity, but only when the relative humidity of the system was increased. This indicates that indeed humidity induced water droplets and not

solvent boiling, which was suggested as breath figure formation mechanism for dip-coating,[118,119] was responsible for the pores. Moreover, the precipitation of the polymer due to increased humidity could even be observed by eye. There also was some evidence supporting the theory that a polymer film forms on top of the water droplets. One drop-cast sample displaying very big pores had some polymer arms extending over the pores that partly were connected to the other side of it (Figure 21). It is unclear whether those arms are remains of a whole polymer layer after bursting or if already they formed this way. To investigate this, it would be useful to observe the formation process *in-situ* with an optical camera. Lastly, a greater stabilization of the system was obtained with greater polymer concentrations, as expected.

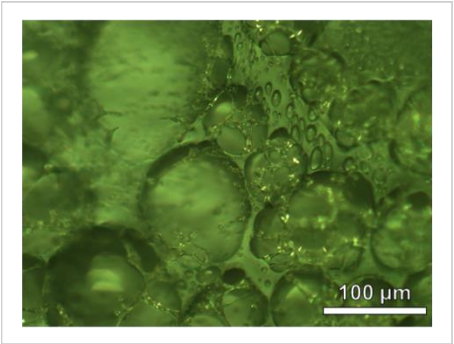

Figure 21. Optical microscopy image of a film created from 74.6 mg/mL PS in chloroform *via* drop-casting onto SiO_x at a relative humidity greater than 80%.

4.2.2 Initial Experiments with Emulsions

After excluding the humidity chamber and humid blow as method to induce water droplets on the films with the available set-up and method combination, the project was shifted towards utilizing the emulsion technique as generalized breath figure technique. This should also allow for more reproducible results, as the atmospheric humidity affects the final pores less and the evaporation should not be as excessive as with the airflow. Moreover, introducing a controlled amount of water to the system should be easier to control than hoping for a specific amount of condensation, which is dependent on many factors.

It was first attempted to stabilize the system of pure polymer solution with the introduced water. Since water is barely soluble in chloroform, sugar was added to the aqueous phase to stabilize the system, as has been done previously in literature.[35] Different methods were tried to create films, which included different withdrawal rates with dip-coating, drop-casting, and blowing dry nitrogen onto the film after dipping. As before, blowing nitrogen lead to very inhomogeneous results and various patterns found within the same sample (Figure 22A). With drop-casting, it seemed like the aqueous phase had recombined before the polymer solidified (Figure 22B), since only few pores were observed. From the two dip-coating speeds tested (Figure 22C), the lower one of 16.8 mm/min yielded more promising results. The films obtained were the first ones to exhibit somewhat ordered and regular pores, so dip-coating in combination with emulsions seemed like the most promising direction to proceed in.

Next, the water content of the emulsion was optimized. For this, 5, 10, 30 and 50 µL aqueous phase per mL organic solvent were tested at the lower withdrawal speed of 16.8 mm/min (Figure 23). The water content of 5 µL/mL was found to be too low to generate enough pores. At water contents of 30 µL/mL and greater, large areas of the substrate were not covered, indicating heavy water droplet aggregation and the droplets rising to the surface of the solution. A greater polymer concentration in the case of 30 µL/mL stabilized the system in a way that areas with ordered pores were found between the larger areas without film. The best water content of the emulsions to create the desired patterns was found to be 10 µL/mL. In comparison to another emulsion of water in chloroform, where 100 µL were dissolved per mL,[130] this seems rather low. This difference likely stems from the fact that the cellulose triacetate used in the other work can stabilize the water droplets much better than linear PS.

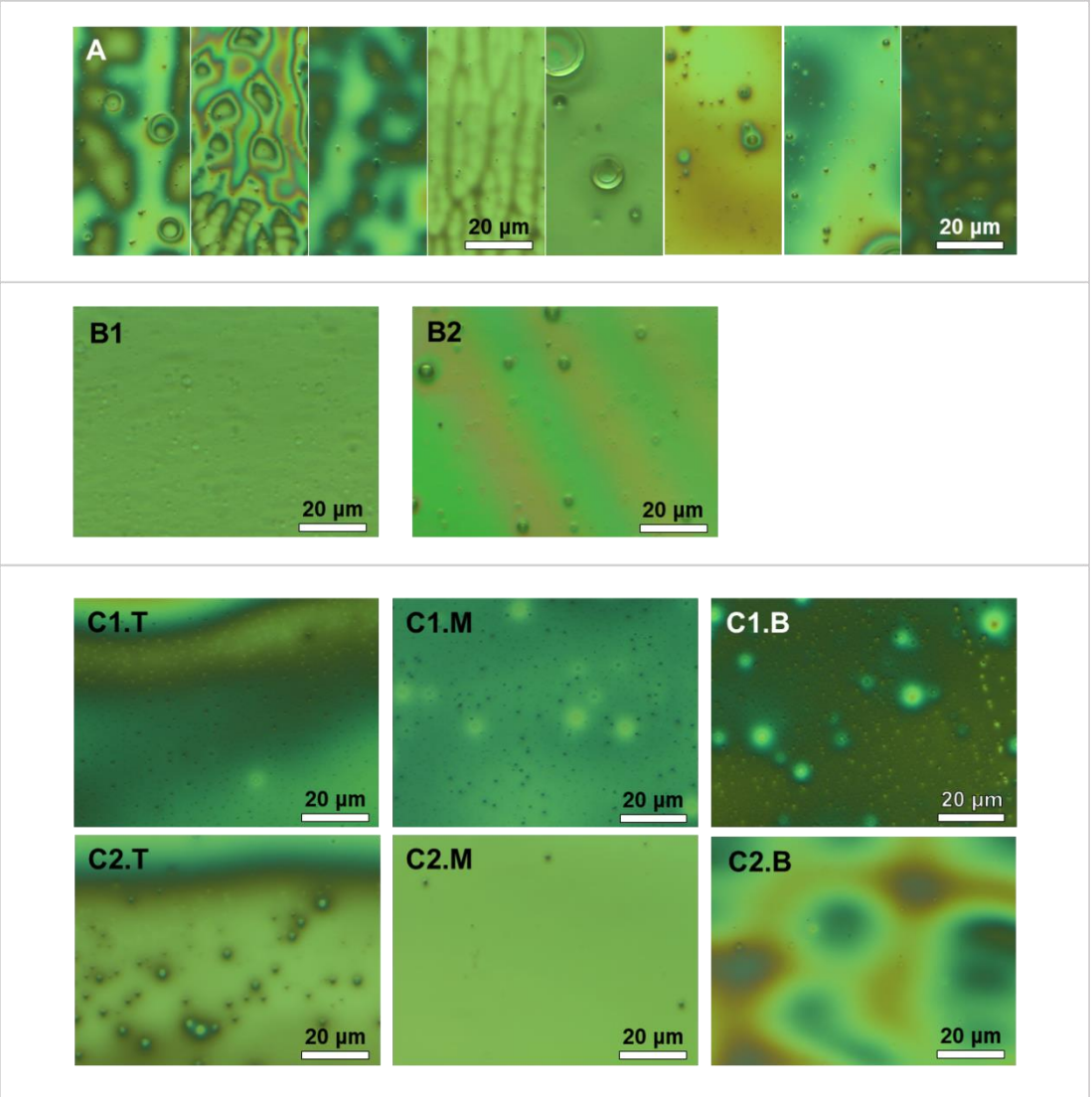

Figure 22. Optical microscopy images of films created *via* dip-coating from 12.8 mg/mL PS in chloroform onto SiO_x. 10 µL of 30 mg/mL sucrose in water were added per mL of chloroform solution. A) The substrate was dipped into the solution and placed vertically under a nitrogen airflow. B) A drop of the solution was cast onto the substrate and left to dry. Images of the outer (1) and inner (2) area of the dried film were taken. C) The film was created *via* dip-coating at 16.8 (1) or 67.2 mm/min (2). Representative sections of top (T), middle (M), and bottom (B) were chosen.

Another observation was that the top and bottom region of the film generally appeared to be more promising for the desired pattern formation than the middle of the film. This is likely to be due to the film being thicker at beginning and end, as is evident from the visible interference colour. The longer evaporation time of the thicker film parts might allow for longer ordering time of the water droplets. Moreover, it is possible that the thicker film is needed for the water droplets to fit

inside properly, thus making it interesting to explore higher and very slow dip-coating rates, as well as greater polymer concentrations.

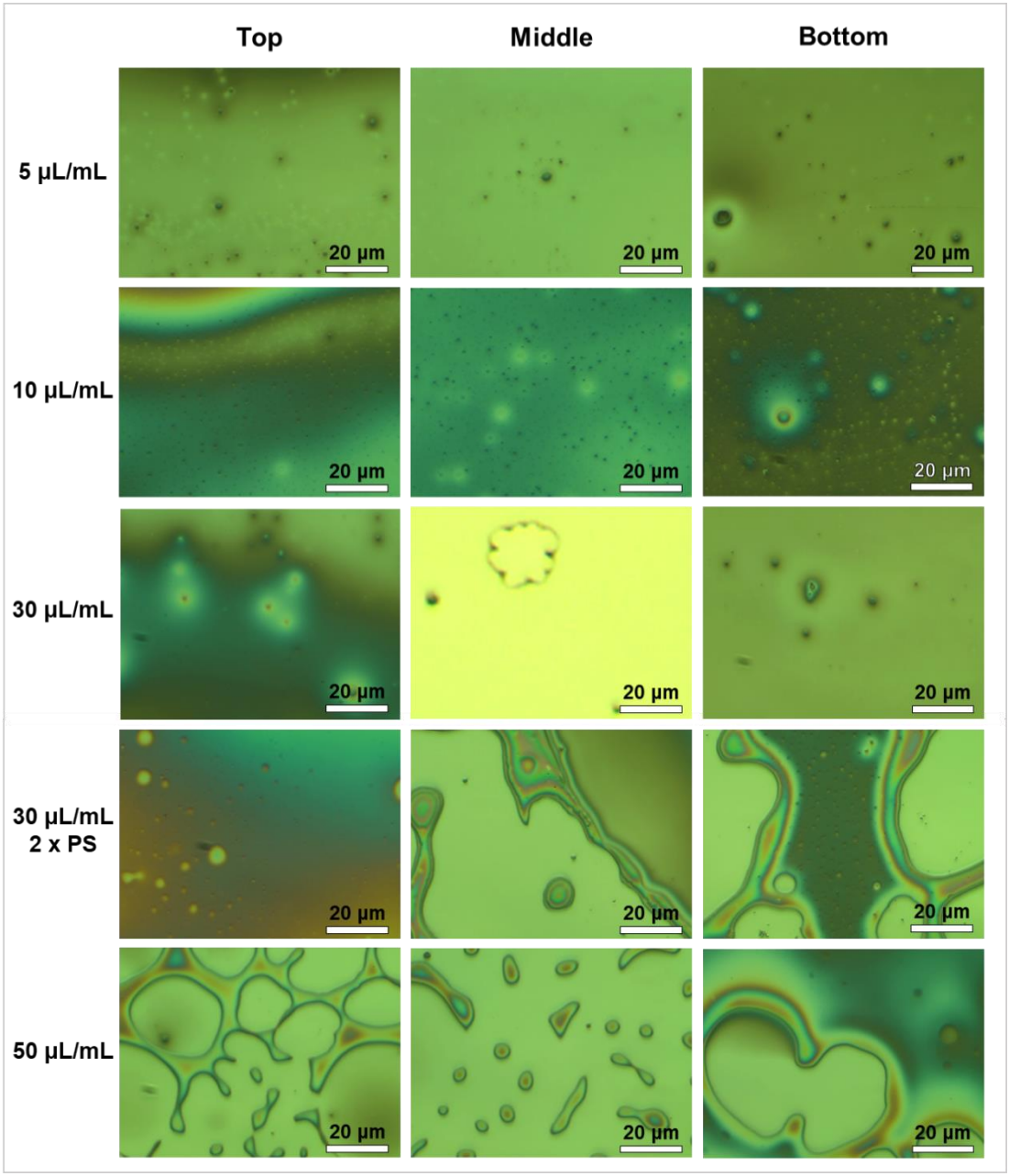

Figure 23. Optical microscopy images of films created via dip-coating with a withdrawal speed of 16.8 mm/min from an emulsion of different amounts of aqueous phase per mL of chloroform onto SiO_x. The chloroform solution contained 12.8 mg PS/mL and the aqueous phase 30 mg sugar/mL.

4.2.3 Introducing Nanoparticles to the Emulsions and Adapting Method

Next, nanoparticles to assemble at the pores were added to the solution. Before optimizing the NP and aqueous phase content with this new addition, it was attempted to verify the necessity of sugar in presence of the NPs, as both should stabilize the emulsion. The same NP content as for previous experiments without the emulsion was chosen for initial experiments. It was also attempted to determine how time-sensitive the experimental procedure is and how temporally stable the emulsions are. For this, two different solutions were prepared: one solution with an aqueous phase with and one without sugar, but both containing an equal weight of nanoparticles. Then, films from the very same solutions were dip-coated at 16.8 mm/min withdrawal speed soon after sonication (around 4 min) and shaking for 10 s, then again after waiting for 10 min, and one final time after shaking them for 30 s.

Both solutions, with and without sugar in the aqueous phase, lost most of the emulsion pattern in the final film after waiting for 10 min as compared to when the solution was used relatively fast after sonication. They both were able to recover some of the pattern after being shaken again for 30 s. The emulsion patterns here exhibit some bigger and some smaller holes in the film, with nanoparticle aggregates inside especially the greater holes. Some of the nanoparticles also still seem well dispersed throughout the polymer film. After waiting for 10 min and coating again, however, only few holes were observed. For the solution without sugar in the aqueous phase, the film created after waiting 10 min and shaking again exhibits greater pores than before, indicating an unstable emulsion and that coalescence continued to occur (Figure 24). Moreover, the pattern recovered less than for the equivalent films created with sugar in the aqueous phase (Figure 25).

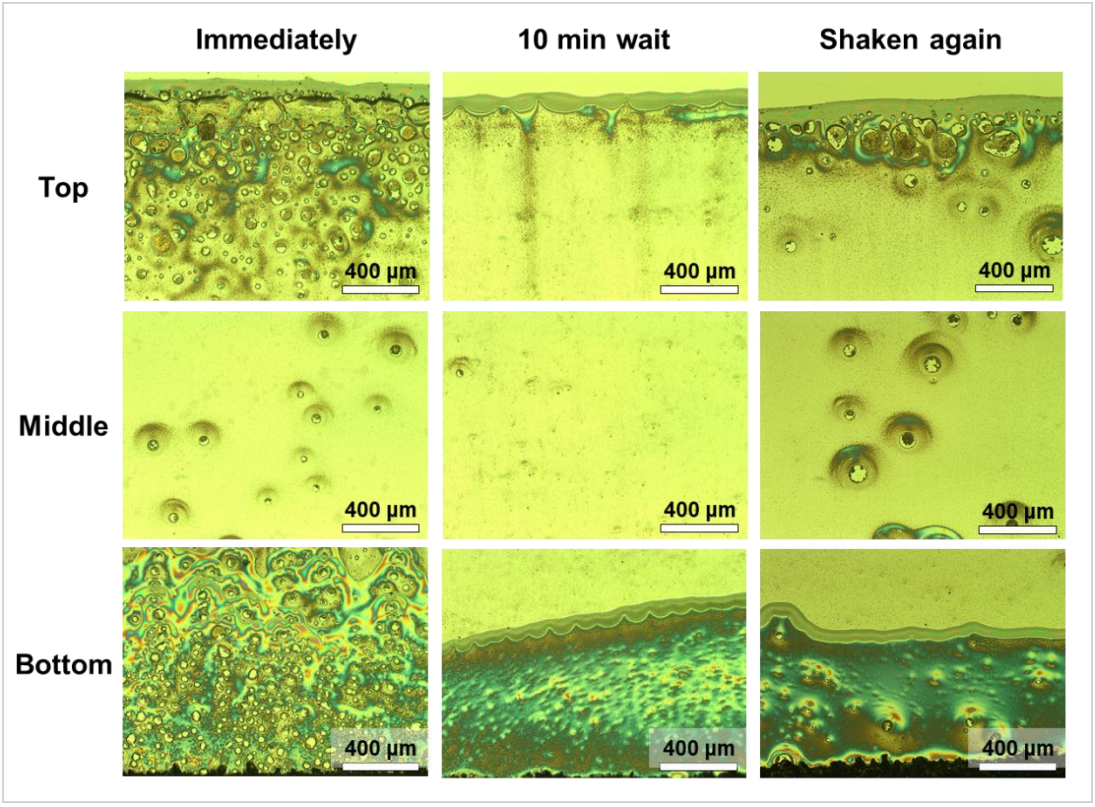

Figure 24. Optical microscopy images of a film created by dip-coating from a solution of 14 µL Milli-Q water (without sugar) per mL of chloroform solution onto SiO_x with a withdrawal rate of 16.8 mm/min. The chloroform solution contained 0.3 mg/mL TiO_2 and 13 mg/mL PS.

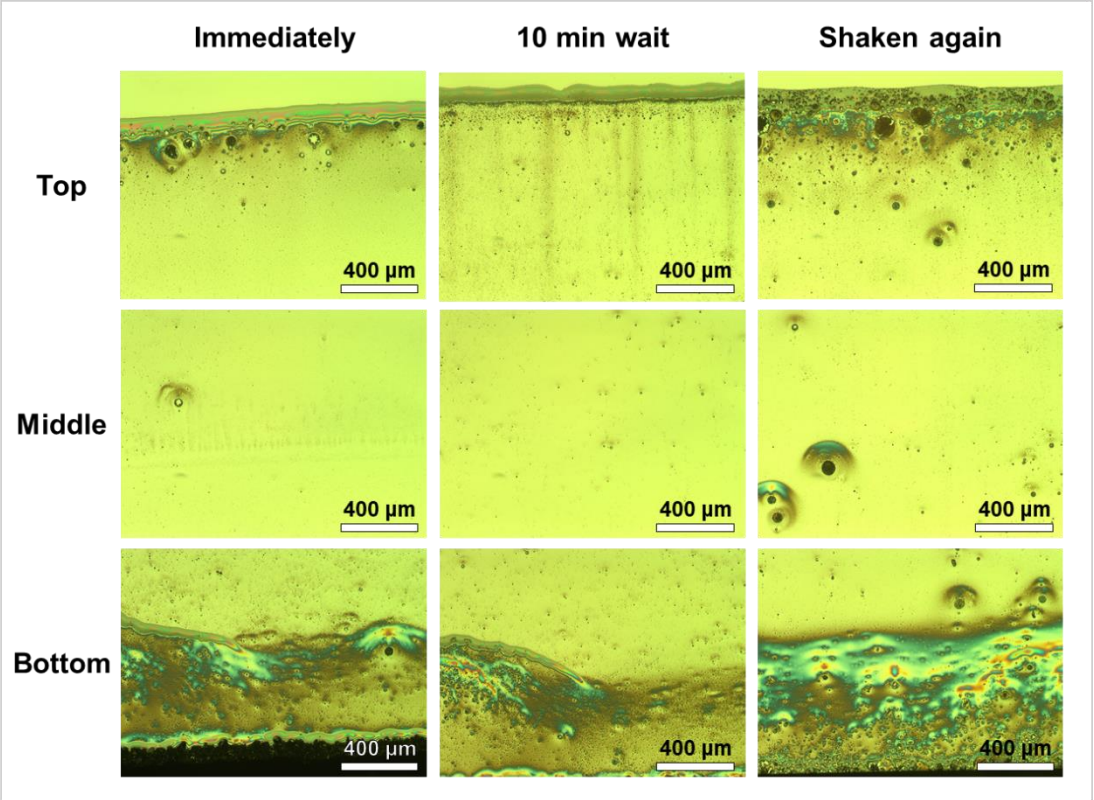

Figure 25. Optical microscopy images of a film created by dip-coating from a solution of 14 µL aqueous phase per mL of chloroform solution onto SiO_x with a withdrawal rate of 16.8 mm/min. The aqueous phase contained 30 mg sugar per mL of Milli-Q water and the chloroform solution contained 0.3 mg/mL TiO_2 and 13 mg/mL PS.

The ability of the emulsion containing sugar to recover better through shaking is even more obvious at a lower withdrawal speed of 8.4 mm/min (Figure 26). The difference with and without shaking is drastic, and the 10 min wait time seemingly influenced the film very little when shaken before the experiment. This indicates that sugar should be used to stabilize the emulsion even with nanoparticles present, and that while the experiments are very time sensitive, shaking directly before the dip-coating should be sufficient to obtain a good mixing for shorter wait times. Therefore, the solutions were shaken by hand for 30 s before beginning an experimental series from here on, and for 10 s between consecutive experiments with the same solution.

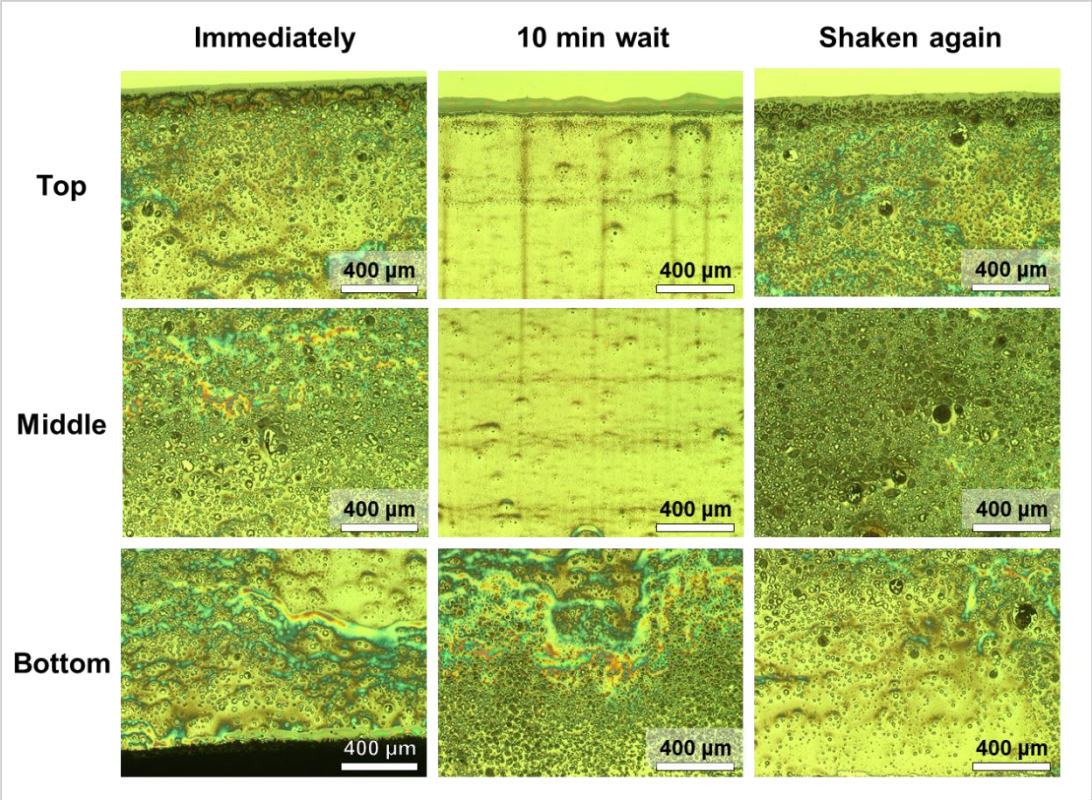

Figure 26. Optical microscopy images of a film created by dip-coating onto SiO_x from a solution of 14 µL aqueous phase per mL of chloroform solution with a withdrawal rate of 8.4 mm/min. The aqueous phase contained 30 mg sugar per mL of Milli-Q water and the chloroform solution contained 0.3 mg/mL TiO_2 and 13 mg/mL PS.

4.2.4 Optimizing the Aqueous Phase Content

Next, the content of the aqueous phase of the emulsion with the same polymer and nanoparticle content was optimized (Figure 27). 16 µL/mL was found to be the best composition, as with a lower aqueous phase content the small pores were further apart and at higher contents the pore size was less homogeneous. This is also closer to the approximately 18.5 µL per mL of benzene of the paper the sucrose method was taken from.[35] Less small pores were found for films created with greater withdrawal speeds, so 8.4 mm/min seemed most promising. These smaller somewhat ordered pores were usually found close to greater pores.

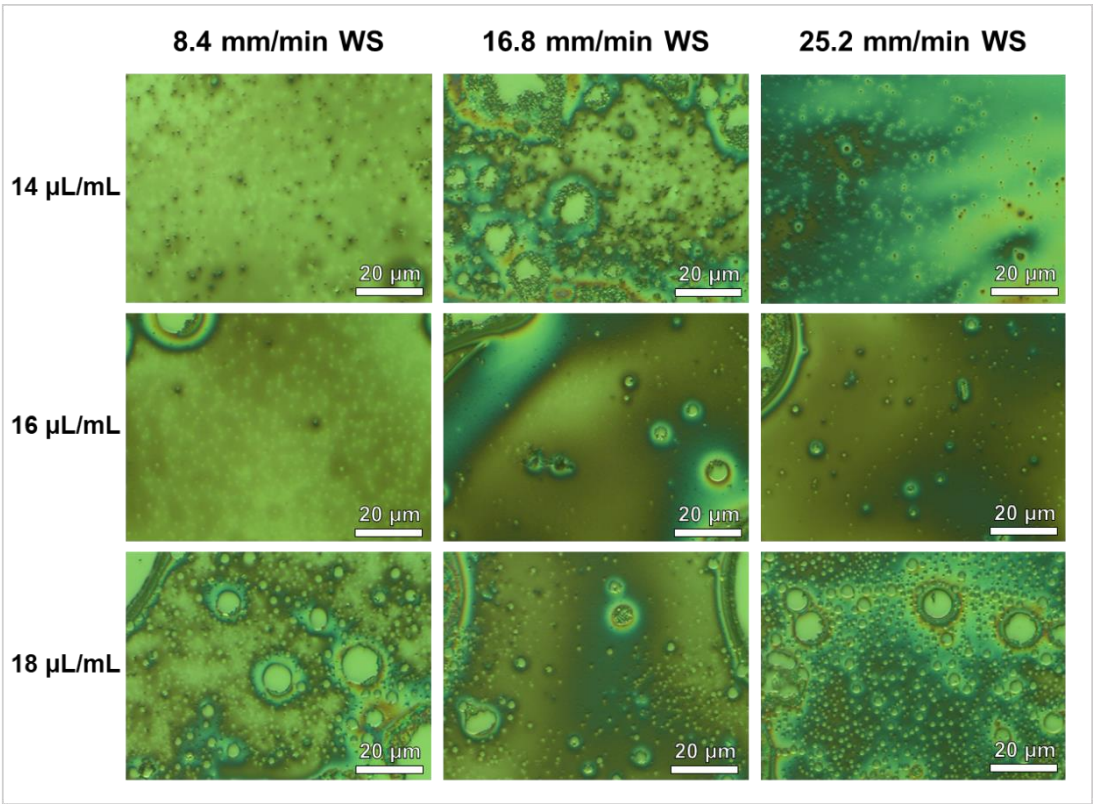

Figure 27. Optical microscopy images of films created *via* dip-coating onto SiO_x with different withdrawal speeds and aqueous phase contents added to the chloroform solution. The images are representative areas at the bottom of the film. The chloroform solution contained 12.8 mg PS/mL and 0.3 mg/mL TiO_2, and the aqueous phase 30 mg sugar/mL.

Overall, the sample containing 16 µL aqueous phase / mL of the chloroform solution exhibited many large iridescent areas stemming from NP agglomerations (Figure 28). Between those NP areas, smaller breath figure like pores could be found, with diameters around 0.2-0.5 µm. The large areas coated with NPs clearly indicated that the current concentration was too high to create a film with the desired features. Therefore, the NP content was optimized next.

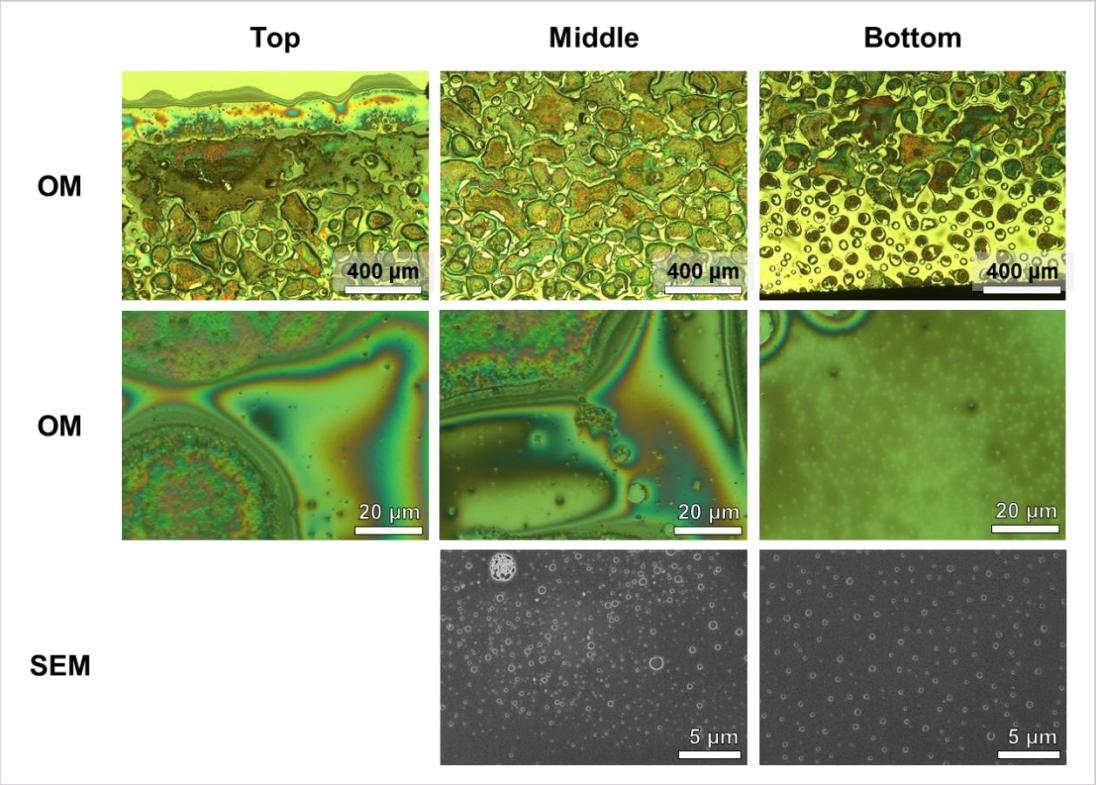

Figure 28. Optical microscopy (OM) and scanning electron microscopy (SEM) images of a film created *via* dip-coating onto SiO_x with 8.4 mm/min withdrawal speed and 16 µL aqueous phase per mL chloroform solution. The chloroform solution contained 12.8 mg PS/mL and 0.3 mg/mL TiO_2, and the aqueous phase 30 mg sugar/mL.

4.2.5 Optimizing NP Content

The corona crisis induced experimental break allowed for a further refinement of the methodology using literature. Therefore, the experimental procedure in the following varied slightly from the one before. From now on, the solutions were shaken for 30 s before use after the 40 min sonication and for 15 s between consecutive experiments. Moreover, the dwell time was increased to 30 s. The general withdrawal speeds used were 8.4, 16.8, and 67.2 mm/min, as they were found to correspond to different dip-coating regimes for similar polymer solutions used within the research group. 8.4 mm/min is therefore likely to correspond to the capillary regime, while 16.8 would likely deposit the thinnest film in the intermediate regime, and 67.2 mm/min should be close to or in the draining regime.

Since the NP content of 0.3 mg/mL still seemed too high, 0.15, 0.1, and 0.05 mg/mL were tested. Such small amounts could not be weighed individually, which is why 2.5 mg NPs were dispersed in 5 mL of chloroform. Then, an amount of the solution corresponding to the desired NP amount was added to the polymer solution to reach the total 5 mL.

For all the experiments (Figure 29), greater pores were found at the top of the film. This is likely to stem from some of the aqueous phase recombining, rising to the surface of the solution due to the lower density, and being pulled out with the substrate. Moreover, it appeared like the bigger pores on the substrates were larger for lower withdrawal speeds and lower NP contents. This makes sense, because during the lower withdrawal speed the aqueous phase has more time to recombine, and a higher NP content is associated with greater stability of the emulsion. However, it must be noted that the greater NP content solutions and of those the higher withdrawal speed experiments were conducted first. Therefore, it might also be that this potential instability phenomenon is related to the time since sonication. Due to this, the experiments were repeated with fresh solutions and in the reverse order. Unfortunately, some experimental difficulties were encountered, which will be further elaborated in 4.2.7, and time did not permit another repetition.

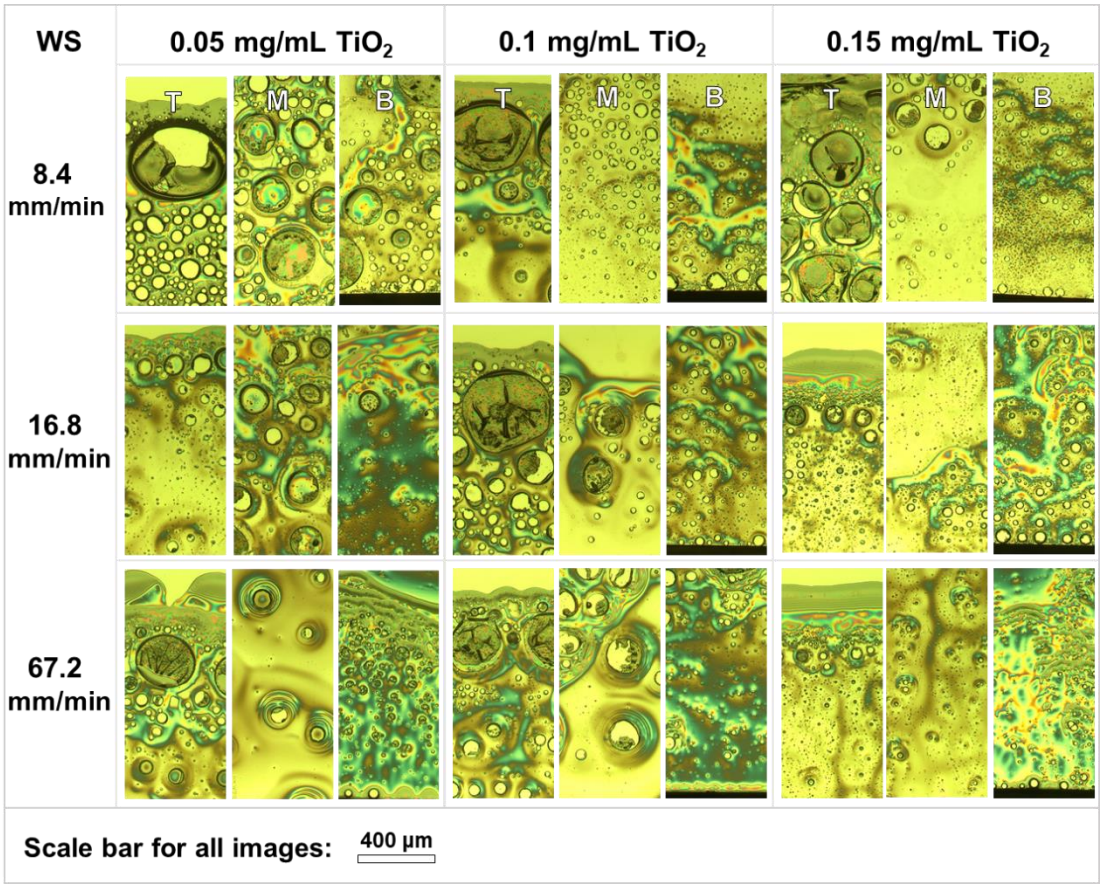

Figure 29. Optical microscopy images of films created from emulsions with different NP contents *via* dip-coating onto SiO_x with different withdrawal speeds (WS). Representative sections of the top (T), middle (M), and bottom (B) of the film were chosen. The chloroform solution contained 12.8 mg PS/mL and different weights of NPs were added to the total 5 mL of the chloroform solution. The aqueous phase contained 30 mg sugar/mL and 16 µL of the aqueous phase were added per mL of chloroform solution.

As for most other samples, the smaller breath figure like pores were mainly located at the bottom of the polymer film. With many substrates, they also reached higher throughout the film, but the best regularity was usually at the bottom. Therefore, the bottom regions with the best order of breath figures created from solutions with different NP contents was compared (Figure 30).

For films created from solutions with 0.15 mg/mL TiO_2, the smaller pores were of rather irregular sizes. Moreover, there were only few of them and those were spread instead of ordered. In addition, the nanoparticles were observed to accumulate at the inside of the pore walls.

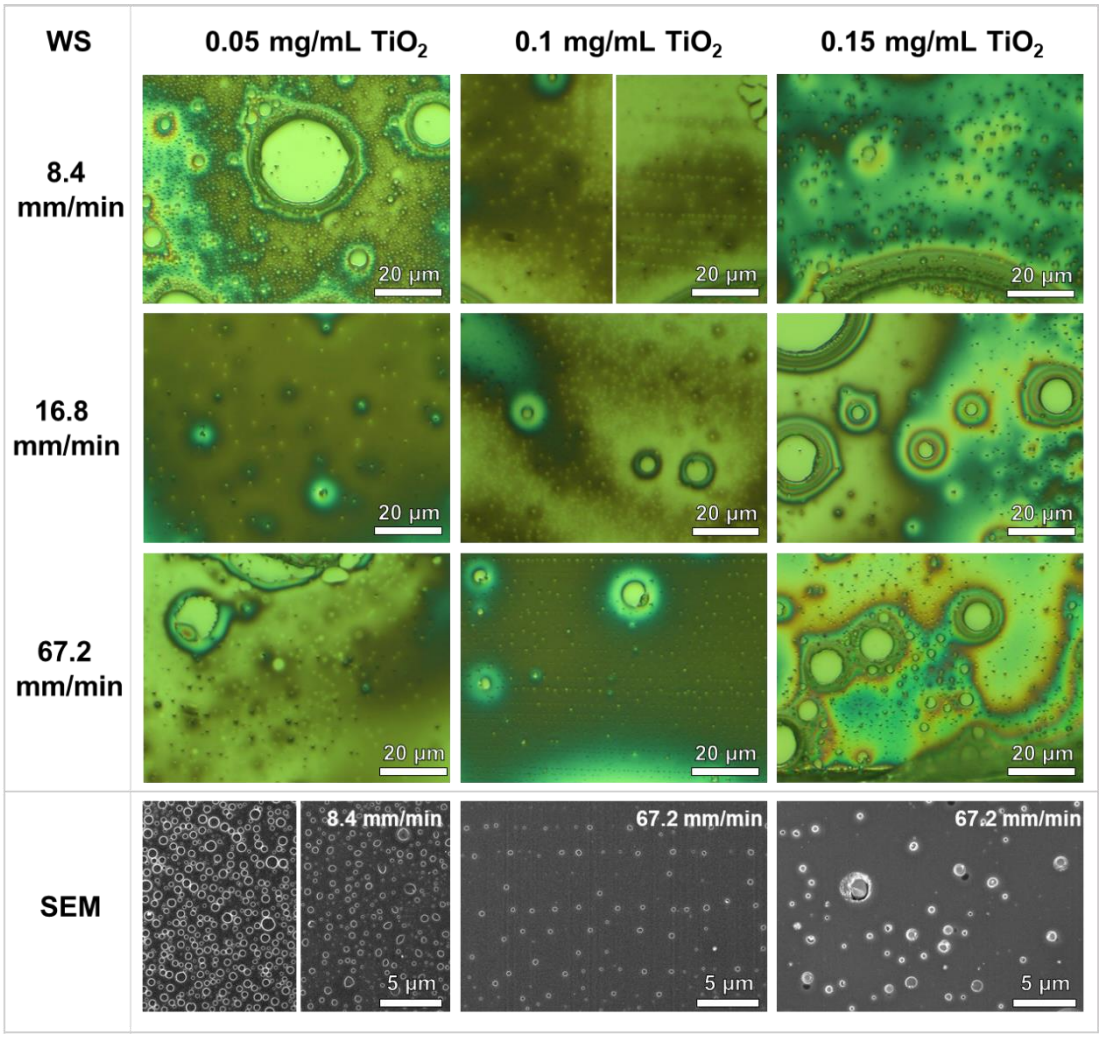

Figure 30. Optical microscopy and scanning electron microscopy (SEM) images of films created from emulsions with different NP contents *via* dip-coating onto SiO_x with different withdrawal speeds (WS). Representative sections of the small breath figure like patterns at the bottom of the films. The chloroform solution contained 12.8 mg PS/mL and different weights of NPs were added to the total 5 mL of the chloroform solution. The aqueous phase contained 30 mg sugar/mL and 16 µL of the aqueous phase were added per mL of chloroform solution.

For films created from 0.1 mg/mL TiO_2 solutions, areas of pores ordered in lines were observed at the bottom of the film for the withdrawal speeds of 8.4 and 67.2 mm/min. These pores are of diameters of about 0.25 µm at a withdrawal speed of 67.2 mm/min. The small pores of films created from 0.05 mg/mL TiO_2 solutions were of less regular diameters. They mainly ranged from 0.25 to 1.3 µm in diameter, most were of sizes around 0.6 µm. There were many more of these pores and they were much denser than for the higher NP concentrations. The areas these pores were

found in also extended to the middle of the films. The greater number of pores together with their irregularity in size might stem from the emulsion being less stable with a lower NP content, since the solution interfaces are less covered and stabilized. This also leads to several greater pores of diameters of 20 μm and more, which likely grow at the expense of the smaller ones *via* an Ostwald ripening mechanism. This poses the question whether it might be beneficial to have a somewhat less stable emulsion to achieve pores of the desired size and spread.

For all films, NPs were found at the walls of the bigger pores (diameter > 10 μm). However, it is unclear whether they also are embedded in the walls of the smaller pores and simply less visible because they do not form aggregates. Overall, it appeared more like the TiO_2 NPs preferred to be in the aqueous phase and assembled at the walls of the pores *via* the coffee ring effect. This indicates that the surface chemistry of the NPs is not optimal for assembling at the interface of the two solvents at this diameter, and the use of bigger particles might be beneficial.

Overall, it was decided to proceed with a nanoparticle content of 0.05 mg/mL in the solution to induce greater areas of small pores, even if that might lead to a greater irregularity in pore size. It should also be noted that the use of the final BCP is expected to increase the stability of the emulsion greatly.

4.2.6 Optimizing Sugar Content

Next, the sugar content in the aqueous phase was optimized. By now, the concentration of 30 mg/mL water was taken straight from literature,[35] where it was noted that a concentration as little as this already stabilized the system greatly. Therefore, it was investigated whether a higher concentration would stabilize the emulsion further.

The tested concentrations were 60, 300, and 600 mg/mL (Figure 31). The reason such ‘‘high’’ concentrations were tested was the very great solubility of sucrose in water

(2 g sucrose in 1 g of water at 20 °C), stemming from its numerous functional groups that can form hydrogen bonds with water molecules.[136] It was found that using a twice as high concentration of sugar did not improve the desired features of the film. Pores of the desired size range were barely observed. It is of course possible that the sugar made the solution stable to an extent that water droplets smaller than what could be observed by optical microscopy were created. This would also be difficult to observe *via* SEM due to charging issues at high magnifications and a double coating that might mask such intricate features. Moreover, such small pores would not be functional to combine with the scale of the BCP features.

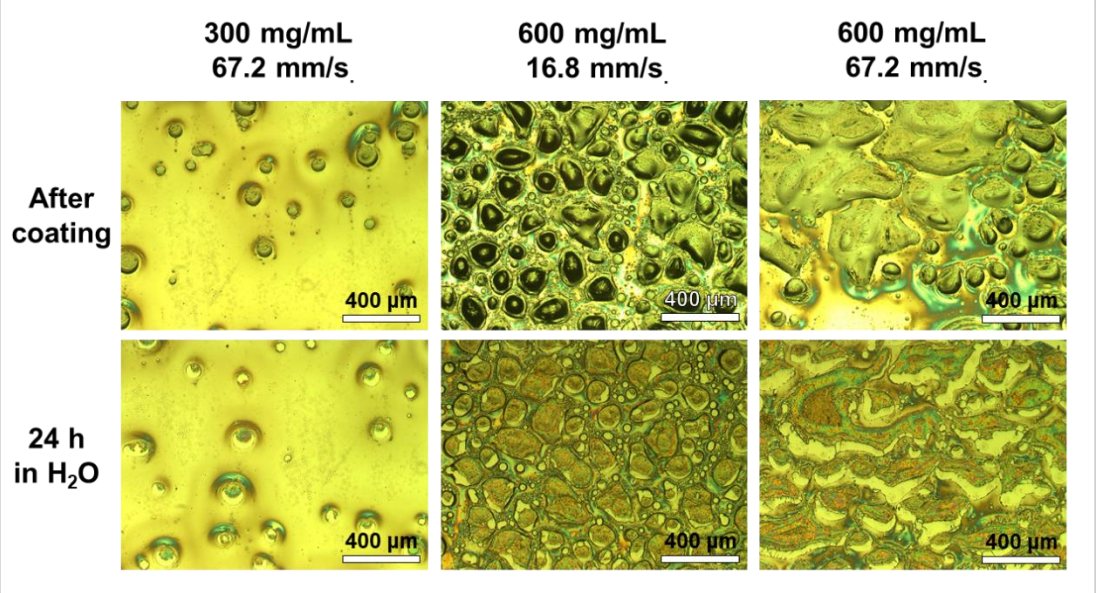

Figure 31. Optical microscopy images of films created from emulsions with different sucrose contents *via* dip-coating onto SiO_x with different withdrawal speeds. Representative sections of the middle of the created films before and after an additional 24 h wash by immersing the substrate in Milli-Q water. The chloroform solution of the emulsion contained 12.8 mg PS/mL and 0.15 mg TiO_2/mL. The aqueous phase contained different amounts of sugar (300 and 600 mg/mL) per mL and 16 µL of the aqueous phase were added per mL of chloroform solution.

At even higher sugar concentrations, the pores were visibly covered with another layer. After immersing the substrates in Milli-Q water for 24 h, this layer disappeared, revealing the iridescent nanoparticle aggregations that were hidden underneath. This strongly suggests that the observed layer was sucrose. At a sucrose concentration of 300 mg/mL in the aqueous phase, many non-spherical big sucrose covered shapes

were observed at the lower withdrawal speeds. It appeared like the sucrose stabilized the droplets in the emulsion to an extent that the minimum surface energy shape of a sphere did not need to be adhered to anymore. While still round, the shapes appear somewhat random. This shows that finding the right emulsion stability to create breath figures is a delicate matter, as the droplets should not be so stable that they begin to deform, but stable enough they do not coalesce, while potentially unstable enough that the right conditions for Ostwald ripening are met in a way that large areas of small pores are created.

At a concentration of 600 mg sucrose per mL Milli-Q water, the sucrose covered large areas of the substrate. It appeared like there was more of the aqueous phase present than for samples with lower sucrose concentrations. It could be that since sucrose is only soluble in water, this higher concentration made the water droplets less miscible, causing them to rise to the surface, instead of more stable when dispersed in the chloroform. This could lead to an appearance of a higher aqueous phase content.

Interestingly, the washing step revealed that most of the TiO_2 particles had aggregated at the top of the pores instead of evenly around the edges. This might be related to a difference in mass of the NPs and the sucrose hydrogen bond network formed in water, leading to a different gravitational force exerted on them within the droplets when dragged vertically. While NP aggregates in pores have not always been evenly spread around the edges for other samples, such a clear trend in position was not observed before. Therefore, this is likely related to the increased viscosity of the water droplets and higher sugar content specifically.

In order to test for the sugar content in a narrower range, aqueous phases of 20, 30, and 40 mg/mL sucrose were tested next. It appeared like there was no clear superiority of either of the concentrations in terms of outcome of the experiments. Therefore, experiments were continued with the initial 30 mg/mL.

Throughout many of the films created, there were iridescent areas at the top or in the pores. By optical microscopy, those areas seemed somewhat patterned, but it was hard to characterize them thoroughly with OM only. Those regions turned out to merely be hilly using SEM (Figure 32A), likely stemming from NPs buried within the film, which can be observed through cracks (Figure 32C) or when those areas got flipped over (Figure 32B). It was interesting to see that the NPs seemed to fully shield the polymer from the substrate at those areas. This might be related to the relative affinities to the substrate, but also to the process in which the polymer precipitated at the NP areas. It is generally assumed, that the pores stem from the aqueous phase, in which the polymer is not soluble in. As the film on top of the NPs was still present after the Milli-Q water washing step, this indicates it is not sucrose. It is currently still unknown how the polymer coats these NP areas. Overall, it was concluded with great confidence that the iridescent colour did not stem from a small breath figure pattern, but from the incorporation of the NPs. The colour likely emerges from the creation of a photonic polycrystal, which is commonly observed in beetles.[156] This would mean that the nanoparticles are arranged in an ordered lattice, but possess long-range disorder induced by different grain orientation and sizes. This disorder leads to structural iridescence, because the domains will interact with light differently.[156]

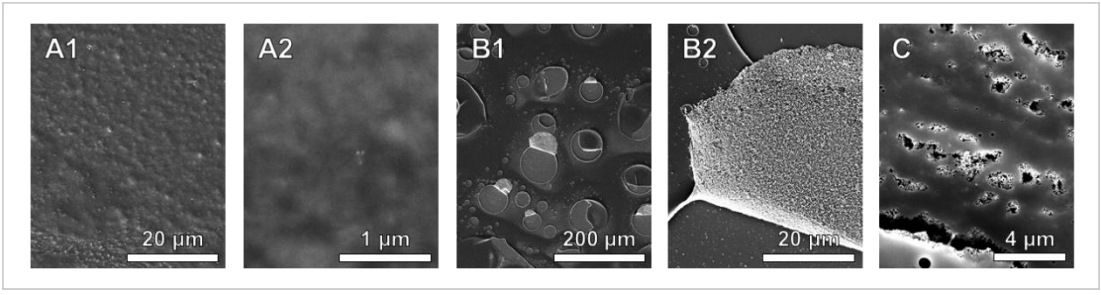

Figure 32. Scanning electron microscopy images of iridescent regions of films created from different emulsions *via* dip-coating onto SiO_x at 16.8 mm/min withdrawal speed. The chloroform solution of the emulsion contained PS and TiO_2 to which an aqueous phase containing sugar was added. A) 25.6 mg PS/mL and 0.05 mg TiO_2/mL chloroform, 30 mg sucrose/mL Milli-Q water, 16 µL aqueous phase per mL chloroform; B) 12.8 mg PS/mL and 0.3 mg TiO_2/mL chloroform, 30 mg sucrose/mL Milli-Q water, 22 µL aqueous phase per mL chloroform; C) 12.8 mg PS/mL and 0.15 mg TiO_2/mL chloroform, 600 mg

sucrose/mL Milli-Q water, 16 µL aqueous phase per mL chloroform, immersed in Milli-Q water for 24 h before imaging.

4.2.7 Wetting Difficulties and Optimizing Solvent and Substrate

The next goal for optimizing the experimental conditions was to test the film creation on freshly piranha cleaned silicon wafers, which should make the substrate more hydrophilic due to the removal of all organic residue and the linking of hydroxyl groups to the native oxide.[153,154] Moreover, benzene and THF were also tested as solvents. The polymer is soluble in both solvents, and while THF has been used a lot to create emulsions in literature,[38,131–134] benzene was used in the paper the sucrose idea was taken from.[35] Solutions with 12.5 mg PS and 0.05 mg TiO_2 per mL of the respective solvent were prepared and 80 µL of the 30 mg/mL aqueous sugar solution added. Freshly cleaned Si wafers and older SiO_x substrates were coated with withdrawal rates of 8.4, 16.8, and 67.2 mm/min.

When the aqueous phase was added while creating the different emulsions, the droplets stayed at the surface with chloroform, sank to the bottom with toluene, and "disappeared" with THF. This is consistent with the relative densities and water being miscible with THF. After sonication, the emulsion with THF was of a translucent white, while the emulsions with chloroform and toluene appeared milky. After three days, the appearance of the emulsions still looked the same by eye and the water did not seem to have separated again, indicating a good stability of the emulsions.

It was found that for all experiments using SiO_x, the final film was very patchy, indicating a bad wetting of the solution just like for the second series of experiments mentioned in 4.2.5. At 67.2 mm/min, however, a thin film covered almost the entire substrate. Only the films created from chloroform exhibited areas of small pores of the desired sizes at all withdrawal speeds, even though they could only be found in small areas that were seemingly unaffected by the poor wetting phenomenon.

The film on freshly cleaned substrates was significantly worse, especially for chloroform. Whereas the film had been very patchy before, now only droplet like areas of polymer solution were sprinkled over the substrate, indicating a very bad wetting of the solution (Figure 33). For toluene, the withdrawal speed of 67.2 mm/min still yielded a thin film, whereas at 16.8 mm/min there was only a web of polymer, and at 8.4 mm/min the polymer also appeared like dried droplets. The THF films seemed the least different from the ones formed on SiO_x. These observations confirm the greater hydrophilicity of the silicon wafers directly after the piranha wash, when a hydroxide layer coats the native oxide.[153,154] This led to an expected decreased wetting of the organic solvents. As THF is the most polar solvent of the three, it makes sense that its films were less affected by this. For a better wetting of the solution, it might be interesting to use substrates right after HF cleaning, which should remove the native oxide layer and make the samples hydrophobic. This should lead to a better spread of the organic solvent, however, as we are dealing with an emulsion with water, it is unclear if it would lead to a more favourable outcome overall. It was concluded that the freshly piranha cleaned substrates were less suitable to dip-coat films from any of the emulsions created.

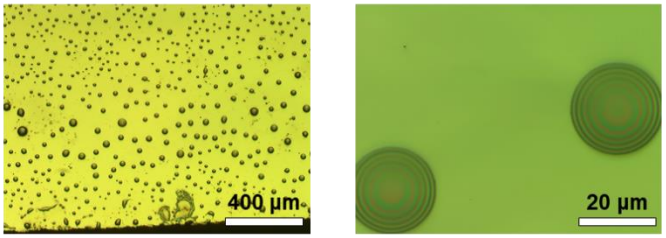

Figure 33. Optical microscopy images of the bottom of a film created from an emulsion *via* dip-coating onto a freshly piranha cleaned Si wafer with 8.4 mm/min withdrawal speed. The chloroform solution of the emulsion contained 12.5 mg PS/mL and 0.05 mg TiO_2/mL. The aqueous phase contained 30 mg sucrose/mL and 16 µL of the aqueous phase were added per mL of chloroform solution.

Since the wetting issue on SiO_x was found for all the different solutions, it was presumed that the solvent itself should have no part in this. It appeared more likely that something was wrong with the substrate, which could be related to the wafer

itself, the acid cleaning, or the Milli-Q water washing step. It should be noted that several different wafers had to be cut for the experiments and even a new batch of wafers used around when these issues first appeared. Therefore, one cannot rule out that the new wafers were slightly but significantly different from the ones before for the purpose of these experiments.

This different film behaviour could also be induced by a greater water content. The amount of aqueous phase added was the same of course, however, changes in the relative humidity of the laboratory and the weather in general could also induce such effects. Due to the enforced break of practical work, the outside weather had changed significantly by the time experiments were continued. Due to this, the relative humidity of the room was reported for each experimental series from now on. Before the experimental break, values should have been around 26% rH, whereas afterwards values from 21.3 to 43.6% rH were measured within two weeks. This shows that the laboratory environment is not very stable with respect to relative humidity, which might affect the experiments. The relative humidity of 21.3%, however, was measured during the experiments with different solvents and freshly cleaned substrates, which indicates that the bad wetting should not have been caused by a higher relative humidity than usual.

Another possibility was that not the humidity during the experiment, but the humidity in the laboratory where the substrates are stored after the cleaning was the real culprit. This was not tracked, however, the relative humidity in Finland in general is lowest in May and June,[157] which was when the troublesome experiments were conducted. This change in relative humidity would affect the surface chemistry of the silicon substrates and therefore their wetting characteristics. It is unclear how great that effect can be, but this should be kept in mind.

An interesting finding was that the lower withdrawal speeds were very much affected by the new observation, while at withdrawal speeds of 67.2 mm/min, the film

covered the substrate almost like before for all experiments (Figure 34). This seems surprising at first, since in theory good wetting is very important for withdrawal in the draining regime.[76,80] However, at lower withdrawal speeds, the solution also has more time to attain its optimum conformation, while at higher withdrawal speeds the solution will be dragged along more as it is. Additionally, in the draining regime some of the solution, as the name already suggests, drains. This means that an excess of aqueous phase might just flow back into the solution. At withdrawal speeds in the capillarity regime, however, the chloroform will evaporate much faster, making the ratio of the water phase in it greater with every second. With a low viscosity of the polymer solution, this might lead to the water solution displacing the polymer solution instead of letting it form an evenly spread film.

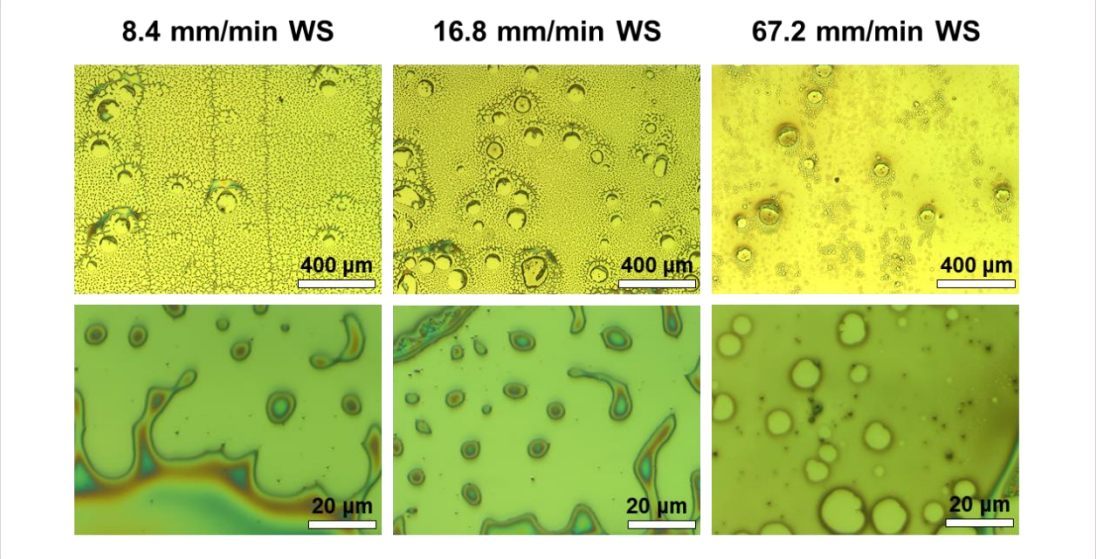

Figure 34. Optical microscopy images of representative sections of the middle of films created from emulsions *via* dip-coating onto SiO_x with different withdrawal speeds (WS). The chloroform solution of the emulsion contained 12.5 mg PS/mL and 0.1 mg TiO_2/mL. The aqueous phase contained 30 mg sucrose per mL and 16 µL of the aqueous phase were added per mL of chloroform solution.

Several experiments were conducted to investigate where this new wetting behaviour stemmed from. For this, the experiments were designed in a way that only one component was changed if possible. Experiments with the new wafers were conducted with just the polymer in the solution, with the aqueous emulsion but no NPs, and with NPs and the emulsion but only 4 µL aqueous phase per mL chloroform.

For all these experiments, the SiO_x substrate was piranha washed as for all previous experiments. Then, two more experiments were conducted using the usual 16 µL/mL aqueous phase and NP and polymer concentration in chloroform. However, for one experiment the wafer was from the new batch, and for one some left over wafer from the previous batch was used. In addition, the cleaning protocol was different to also exclude that as potential source. Now, the substrates were sonicated in acetone for 10 min, then sonicated in 2-propanol for 10 min, subsequently rinsed with Milli-Q water, and blown dry with N_2. All experiments were conducted at both lower withdrawal speeds, where the effect of the wetting issue was more prominent. The results were summarized in Table 2 and will be further discussed in the following.

Table 2. Summary of a series of experiments to determine which part of the experimental procedure induced the wetting difficulties. Films were created from the respective solutions at withdrawal speeds of 8.4 and 16.8 mm/min. The X means that small breath figure like pores were present. Poor wetting describes the very patchy film creation as seen before. The new and old substrates refer to the old and new batch of substrates with the same specifications.

62 mg PS in 5 mL $CHCl_3$					
NPs (mg/mL)	**Sugar water (µL)**	**Substrate**	**Washing**	**Breath Figures**	**Wetting**
0	0	New	Piranha		Good
0	80	New	Piranha	X	Poor
0.05	20	New	Piranha		Very poor
0.05	80	Old	Sonication	X	Fine
0.05	80	New	Sonication	X	Fine

The results of the experimental procedure to determine the sudden change in wetting behaviour of the solution show that the issue must be related to the aqueous phase added to the solution, as the film created from just the polymer solution looks as expected and covers the whole substrate well. However, reducing the water content of the emulsion did not appear to make a difference for the wetting. Interestingly, the films obtained from the sonication washing regime displayed a better wetting behaviour than the piranha washed substrates. This might indicate that the cleaning step does somehow not work anymore. As the Milli-Q water rinse is used in both cleaning regimes, this could be related to one of the components of

the piranha solution (hydrogen peroxide or sulfuric acid) being oxidized. However, the vigorous bubbling was still observed during the piranha cleaning, which would indicate otherwise. It could also be that a change in environmental atmosphere in the room where the substrates are stored before use lead to a higher water molecule and hydroxyl group content being left on the substrate surface in comparison to before, making the substrate more hydrophilic. The alternative washing should not oxidize the wafer, so the wafer should be more hydrophobic directly afterwards. It is not entirely clear how the piranha cleaning step suddenly leads to a different surface chemistry than before, however, for the purpose of this work, it was decided to change to the sonication cleaning regime to avoid this issue.

Another interesting finding with this experimental series was that the substrates from the old and the new batch did yield somewhat similar, but still significantly different results (Figure 35). Both films displayed very great pores, so a great amount of the wafer was not coated with a polymer film. However, the pores of the old wafer still were close to spherical, whereas the pores of the new wafer were much bigger on average and somewhat randomly shaped. Therefore, it seems like the new batch of wafers, despite having the same specification, is slightly different, therefore affecting the outcome of the results. It could be that the impurities of the material are different, influencing the interaction with water and/or the polymer solution. This difference might be enhanced by the piranha cleaning. This difference in wafer batches is something to be aware of when comparing the experiments, however, it is likely also something that cannot be controlled.

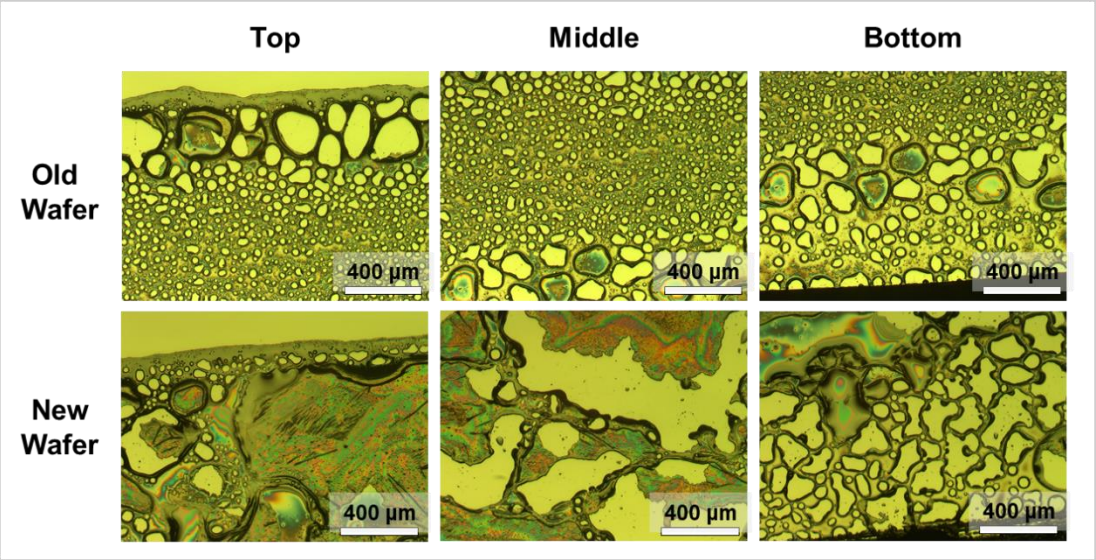

Figure 35. Optical microscopy images of films created from emulsions *via* dip-coating onto SiO_x. The chloroform solution of the emulsion contained 12.5 mg PS/mL and 0.1 mg TiO_2/mL. The aqueous phase contained 30 mg sucrose per mL and 16 µL of the aqueous phase were added per mL of chloroform solution. Images of experiments at 8.4 mm/min withdrawal speed were compared between different silicon wafer batches used as substrate.

After the decision to change to the other cleaning regime was made, the experiments with the different solvents were repeated on the sonication regime cleaned SiO_x substrates. Two THF solutions were prepared, one with and one without sucrose in the aqueous phase, since the sucrose might hinder the even distribution of the aqueous phase in miscible THF. Again, the films at the withdrawal speed of 67.2 mm/min were the most even.

At lower withdrawal speeds, the THF solution exhibited poor wetting of the substrate again. This was surprising, as a polymer emulsion in THF was successfully spin cast on SiO_x before, indicating good wetting.[38] However, it should be noted that in those experiments, the desired porous patterns were only obtained for PMMA and not PS,[38] which shows how challenging working with linear PS is for such purposes. Therefore, it was a pleasant surprise to find an area on the films formed from both THF solutions at the highest withdrawal displaying a somewhat ordered porous pattern. These areas were only small and found at the beginning of the bottom section of the respective films. Moreover, these pores do not penetrate the film fully

to the substrate. In comparison, the pattern of the film created from an emulsion without sucrose had a more regular pattern with more spherical pores. This shows that the sucrose in the other solution likely did not allow for the complete mixing of the aqueous phase in the organic solvent and hindered the water droplets from adapting a spherical shape. The great miscibility of water in THF likely also is the reason why the porous area was comparatively small. With a greater water content, this pattern might easily extend through the entire film. This also agrees with literature, where the water content range reported to work well was from around 30 to 50 µL water per mL THF.[38,132–134]

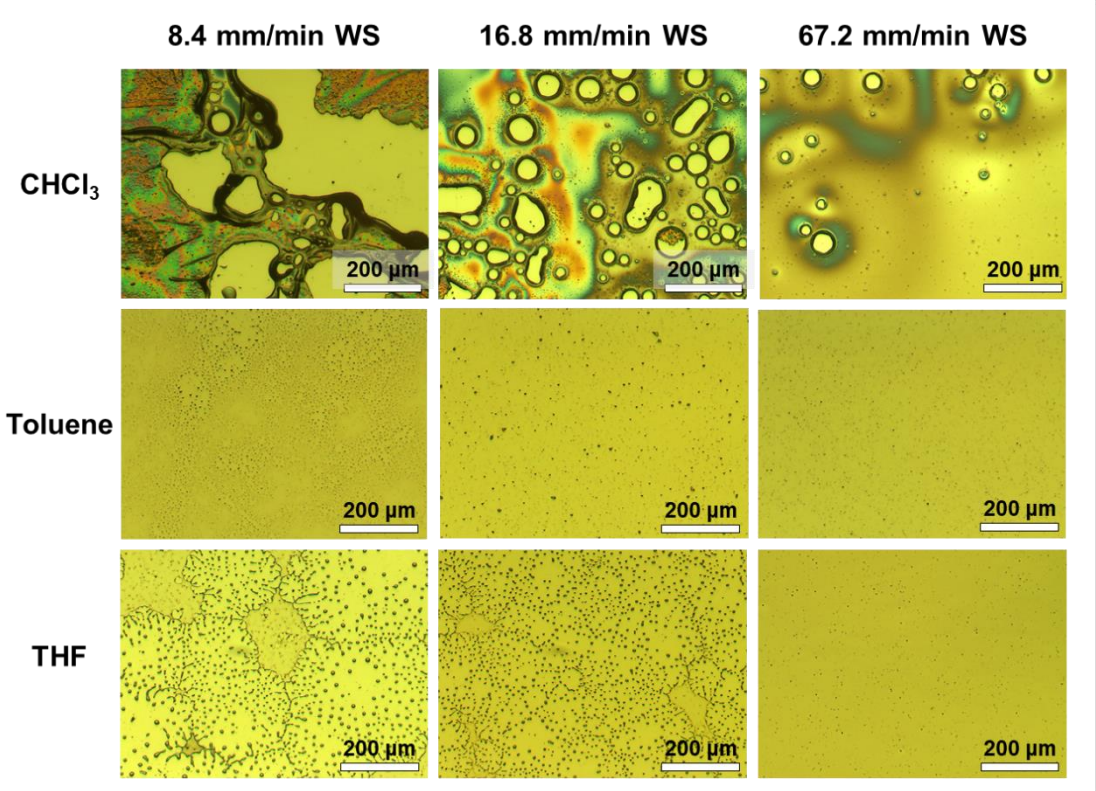

Figure 36. Optical microscopy images of representative middle sections of films created from emulsions *via* dip-coating onto SiO_x with different withdrawal speeds (WS). The solutions of the emulsion used different solvents ($CHCl_3$, toluene or THF) with 12.5 mg PS/mL and 0.1 mg TiO_2/mL. The aqueous phase contained 30 mg sucrose per mL and 16 µL of the aqueous phase were added per mL of the other solution.

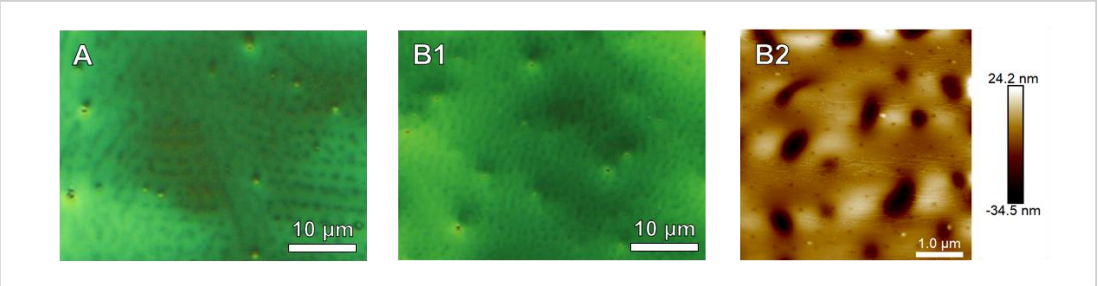

Figure 37. Microscopy images of representative bottom areas of films created from emulsions *via* dip-coating onto SiO_x with 67.2 mm/min withdrawal speed. The THF solution contained 12.5 mg PS/mL and 0.1 mg TiO_2/mL. 16 µL of the aqueous phase were added per mL of the other solution. A) Optical microscopy image of a film created from a solution with pure Milli-Q water as aqueous phase. B) Optical microscopy (1) and atomic force microscopy height (2) images of a film created from a solution with 30 mg sucrose/mL in the aqueous phase.

While the wetting of the toluene solution was fine, no proper pores were formed on the film. This might be because the density of water is greater, so while the emulsion seemed stable, there might not have been enough water droplets at the surface of the solution to be dragged along or they drained more than the rest of the solution. Another reason might be that films created from toluene are typically thinner than the ones from chloroform,[158] which might not allow for enough space for the water droplets to be incorporated. For the purpose of this work, the bad wetting of the THF solution and the absence of pores in films created from the benzene solution did not seem functional, therefore, it was decided to stick with chloroform as solvent.

4.2.8 Effect of Greater Polymer Concentration

In general, increasing the concentration of the polymer should promote the stability of the emulsion and breath figures. Therefore, the effect of doubling the PS concentration was tested. Surprisingly, the greater PS concentration did not seem to lead to an increased stability of the emulsion. Instead, when all other parameters were kept the same, much greater water droplets must have formed judging from the film that was created (Figure 38).

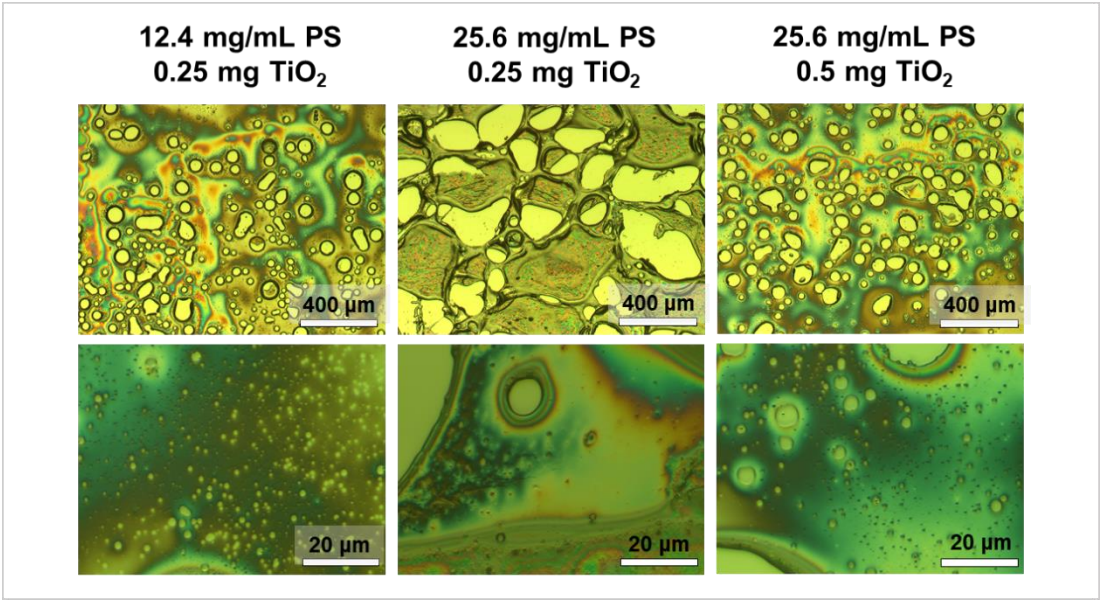

Figure 38. Optical microscopy images of films created from emulsions *via* dip-coating onto SiO_x with 16.8 mm/min withdrawal speed. Representative sections of the middle of the films were chosen. The chloroform solution contained either 12.4 or 25.6 mg PS/mL and either 0.25 or 0.5 mg TiO_2 NPs were added to the total 5 mL of the chloroform solution. The aqueous phase contained 30 mg sugar/mL and 16 µL of the aqueous phase were added per mL of chloroform solution.

When the NP content of the solution was also doubled like the PS concentration, the films created appeared reminiscent of the ones with half the concentrations of both again. This poses the question whether a certain ratio of NP:polymer is required. Another interesting finding is that there seem to be much greater areas covered with NPs for films created from solutions with a lower NP concentration. Both observations might have been weird coincidences, so this should be investigated further to draw reliable conclusions, which is not within the scope of this work.

In both cases of increasing the PS concentration, the smaller breath figure like pores were not more ordered or frequent than at a lower concentration. As no improvement in the films formed from solutions with a higher PS concentration could be found, it was decided to continue with the lower concentration.

4.3 Block Copolymer Self-Assembly

Films of PS_{32k}-*b*-$P4VP_{4.5k}$ and $PS_{3.3k}$-*b*-$P4VP_{18.7k}$ were created by dip-coating from solutions of 10 mg/mL in chloroform. The different withdrawal speeds used were 8.4, 42, and 67.2 mm/min. Optical microscopy revealed evenly coated films. Atomic force microscopy revealed hexagonally ordered circular structures with a distance of roughly 30 nm to another for PS_{32k}-*b*-$P4VP_{4.5k}$ (Figure 39). The circular structures observed could stem from either a spherical or perpendicular cylindrical domain morphology. The spherical morphology could also stem from micelles from the solution being incorporated into the film as spheres. It is not completely clear if the polymer would form micelles in chloroform, as it was only suggested in one paper that chloroform should dissolve P4VP significantly less well than PS,[101] and most others indicate that chloroform should be a good enough solvent for both blocks for no micelles to form in solution.[159,160] It should be noted, however, that a higher molecular weight of the block will make it less soluble, and that the interaction of the polymer with other molecules or particles with different solubilities can also induce micelle formation.[160] Judging from the comparatively low P4VP volume fractions, a spherical domain morphology is the likeliest explanation for the circular pattern.

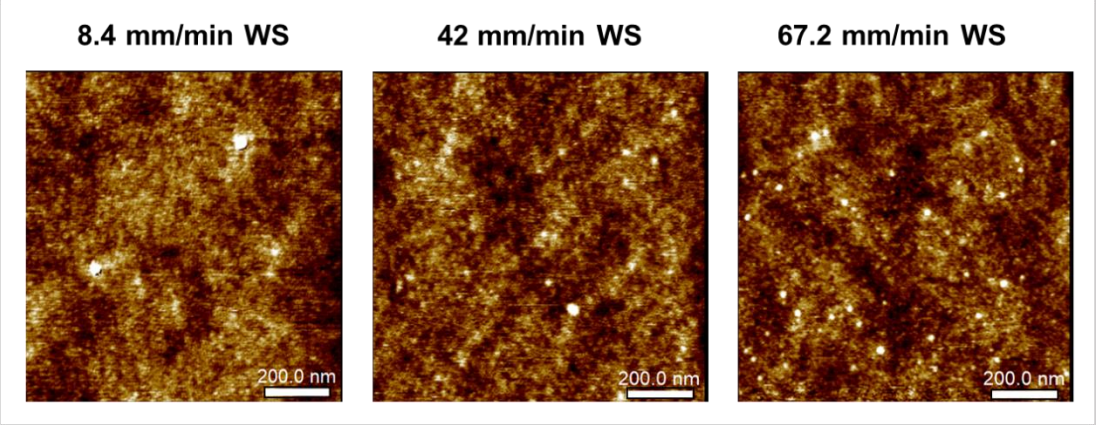

Figure 39. AFM images of representative sections of films formed *via* dip-coating onto SiO_x with different withdrawal speeds (WS). The solution contained 10.1 mg PS_{32k}-*b*-$P4VP_{4.5k}$ per mL chloroform. The height of the images goes from approximately -1 to +1 nm.

No surface pattern was observed for $PS_{3.3k}$-*b*-$P4VP_{18.7k}$ films with AFM. This might stem from the lower molecular weights of the individual blocks or their changed ratio not matching the solvent, since P4VP is less soluble in chloroform than PS.[101] The domains might have attained a parallel morphology to the substrate. Lower molecular weight also increases the polymer chain mobility, which would aid potential micelles in the solution to change their morphology during the drying of the film. Furthermore, a lower molecular weight also decreases the size of the individual domains and their spacing, as well as the tendency to phase separate. The formed film might have also been so thin that a brush layer was created. Even though the experimental conditions for both BCPs used were the same and a comparable thickness would be expected, the actual thickness has not been measured and the critical thickness below which a brush layer forms is also related to the specific block molecular weights.[106] Overall, these results showed that $PS_{3.3k}$-*b*-$P4VP_{18.7k}$ was unfit for the purpose of creating a BCP pattern under conditions suitable for BF creation. Therefore, experiments were continued with PS_{32k}-*b*-$P4VP_{4.5k}$ only, which is also closer to the PS model system.

The film created from the PS_{32k}-*b*-$P4VP_{4.5k}$ solution with a withdrawal speed of 67.2 mm/min was imaged with AFM again after being immersed in Milli-Q water for 24 h. This was done to compare the pattern to the one formed for the experiments combining the BCP and an emulsion, for which the washing step was necessary to remove the sugar from the sample. After the solvent annealing with water, the film displayed a well-ordered hexagonal pore structure with pore-pore distances of around 30 nm and pore diameters around 10 nm (Figure 40). This likely stems from the P4VP block swelling and collapsing upon air drying, forming the pores, as has been observed for PS-*b*-P4VP in literature with ethanol.[99,101–103] The order of the film also seemed enhanced after the immersion in water, so the presumably spherical micellar domains might have turned into perpendicularly ordered cylindrical domains, in addition. To investigate this, a cross section of thin films before and after washing with water should be created and imaged using SEM or TEM. Moreover, the films

could be additionally stained by I_2, which selectively binds to the PVP phase,[101,109,110] to prove whether the P4VP phase spread over the surface of the film in the washing step, as would be expected after pore formation.[99,101]

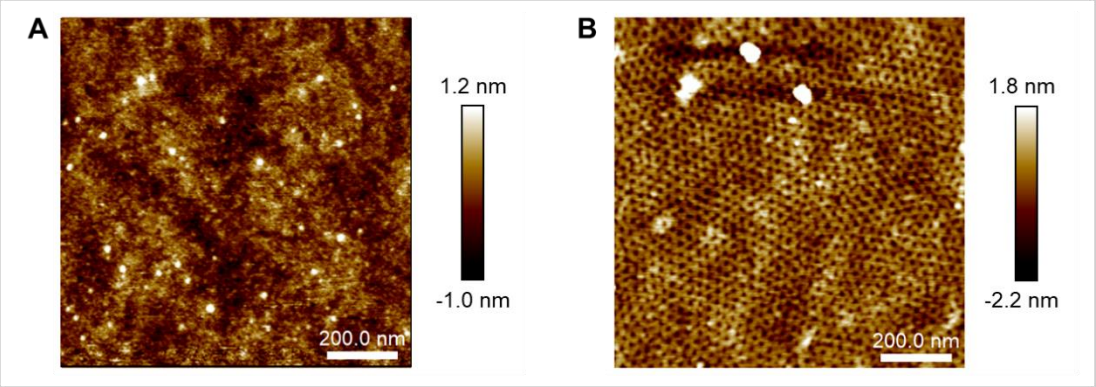

Figure 40. AFM height images of a film dip-coated from 10 mg/mL PS_{32k}-*b*-$P4VP_{4.5k}$ in chloroform with a withdrawal speed of 67.2 mm/min. A) After coating, B) after being immersed in Milli-Q water for 24 h.

The pore formation might also be useful to later incorporate a second type of ordered NPs into the BCP pattern physically rather than chemically. On the other hand, if the P4VP really covers the entire air interface, NPs interacting with pyridine might cover the entire film instead of just the pores, which would not conform with the aim of the multi-hierarchical ordering. Moreover, if the NPs are incorporated before the water washing, this might lead to a complete reorganization of the film in an undesired way. Therefore, it should be tested whether the washing step is necessary or if the AFM measurements can also be conducted with the sugar present. Another way might be to replace the sugar with a surfactant or stabilize the emulsion sufficiently with just the different NPs. Future experiments will show whether the pores are detrimental or beneficial for the ordering of NPs.

4.4 Introducing Breath Figures for a Block Copolymer Film with Nanoparticles

After the preliminary optimization of a polymer emulsion with the cheaper PS, it was attempted to replace the polymer by the chosen BCP to obtain similar patterns.

Therefore, a solution with 50 mg/mL BCP and 0.05 mg/mL TiO_2 in chloroform was mixed with 80 µm of a 30 mg/mL aqueous sucrose solution. Films were created by dip-coating with the previously used 8.4, 16.8, and 67.2 mm/min withdrawal speeds.

For the films created with 16.8 and 67.2 mm/min withdrawal speed, several oval areas of honeycomb patterns could be found at the bottom (Figure 41). The pores of this pattern extended throughout the whole film and were open toward the substrate. The around 10 to 50 µm wide pores became smaller towards the edges of the cage like structures. Around those honeycomb areas, porous areas similar to those found for films consisting of homopolymer PS were observed too. However, after observing the honeycomb areas, it was clear that the "real" breath figure patterns had been created. At the withdrawal speed of 8.4 mm/min, an oval area that looked like a pre-stage of the cage structures found on the other samples was observed. Here, the pores did not penetrate to the substrate, but the different colours clearly showed the thickness of the film changing within each pore, giving it the distinct appearance of stemming from an assembled water droplet cluster.

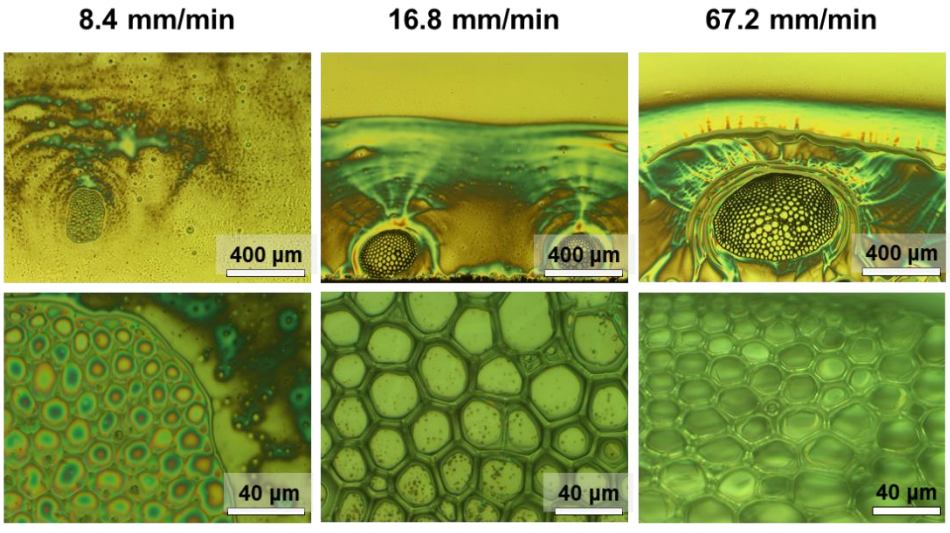

Figure 41. Optical microscopy images of films created from emulsions *via* dip-coating onto SiO_x at different withdrawal speeds (8.4, 16.8, 67.2 mm/min). The chloroform solution of the emulsion contained 10 mg PS-*b*-P4VP (32-*b*-4.5)/mL and 0.1 mg TiO_2/mL. The aqueous phase contained 30 mg sucrose per mL and 16 µL of the aqueous phase were added per mL of chloroform solution.

Due to the exciting nature of these results, an additional 80 µL of the sugar solution was added to the emulsion to create more films in hope to create larger areas with a honeycomb pattern. This was at least partly achieved (Figure 42). At the two lower withdrawal speeds, small oval areas of blueish colour, partly with a tiny honeycomb pattern, were found throughout the film. At the withdrawal speed of 67.2 mm/min, entire honeycomb lines stretching from one side of the substrate to the other were found at the very top of the film and at the beginning of the bottom area. In such areas, the pore sizes commonly ranged from 1 to 5 µm diameter. Moreover, in addition to the cages at the bottom with relatively huge pores, as for the films with a lower aqueous phase content, many cages with pores of the smaller size (around 1 to 5 µm) could be found throughout the sample. The latter also had the characteristic iridescent colour of breath figures. It was further observed by optical microscopy that the walls of the cage with greater pores at the bottom was still made of a web of smaller pores (Figure 43A3).

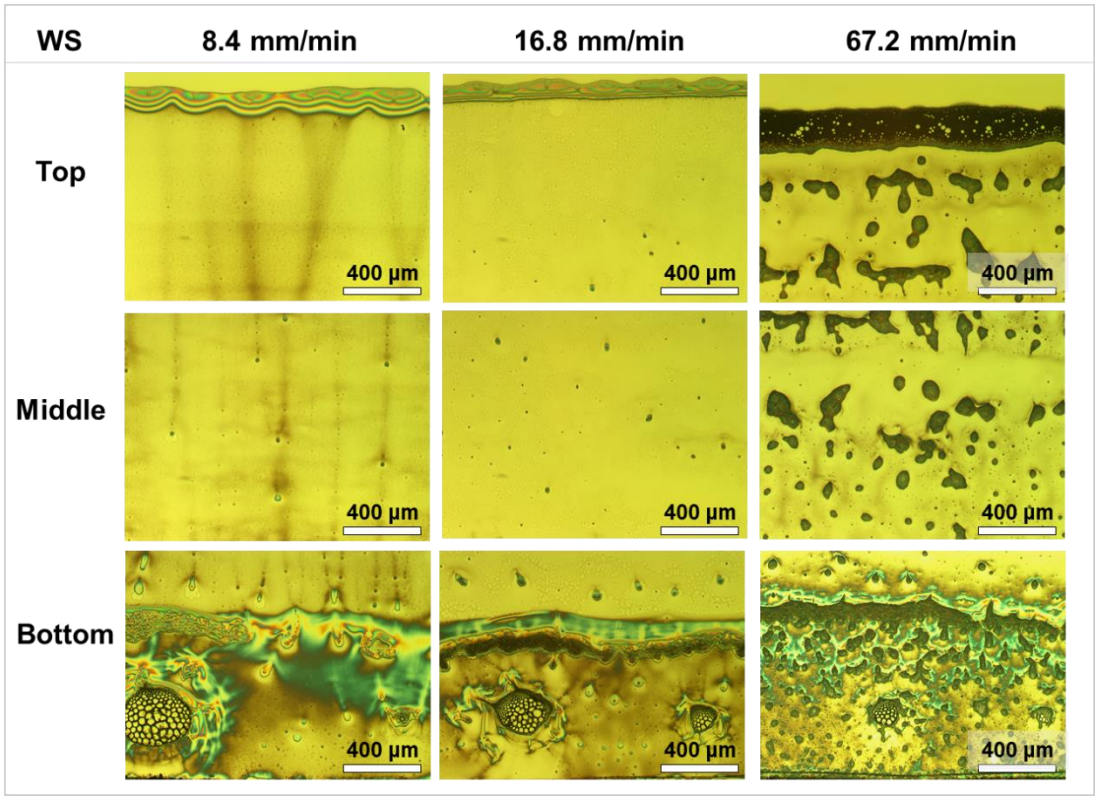

Figure 42. Optical microscopy images of films created from emulsions *via* dip-coating onto SiO_x at different withdrawal speeds (8.4, 16.8, 67.2 mm/min). The chloroform solution of the emulsion

contained 10 mg PS-*b*-P4VP (32-*b*-4.5)/mL and 0.1 mg TiO_2/mL. The aqueous phase contained 30 mg sucrose per mL and 32 µL of the aqueous phase were added per mL of chloroform solution.

The honeycomb areas appearing rather dark with optical microscopy were found to consist of multiple layers of the honeycomb network with SEM and even AFM. Moreover, AFM revealed that the BCP did indeed assemble into a pattern throughout the entire film including the cage walls. The pattern was hexagonally ordered pores, with pore to pore distances of 40 to 140 nm and pore diameters of 10 to 80 nm (Figure 43C). The pores might be induced by the solvent annealing from the water washing step to remove the sucrose. However, the pores are bigger and further apart, and the pattern is overall less ordered in comparison to the pure BCP film. Therefore, it is likely that the water content in the emulsion already influenced the pattern during the film creation. The water droplets of the emulsion could have already swollen the P4VP domains, which would likely lead to greater pores, as the PS matrix was not solidified yet. It is possible that a greater water content in the emulsion might lead to a more uniform swelling of the P4VP domains and a more homogeneous pore pattern. It should also be tested whether the water washing step affects the final pattern or if the pores are already created during film formation due to the emulsion. Overall, this result shows that a bi-hierarchical polymer pattern was successfully created.

One curious finding about the final films is that the TiO_2 nanoparticles were not observed. This might be caused by the NPs mixing better into the BCP than into the PS. They likely are dissolved in the new P4VP phase and bound to the pyridine.[150] This might have also influenced the final domain morphology. In order to test the effect of the NPs on the pore formation, a film of the BCP with NPs should be created without the water phase. The domain the NPs are dispersed in cannot be accurately proven by EDS due to the resolution limit of this technique, however, it should be possible to prove the presence or absence of Ti in the film that way. The visual absence of the particles indicates bigger particles should be chosen to ensure they will assemble at the water/solvent interface.

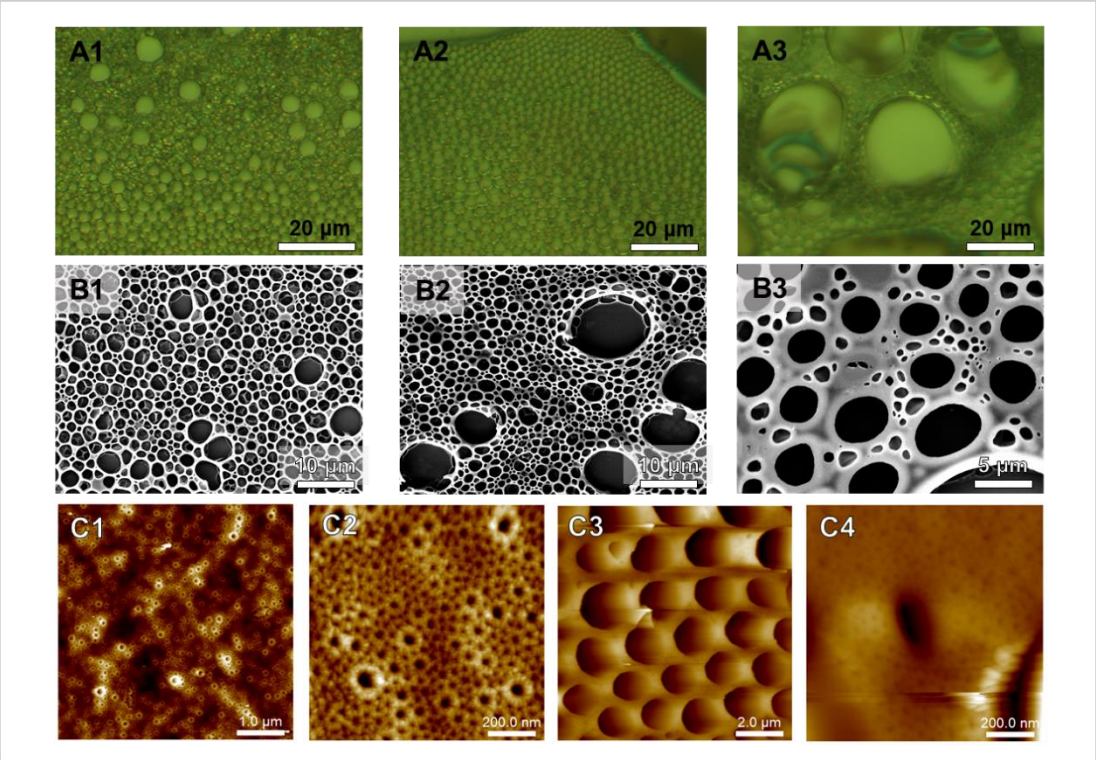

Figure 43. Microscopy images of a film created from an emulsion *via* dip-coating onto SiO_x at a withdrawal speed of 67.2 mm/min. The chloroform solution of the emulsion contained 10 mg PS-*b*-P4VP (32-*b*-4.5)/mL and 0.1 mg TiO_2/mL. The aqueous phase contained 30 mg sucrose per mL and 32 µL of the aqueous phase were added per mL of chloroform solution. A) Optical microscopy images. B) Scanning electron microscopy images. C) Atomic force microscopy height images of the flat polymer film (1,2) and of the cage structures (3,4).

The experiments showed that a higher withdrawal speed is preferable for honeycomb patterns to form. At even higher withdrawal speeds than the ones tested by now, more of the substrate might be covered with this pattern. This might be due to the emulsion droplets diffusing back into the solution at lower withdrawal speeds, similarly to what was hypothesized for the small molecules[106] and micelles in dip-coated films.[105] Alternatively, this might not be a pure time issue, but it could also be that the film simply needs to be thicker to accommodate for the big droplets in the solution. It appears like the cages that were formed are thicker than the rest of the film. Therefore, it would be interesting to repeat this experiment at very low and high withdrawal speeds, which should both yield a thicker film due to the V-shaped thickness withdrawal speed relationship.

The BCP solution is stable with higher water contents in the emulsion than PS, as expected. Being able to use a higher water content likely enables the creation of larger honeycomb areas. Therefore, the solution with the final BCP should further be optimized with regard to water content, and likely also NP content.

4.5 Suggestions for Future Directions

There still are several questions about the BCP films to be answered. The assumed domain morphologies of the BCP domains should be confirmed by creating a cross section and imaging it with SEM or TEM. This should clarify whether spheres or perpendicular cylinders resulted in the circular surface morphologies. Moreover, by dyeing the P4VP phase, the domain locations of the respective blocks can be confirmed. The effect of the water droplets in the emulsion and the NPs on the formed BCP pattern should also be tested individually by creating a pure BCP film from an aqueous emulsion and by creating a BCP film with NPs from a solution without water. The effect of the water annealing on the BCP and NP film can then be tested subsequently. All these experiments should yield a good idea of the part each individual component of the system plays for the domain pattern formation.

It appeared like more of the honeycomb pattern from the BCP solution assembles at higher withdrawal speeds. Therefore, the BCP experiments should be conducted at even higher speeds than previously. While the maximum for the current machines is 84 mm/min, which has not been tried yet, another available machine will be able to withdraw at speeds of 0.1 to 100 mm/min. Moreover, this machine will not be limited to 8.4 mm/min steps in speed, which will allow a more detailed examination of the system in the different withdrawal regimes. This will allow for different film thicknesses, which is likely going to affect the pattern formation.

The introduced TiO_2 NPs did not fully assemble at the walls of the pores as desired. Instead, there were greater aggregates found in bigger pores of PS solutions, whereas it was unclear whether any NPs were present in smaller pores. In the final BCP film,

the NPs were not visible at all, indicating they likely resided inside the P4VP domains. Therefore, while the size of the TiO_2 NPs with 20 nm diameter is close to some literature,[70] it might be useful to conduct the experiments with even bigger particles, maybe around 200 nm. This would stabilize the emulsion more and the greater size would increase the likelihood of the particles to get stuck at the solvent-water interface without having to adapt the surface chemistry.

It was found that the synthesis of TiO_2 in the desired size range is not easily achievable, and there also are no reliable commercial sources for similar sizes. Therefore, it might be a good idea to switch to SiO_2 NPs, which are easily and cheaply available over a broad size range. Moreover, these particles have also been proven to work well to assemble at the breath figure interface in chloroform.[51,70] Sizes of 1 µm silica particles were proven to still be much more effective than 200 nm.[51] Greater sizes would likely not be suitable for the ordered small pores created from PS solutions, however, the honeycomb pattern created from the final BCP solution exhibits much bigger features, which would allow for the use of even larger particles. This would also aid the differentiation of the different NPs in the solution once the gold NPs for the BCP phase are introduced, as the greater NPs will be much preferred for assembly at the solvent-water interface. Therefore, changing from 20 nm TiO2 NPs to 1 µm SiO_2 NPs is suggested.

For the BF pattern created from the BCP, the water and nanoparticle content should still be adapted. It was evident that the BCP solution can stabilize much greater amounts of water. It would also be interesting to image the films with AFM before and after the sugar wash, which should be possible by focusing the tip on the area between larger BF pores, where there should be less sugar. This would irrefutably show whether the pore pattern for this system already exists before the water washing step.

Once the first type of nanoparticles is proven to be incorporated into this multi-hierarchical film at the breath figure pores as desired, the next step would be to introduce the second type of nanoparticles to the BCP pattern. For this, smaller nanoparticles should be used, so they are not favoured for assembly at the water-solvent interface. Moreover, it would be good if those NPs were hydrophobic. Therefore, the dodecanethiol stabilized 4 nm Au NPs still seem feasible. First, it should be tried to assemble those in the polymer phase by simply dipping the dried film in a solution of the NPs. Once that works, it might then be tried to assembly the whole film with polymer and NP patterns at two different size ranges as one pot synthesis. It is possible that the stabilized Au NPs will not interact favourably enough with the P4VP block, as the dodecanethiol ligand will likely not bind to the pyridine unit. The NPs might be physically stuck inside the BCP pores anyway, but alternatively pure Au NPs could be reduced in the solution, as those should form complexes with the pyridine.[65] The use of pure NPs was not suggested at first, as the ligands ensure they will favour the polymer phase. However, if the Au NPs are introduced after film formation, this precaution might be less necessary. Attention must be paid to the solvent the NPs will be dispersed in to immerse the dried film into though, as the solvent could change the domain pattern again. Overall, there are many things to try to incorporate a second type of NP into the film, and it must simply be tried what will work in the end.

Lastly, there still are some questions of a more fundamental nature, that are less relevant to create the desired film, for example, whether the BCP forms micelles in solution. This can be tested by dynamic light scattering. There also still are no clear answers about the effect of the dip-coating regimes on the breath figure formation, which should be investigated further, which will be easier with the new dip-coater with a wider speed range and smaller speed intervals. It would be especially interesting to find out whether there is a relation between film thickness and honeycomb pattern formation in terms of a certain thickness being met to incorporate the droplets. For this, thickness measurements will need to be combined

with an experimental series of withdrawal speeds and the corresponding film morphologies. Such experiments will likely be more valuable once the system has been optimized and films of desired quality can be created.

5 Conclusion

It was attempted to create a multi-hierarchical polymer thin film, incorporating two different levels of organized nanoparticles, *via* dip-coating. For this, block copolymer, breath figure, and NP self-assembly was combined. This ambitious goal was not met fully, in part due to unforeseen global events limiting laboratory time.

It was decided to induce the breath figure pattern by forming an emulsion, because a self-built humidity chamber and a humid airflow did not yield enough control. The emulsion with the PS model system was optimized for water content, NP content, sugar content to stabilize the water droplets, and process conditions. Partly ordered pores of the desired size were mainly observed at the bottom of the substrates, which might be related to the film being thicker there. TiO_2 NPs were found at the edges of the pores. Different solvents and substrate conditions were tested, and chloroform was found to be the best solvent for the purpose of this research. Wetting difficulties that might have been related to weather conditions were encountered and investigated.

The PS_{32k}-*b*-$P4VP_{4.5k}$ BCP film lead to a desired circular surface pattern when dip-coated under similar circumstances as the optimized PS emulsion. When immersed in water after the film creation, the pattern changed to hexagonally ordered pores. Creating an emulsion with the BCP and TiO_2 NPs, the desired honeycomb like areas were found on the substrate. This illustrates the limitations of using a homopolymer as model system for a block copolymer, since no such patterns were created using PS and the BCP emulsion could hold significantly more water. Higher withdrawal speeds lead to greater honeycomb areas, with the best sample containing cage like areas scattered through the entire film and entire lines of the pattern at the top and bottom.

The NPs could not be observed in the film, indicating that they dissolved in the P4VP block. Therefore, larger particles should be used to increase their energy of detachment at the water/solvent interface in the emulsion. Overall, two levels of hierarchy in the polymer film were obtained with pores of 1-50 μm in the breath figure pattern and pores of 10-80 nm diameter in the BCP pattern between the large pores and throughout the rest of the film. The BCP emulsion should be further optimized, but the results already look promising. Several suggestions for continuation of this research were made. By choosing the right NP types and sizes, it should be possible to independently decorate the patterns at two different length scales. This would mean the combination of several self-assembly techniques into a facile way to enrich a range of materials with new surface functionalities in one step by creating a higher level of fully self-assembled hierarchy in a thin film than reported by now, thereby paving the way for novel advanced applications.

References

(1) Fratzl, P.; Weinkamer, R. Nature's Hierarchical Materials. *Progress in Materials Science*. Pergamon November 1, 2007, pp 1263–1334.

(2) Shin, D. O.; Mun, J. H.; Hwang, G. T.; Yoon, J. M.; Kim, J. Y.; Yun, J. M.; Yang, Y. B.; Oh, Y.; Lee, J. Y.; Shin, J.; et al. Multicomponent Nanopatterns by Directed Block Copolymer Self-Assembly. *ACS Nano* **2013**, *7* (10), 8899–8907, DOI: 10.1021/nn403379k.

(3) Ozin, G. A. Panoscopic Materials: Synthesis over "all" Length Scales. *Chemical Communications*. Royal Society of Chemistry March 21, 2000, pp 419–432.

(4) Lee, L. R.; Liu, C. T.; Tseng, H. F.; Lin, K. T.; Chu, C. W.; Chen, J. T. Hierarchical Polymer Structures Using Templates and the Modified Breath Figure Method. *Langmuir* **2018**, *34* (25), 7472–7478, DOI: 10.1021/acs.langmuir.8b01381.

(5) Whitesides, G. M.; Grzybowski, B. Self-Assembly at All Scales. *Science*. American Association for the Advancement of Science March 29, 2002, pp 2418–2421.

(6) Sun, W.; Ji, A.; Shen, J. Rings of Nanoparticle-Decorated Honeycomb-Structured Polymeric Film: The Combination of Pickering Emulsions and Capillary Flow in the Breath Figures Method. *Langmuir* **2008**, *24* (20), 11338–11341, DOI: 10.1021/la8024217.

(7) Aizenberg, J.; Braun, P. V.; Wiltzius, P. Patterned Colloidal Deposition Controlled by Electrostatic and Capillary Forces. *Phys. Rev. Lett.* **2000**, *84* (13), 2997, DOI: 10.1103/PhysRevLett.84.2997.

(8) Jonas, U.; Del Campo, A.; Krüger, C.; Glasser, G.; Boos, D. Colloidal Assemblies on Patterned Silane Layers. *Proc. Natl. Acad. Sci. U. S. A.* **2002**, *99* (8), 5034–5039, DOI: 10.1073/pnas.082634799.

(9) Luo, M.; Epps, T. H. Directed Block Copolymer Thin Film Self-Assembly: Emerging Trends in Nanopattern Fabrication. *Macromolecules*. October 8, 2013, pp 7567–7579.

(10) Hayakawa, T.; Horiuchi, S. From Angstroms to Micrometers: Self-Organized Hierarchical Structure within a Polymer Film. *Angew. Chemie Int. Ed.* **2003**, *42* (20), 2285–2289, DOI: 10.1002/anie.200219877.

(11) Darling, S. B. Directing the Self-Assembly of Block Copolymers. *Progress in Polymer Science (Oxford)*. Pergamon October 1, 2007, pp 1152–1204.

(12) Albert, J. N. L.; Epps, T. H. Self-Assembly of Block Copolymer Thin Films. *Materials Today*. Elsevier June 1, 2010, pp 24–33.

(13) Tokarev, I.; Krenek, R.; Burkov, Y.; Schmeisser, D.; Sidorenko, A.; Minko, S.; Stamm, M. Microphase Separation in Thin Films of Poly(Styrene-Block-4-Vinylpyridine) Copolymer-2-(4'-Hydroxybenzeneazo)Benzoic Acid Assembly. *Macromolecules* **2005**, *38* (2), 507–516, DOI: 10.1021/ma048864i.

(14) Xu, X.; Heng, L.; Zhao, X.; Ma, J.; Lin, L.; Jiang, L. Multiscale Bio-Inspired Honeycomb Structure Material with High Mechanical Strength and Low Density. *J. Mater. Chem.* **2012**, *22* (21), 10883–10888, DOI:

10.1039/c2jm31510f.
(15) Gong, J.; Xu, B.; Tao, X. Three-Dimensionally Conformal Porous Microstructured Fabrics via Breath Figures: A Nature-Inspired Approach for Novel Surface Modification of Textiles. *Sci. Rep.* **2017**, *7* (1), 1–9, DOI: 10.1038/s41598-017-02615-1.
(16) Trindade, T.; O'Brien, P.; Pickett, N. L. Nanocrystalline Semiconductors: Synthesis, Properties, and Perspectives. *Chemistry of Materials*. American Chemical Society 2001, pp 3843–3858.
(17) Sawitowski, T.; Miquel, Y.; Heilmann, A.; Schmid, G. Optical Properties of Quasi One-Dimensional Chains of Gold Nanoparticles. *Adv. Funct. Mater.* **2001**, *11* (6), 435–440, DOI: 10.1002/1616-3028(200112)11:6<435::AID-ADFM435>3.0.CO;2-X.
(18) Pileni, M. P. Nanocrystal Self-Assemblies: Fabrication and Collective Properties. *J. Phys. Chem. B* **2001**, *105* (17), 3358–3371, DOI: 10.1021/jp0039520.
(19) Alivisatos, A. P. Semiconductor Clusters, Nanocrystals, and Quantum Dots. *Science* **1996**, *271* (5251), 933–937, DOI: 10.1126/science.271.5251.933.
(20) Collier, C. P.; Saykally, R. J.; Shiang, J. J.; Henrichs, S. E.; Heath, J. R. Reversible Tuning of Silver Quantum Dot Monolayers through the Metal- Insulator Transition. *Science* **1997**, *277* (5334), 1978–1981, DOI: 10.1126/science.277.5334.1978.
(21) Ruokolainen, J.; Saariaho, M.; Ikkala, O.; Ten Brinke, G.; Thomas, E. L.; Torkkeli, M.; Serimaa, R. Supramolecular Routes to Hierarchical Structures: Comb-Coil Diblock Copolymers Organized with Two Length Scales. *Macromolecules* **1999**, *32* (4), 1152–1158, DOI: 10.1021/ma980189n.
(22) Bates, F. S.; Fredrickson, G. H. Block Copolymer Thermodynamics: Theory and Experiment. *Annu. Rev. Phys. Chem.* **1990**, *41* (1), 525–557.
(23) Van Zoelen, W.; Ten Brinke, G. Thin Films of Complexed Block Copolymers. *Soft Matter*. Royal Society of Chemistry April 8, 2009, pp 1568–1582.
(24) Bormashenko, E.; Balter, S.; Aurbach, D. On the Nature of the Breath Figures Self-Assembly in Evaporated Polymer Solutions: Revisiting Physical Factors Governing the Patterning. *Macromol. Chem. Phys.* **2012**, *213* (16), 1742–1747, DOI: 10.1002/macp.201200272.
(25) Sunami, H.; Ito, E.; Tanaka, M.; Yamamoto, S.; Shimomura, M. Effect of Honeycomb Film on Protein Adsorption, Cell Adhesion and Proliferation. *Colloids Surfaces A Physicochem. Eng. Asp.* **2006**, *284–285*, 548–551, DOI: 10.1016/j.colsurfa.2005.11.041.
(26) Tanaka, M.; Takayama, A.; Ito, E.; Sunami, H.; Yamamoto, S.; Shimomura, M. Effect of Pore Size of Self-Organized Honeycomb-Patterned Polymer Films on Spreading, Focal Adhesion, Proliferation, and Function of Endothelial Cells. In *Journal of Nanoscience and Nanotechnology*; 2007; Vol. 7, pp 763–772.
(27) Yamamoto, S.; Tanaka, M.; Sunami, H.; Arai, K.; Takayama, A.; Yamashita, S.; Morita, Y.; Shimomura, M. Relationship between Adsorbed Fibronectin and Cell Adhesion on a Honeycomb-Patterned Film. *Surf. Sci.* **2006**, *600* (18), 3785–

3791, DOI: 10.1016/j.susc.2006.01.085.
(28) Kawano, T.; Sato, M.; Yabu, H.; Shimomura, M. Honeycomb-Shaped Surface Topography Induces Differentiation of Human Mesenchymal Stem Cells (HMSCs): Uniform Porous Polymer Scaffolds Prepared by the Breath Figure Technique. *Biomater. Sci.* **2014**, *2* (1), 52–56, DOI: 10.1039/c3bm60195a.
(29) Eniwumide, J. O.; Tanaka, M.; Nagai, N.; Morita, Y.; De Bruijn, J.; Yamamoto, S.; Onodera, S.; Kondo, E.; Yasuda, K.; Shimomura, M. The Morphology and Functions of Articular Chondrocytes on a Honeycomb-Patterned Surface. *Biomed Res. Int.* **2014**, *2014*, DOI: 10.1155/2014/710354.
(30) Tanaka, M.; Nishikawa, K.; Okubo, H.; Kamachi, H.; Kawai, T.; Matsushita, M.; Todo, S.; Shimomura, M. Control of Hepatocyte Adhesion and Function on Self-Organized Honeycomb-Patterned Polymer Film. *Colloids Surfaces A Physicochem. Eng. Asp.* **2006**, *284–285*, 464–469, DOI: 10.1016/j.colsurfa.2005.11.098.
(31) Muñoz-Bonilla, A.; Fernández-García, M.; Rodríguez-Hernández, J. Towards Hierarchically Ordered Functional Porous Polymeric Surfaces Prepared by the Breath Figures Approach. *Prog. Polym. Sci.* **2014**, *39* (3), 510–554, DOI: 10.1016/j.progpolymsci.2013.08.006.
(32) Pitois, O.; François, B. Formation of Ordered Micro-Porous Membranes. *Eur. Phys. J. B* **1999**, *8* (2), 225–231, DOI: 10.1007/s100510050685.
(33) Pitois, O.; François, B. Crystallization of Condensation Droplets on a Liquid Surface. *Colloid Polym. Sci.* **1999**, *277* (6), 574–578, DOI: 10.1007/s003960050427.
(34) Karthaus, O.; Maruyama, N.; Cieren, X.; Shimomura, M.; Hasegawa, H.; Hashimoto, T. Water-Assisted Formation of Micrometer-Size Honeycomb Patterns of Polymers. *Langmuir* **2000**, *16* (15), 6071–6076, DOI: 10.1021/la0001732.
(35) Ham, H. T.; Chung, I. J.; Choi, Y. S.; Lee, S. H.; Kim, S. O. Macroporous Polymer Thin Film Prepared from Temporarily Stabilized Water-in-Oil Emulsion. *J. Phys. Chem. B* **2006**, *110* (28), 13959–13964, DOI: 10.1021/jp0616361.
(36) Liang, J.; Ma, Y.; Sun, H.; Li, W.; Wu, L. Polyanion Cluster Patterning on Polymer Surface through Microemulsion Approach for Selective Adsorption of Proteins. *J. Colloid Interface Sci.* **2013**, *409*, 80–87, DOI: 10.1016/j.jcis.2013.08.004.
(37) Zhang, W. X.; Wan, L. S.; Meng, X. L.; Li, J. W.; Ke, B. B.; Chen, P. C.; Xu, Z. K. Macroporous, Protein-Containing Films Cast from Water-in-Oil Emulsions Featuring a Block-Copolymer. *Soft Matter* **2011**, *7* (9), 4221–4227, DOI: 10.1039/c0sm01447h.
(38) Madej, W.; Budkowski, A.; Raczkowska, J.; Rysz, J. Breath Figures in Polymer and Polymer Blend Films Spin-Coated in Dry and Humid Ambience. *Langmuir* **2008**, *24* (7), 3517–3524, DOI: 10.1021/la703363a.
(39) Park, M. S.; Kim, J. K. Breath Figure Patterns Prepared by Spin Coating in a Dry Environment. *Langmuir* **2004**, *20* (13), 5347–5352, DOI: 10.1021/la035915g.
(40) Stenzel, M. H.; Barner-Kowollik, C.; Davis, T. P. Formation of Honeycomb-Structured, Porous Films via Breath Figures with Different Polymer

Architectures. *J. Polym. Sci. Part A Polym. Chem.* **2006**, *44* (8), 2363–2375, DOI: 10.1002/pola.21334.

(41) Cui, L.; Wang, H.; Ding, Y.; Han, Y. Tunable Ordered Droplets Induced by Convection in Phase-Separating P2VP/PS Blend Film. *Polymer (Guildf).* **2004**, *45* (24), 8139–8146, DOI: 10.1016/j.polymer.2004.09.065.

(42) Lin, C. L.; Tung, P. H.; Chang, F. C. Synthesis of Rod-Coil Diblock Copolymers by ATRP and Their Honeycomb Morphologies Formed by the "breath Figures" Method. *Polymer (Guildf).* **2005**, *46* (22), 9304–9313, DOI: 10.1016/j.polymer.2005.07.051.

(43) Tian, Y.; Jiao, Q.; Ding, H.; Shi, Y.; Liu, B. The Formation of Honeycomb Structure in Polyphenylene Oxide Films. *Polymer (Guildf).* **2006**, *47* (11), 3866–3873, DOI: 10.1016/j.polymer.2006.03.081.

(44) Han, X.; Tian, Y.; Wang, L.; Xiao, C. Formation of Honeycomb Films Based on a Soluble Polyimide Synthesized from 2,2′-Bis[4-(3,4-Dicarboxyphenoxy)Phenyl]Hexafluoropropane Dianhydride and 3,3′-Dimethyl-4,4′-Diaminodiphenylmethane. *J. Appl. Polym. Sci.* **2008**, *107* (1), 618–623, DOI: 10.1002/app.27109.

(45) Cheng, C. X.; Tian, Y.; Shi, Y. Q.; Tang, R. P.; Xi, F. Porous Polymer Films and Honeycomb Structures Based on Amphiphilic Dendronized Block Copolymers. *Langmuir* **2005**, *21* (14), 6576–6581, DOI: 10.1021/la050187d.

(46) Chiu, Y. C.; Kuo, C. C.; Lin, C. J.; Chen, W. C. Highly Ordered Luminescent Microporous Films Prepared from Crystalline Conjugated Rod-Coil Diblock Copolymers of PF-b-PSA and Their Superhydrophobic Characteristics. *Soft Matter* **2011**, *7* (19), 9350–9358, DOI: 10.1039/c1sm05712j.

(47) Hiwatari, K. I.; Serizawa, T.; Seto, F.; Kishida, A.; Muraoka, Y.; Akashi, M. Graft Copolymers Having Hydrophobic Backbone and Hydrophilic Branches Xxxiv. Fabrication and Control of Honeycomb Structure Prepared from Amphiphilic Graft Copolymers. *Polym. J.* **2001**, *33* (9), 669–675, DOI: 10.1295/polymj.33.669.

(48) Peng, J.; Han, Y.; Yang, Y.; Li, B. The Influencing Factors on the Macroporous Formation in Polymer Films by Water Droplet Templating. *Polymer (Guildf).* **2004**, *45* (2), 447–452, DOI: 10.1016/j.polymer.2003.11.019.

(49) Srinivasarao, M.; Collings, D.; Philips, A.; Patel, S. Three-Dimensionally Ordered Array of Air Bubbles in a Polymer Film. *Science* **2001**, *292* (5514), 79–83, DOI: 10.1126/science.1057887.

(50) Pickering, S. U. CXCVI. - Emulsions. *Journal of the Chemical Society, Transactions*. The Royal Society of Chemistry January 1, 1907, pp 2001–2021.

(51) Sun, W.; Ji, J.; Shen, J. Rings of Nanoparticle-Decorated Honeycomb-Structured Polymeric Film: The Combination of Pickering Emulsions and Capillary Flow in the Breath Figures Method. *Langmuir* **2008**, *24* (20), 11338–11341, DOI: 10.1021/la8024217.

(52) Sun, W.; Shao, Z.; Ji, J. Particle-Assisted Fabrication of Honeycomb-Structured Hybrid Films via Breath Figures Method. *Polymer (Guildf).* **2010**, *51* (18), 4169–4175, DOI: 10.1016/j.polymer.2010.07.008.

(53) Zhang, A.; Bai, H.; Li, L. Breath Figure: A Nature-Inspired Preparation Method for Ordered Porous Films. *Chem. Rev.* **2015**, *115* (18), 9801–9868, DOI: 10.1021/acs.chemrev.5b00069.

(54) Yin, D.; Horiuchi, S.; Masuoka, T. Lateral Assembly of Metal Nanoparticles Directed by Nanodomain Control in Block Copolymer Thin Films. *Chem. Mater.* **2005**, *17* (3), 463–469, DOI: 10.1021/cm048695g.

(55) Li, Q.; He, J.; Glogowski, E.; Li, X.; Wang, J.; Emrick, T.; Russell, T. P. Responsive Assemblies: Gold Nanoparticles with Mixed Ligands in Microphase Separated Block Copolymers. *Adv. Mater.* **2008**, *20* (8), 1462–1466, DOI: 10.1002/adma.200702004.

(56) Zehner, R. W.; Lopes, W. A.; Morkved, T. L.; Jaeger, H.; Sita, L. R. Selective Decoration of a Phase-Separated Diblock Copolymer with Thiol-Passivated Gold Nanocrystals. *Langmuir* **1998**, *14* (2), 241–244, DOI: 10.1021/la971086l.

(57) Niskanen, J.; Shan, J.; Tenhu, H.; Jiang, H.; Kauppinen, E.; Barranco, V.; Picó, F.; Yliniemi, K.; Kontturi, K. Synthesis of Copolymer-Stabilized Silver Nanoparticles for Coating Materials. *Colloid Polym. Sci.* **2010**, *288* (5), 543–553, DOI: 10.1007/s00396-009-2178-x.

(58) Lin, Y.; Böker, A.; He, J.; Sill, K.; Xiang, H.; Abetz, C.; Li, X.; Wang, J.; Emrick, T.; Long, S.; et al. Self-Directed Self-Assembly of Nanoparticle/Copolymer Mixtures. *Nature* **2005**, *434* (7029), 55–59, DOI: 10.1038/nature03310.

(59) Binder, W. H.; Kluger, C.; Straif, C. J.; Friedbacher, G. Directed Nanoparticle Binding onto Microphase-Separated Block Copolymer Thin Films. *Macromolecules* **2005**, *38* (23), 9405–9410, DOI: 10.1021/ma0518252.

(60) Watanabe, S.; Fujiwara, R.; Hada, M.; Okazaki, Y.; Iyoda, T. Site-Specific Recognition of Nanophase-Separated Surfaces of Amphiphilic Block Copolymers by Hydrophilic and Hydrophobic Gold Nanoparticles. *Angew. Chemie - Int. Ed.* **2007**, *46* (7), 1120–1123, DOI: 10.1002/anie.200603516.

(61) Sun, Z.; Kim, D. H.; Wolkenhauer, M.; Bumbu, G. G.; Knoll, W.; Gutmann, J. S. Synthesis and Photoluminescence of Titania Nanoparticle Arrays Templated by Block-Copolymer Thin Films. *ChemPhysChem* **2006**, *7* (2), 370–378, DOI: 10.1002/cphc.200500340.

(62) Yang, T.; Zhang, S.; Komura, M.; Iyoda, T.; Nagai, K. Site-Selective Self-Assembly of Fullerene Nanoparticles on Amphiphilic Block Copolymer Thin Film from Water Suspension. *Jpn. J. Appl. Phys.* **2012**, *51* (7 PART 1), DOI: 10.1143/JJAP.51.070201.

(63) Misner, M. J.; Skaff, H.; Emrick, T.; Russell, T. P. Directed Deposition of Nanoparticles Using Diblock Copolymer Templates. *Adv. Mater.* **2003**, *15* (3), 221–224, DOI: 10.1002/adma.200390050.

(64) Minelli, C.; Geissbuehler, I.; Hinderung, C.; Heinzelmann, H.; Vogel, H.; Pugin, R.; Liley, M. Organization of Nanoparticles on Hard Substrates Using Block Copolymer Films as Templates. *J. Nanosci. Nanotechnol.* **2006**, *6* (6), 1611–1619, DOI: 10.1166/jnn.2006.241.

(65) Hwang, Y. K.; Lee, J. M.; Sathaye, S. D.; Cho, G.; Hwang, J. S.; Chang, J. S. Palladium and Gold Nanoparticle Array Films Formed by Using Self-Assembly

of Block Copolymer. *J. Nanosci. Nanotechnol.* **2006**, *6* (6), 1850–1853, DOI: 10.1166/jnn.2006.206.

(66) Jiang, X.; Zhou, X.; Zhang, Y.; Zhang, T.; Guo, Z.; Gu, N. Interfacial Effects of *In Situ* -Synthesized Ag Nanoparticles on Breath Figures. *Langmuir* **2010**, *26* (4), 2477–2483, DOI: 10.1021/la9027139.

(67) Sun, H.; Li, H.; Wu, L. Micro-Patterned Polystyrene Surfaces Directed by Surfactant-Encapsulated Polyoxometalate Complex via Breath Figures. *Polymer (Guildf).* **2009**, *50* (9), 2113–2122, DOI: 10.1016/j.polymer.2009.02.036.

(68) Böker, A.; Lin, Y.; Chiapperini, K.; Horowitz, R.; Thompson, M.; Carreon, V.; Xu, T.; Abetz, C.; Skaff, H.; Dinsmore, A. D.; et al. Hierarchical Nanoparticle Assemblies Formed by Decorating Breath Figures. *Nat. Mater.* **2004**, *3* (5), 302–306, DOI: 10.1038/nmat1110.

(69) Escalé, P.; Rubatat, L.; Billon, L.; Save, M. Recent Advances in Honeycomb-Structured Porous Polymer Films Prepared via Breath Figures. *Eur. Polym. J.* **2012**, *48* (6), 1001–1025, DOI: 10.1016/j.eurpolymj.2012.03.001.

(70) Saito, Y.; Shimomura, M.; Yabu, H. Breath Figures of Nanoscale Bricks: A Universal Method for Creating Hierarchic Porous Materials from Inorganic Nanoparticles Stabilized with Mussel-Inspired Copolymers. *Macromol. Rapid Commun.* **2014**, *35* (20), 1763–1769, DOI: 10.1002/marc.201400363.

(71) Ma, H.; Cui, J.; Song, A.; Hao, J. Fabrication of Freestanding Honeycomb Films with Through-Pore Structures via Air/Water Interfacial Self-Assembly. *Chem. Commun.* **2011**, *47* (4), 1154–1156, DOI: 10.1039/c0cc02680h.

(72) Ma, H.; Cui, J.; Chen, J.; Hao, J. Self-Organized Polymer Nanocomposite Inverse Opal Films with Combined Optical Properties. *Chem. - A Eur. J.* **2011**, *17* (2), 655–660, DOI: 10.1002/chem.201001147.

(73) Widawski, G.; Rawiso, M.; François, B. Self-Organized Honeycomb Morphology of Star-Polymer Polystyrene Films. *Nature* **1994**, *369* (6479), 387–389, DOI: 10.1038/369387a0.

(74) Pietsch, T.; Müller-Buschbaum, P.; Mahltig, B.; Fahmi, A. Nanoporous Thin Films and Binary Nanoparticle Superlattices Created by Directed Self-Assembly of Block Copolymer Hybrid Materials. *ACS Appl. Mater. Interfaces* **2015**, *7* (23), 12440–12449, DOI: 10.1021/am5076056.

(75) Puetz, J.; Aegerter, M. A. Dip Coating Technique. In *Sol-Gel Technologies for Glass Producers and Users*; Springer US, 2004; pp 37–48.

(76) Grosso, D. How to Exploit the Full Potential of the Dip-Coating Process to Better Control Film Formation. *J. Mater. Chem.* **2011**, *21* (43), 17033–17038, DOI: 10.1039/c1jm12837j.

(77) Geffcken, W.; Berger, E. Verfahren Zur Änderung Des Reflexionsvermögens Optischer Gläser. *Dtsch. Reichspatent, assigned to Jenaer Glas. Schott Gen., Jena* **1939**, *736*, 411.

(78) Brinker, C. J. Dip Coating. In *Chemical Solution Deposition of Functional Oxide Thin Films*; Springer-Verlag Wien, 2013; Vol. 9783211993118, pp 233–261.

(79) Zhu, H.; Masson, J. F.; Bazuin, C. G. Monolayer Arrays of Nanoparticles on Block

Copolymer Brush Films. *Langmuir* **2019**, *35* (15), 5114–5124, DOI: 10.1021/acs.langmuir.8b04085.

(80) Faustini, M.; Louis, B.; Albouy, P. A.; Kuemmel, M.; Grosso, D. Preparation of Sol-Gel Films by Dip-Coating in Extreme Conditions. *J. Phys. Chem. C* **2010**, *114* (17), 7637–7645, DOI: 10.1021/jp9114755.

(81) Faustini, M.; Ceratti, D. R.; Louis, B.; Boudot, M.; Albouy, P. A.; Boissière, C.; Grosso, D. Engineering Functionality Gradients by Dip Coating Process in Acceleration Mode. *ACS Appl. Mater. Interfaces* **2014**, *6* (19), 17102–17110, DOI: 10.1021/am504770x.

(82) Landau, L.; Levich, B. Dragging of a Liquid by a Moving Plate. In *Dynamics of Curved Fronts*; Elsevier, 1988; pp 141–153.

(83) Matsen, M. W.; Bates, F. S. Unifying Weak- and Strong-Segregation Block Copolymer Theories. *Macromolecules* **1996**, *29* (4), 1091–1098, DOI: 10.1021/ma951138i.

(84) Leibler, L. Theory of Microphase Separation in Block Copolymers. *Macromolecules* **1980**, *13* (6), 1602–1617, DOI: 10.1021/ma60078a047.

(85) Olson, D. A.; Chen, L.; Hillmyer, M. A. Templating Nanoporous Polymers with Ordered Block Copolymers. *Chemistry of Materials*. American Chemical Society February 12, 2008, pp 869–890.

(86) Hamley, I. W. Ordering in Thin Films of Block Copolymers: Fundamentals to Potential Applications. *Progress in Polymer Science (Oxford)*. Pergamon November 1, 2009, pp 1161–1210.

(87) Li, M.; Coenjarts, C. A.; Ober, C. K. Patternable Block Copolymers. *Advances in Polymer Science*. Springer, Berlin, Heidelberg 2005, pp 183–226.

(88) Fasolka, M. J.; Mayes, A. M. Block Copolymer Thin Films: Physics and Applications. *Annu. Rev. Mater. Res.* **2001**, *31* (1), 323–355, DOI: 10.1146/annurev.matsci.31.1.323.

(89) Segalman, R. A. Patterning with Block Copolymer Thin Films. *Materials Science and Engineering R: Reports*. Elsevier February 28, 2005, pp 191–226.

(90) Green, P. F.; Limary, R. Block Copolymer Thin Films: Pattern Formation and Phase Behavior. *Adv. Colloid Interface Sci.* **2001**, *94* (1–3), 53–81, DOI: 10.1016/S0001-8686(01)00055-0.

(91) Fasolka, M. J.; Banerjee, P.; Mayes, A. M.; Pickett, G.; Balazs, A. C. Morphology of Ultrathin Supported Diblock Copolymer Films: Theory and Experiment. *Macromolecules* **2000**, *33* (15), 5702–5712, DOI: 10.1021/ma990021h.

(92) Morkved, T. L.; Jaeger, H. M. Thickness-Induced Morphology Changes in Lamellar Diblock Copolymer Ultrathin Films. *EPL (Europhysics Lett.* **1997**, *40* (6), 643, DOI: 10.1209/EPL/I1997-00517-6.

(93) Sidorenko, A.; Tokarev, I.; Minko, S.; Stamm, M. Ordered Reactive Nanomembranes/Nanotemplates from Thin Films of Block Copolymer Supramolecular Assembly. *J. Am. Chem. Soc.* **2003**, *125* (40), 12211–12216, DOI: 10.1021/ja036085w.

(94) Cavicchi, K. A.; Berthiaume, K. J.; Russell, T. P. Solvent Annealing Thin Films of Poly(Isoprene-b-Lactide). *Polymer (Guildf).* **2005**, *46* (25), 11635–11639, DOI:

10.1016/j.polymer.2005.09.072.
(95) Yu, X.; Peng, J.; Cui, L.; Wang, H.; Li, B.; Han, Y. Morphology Development of Ultrathin Symmetric Diblock Copolymer Film via Solvent Vapor Treatment. *Macromolecules* **2004**, *37* (19), 7301–7307, DOI: 10.1021/ma0497761.
(96) Jung, Y. S.; Ross, C. A. Solvent-Vapor-Induced Tunability of Self-Assembled Block Copolymer Patterns. *Adv. Mater.* **2009**, *21* (24), 2540–2545, DOI: 10.1002/adma.200802855.
(97) Phillip, W. A.; Hillmyer, M. A.; Cussler, E. L. Cylinder Orientation Mechanism in Block Copolymer Thin Films upon Solvent Evaporation. *Macromolecules* **2010**, *43* (18), 7763–7770, DOI: 10.1021/ma1012946.
(98) Lodge, T. P.; Pudil, B.; Hanley, K. J. The Full Phase Behavior for Block Copolymers in Solvents of Varying Selectivity. *Macromolecules* **2002**, *35* (12), 4707–4717, DOI: 10.1021/ma0200975.
(99) Wang, Y.; Li, F. An Emerging Pore-Making Strategy: Confined Swelling-Induced Pore Generation in Block Copolymer Materials. *Adv. Mater.* **2011**, *23* (19), 2134–2148, DOI: 10.1002/adma.201004022.
(100) Wang, Y. Nondestructive Creation of Ordered Nanopores by Selective Swelling of Block Copolymers: Toward Homoporous Membranes. *Acc. Chem. Res.* **2016**, *49* (7), 1401–1408, DOI: 10.1021/acs.accounts.6b00233.
(101) Yin, J.; Yao, X.; Liou, J. Y.; Sun, W.; Sun, Y. Sen; Wang, Y. Membranes with Highly Ordered Straight Nanopores by Selective Swelling of Fast Perpendicularly Aligned Block Copolymers. *ACS Nano* **2013**, *7* (11), 9961–9974, DOI: 10.1021/nn403847z.
(102) Guo, L.; Wang, Y. Monolithic Membranes with Designable Pore Geometries and Sizes via Retarded Evaporation of Block Copolymer Supramolecules. *Macromolecules* **2015**, *48* (23), 8471–8479, DOI: 10.1021/acs.macromol.5b01992.
(103) Sun, W.; Wang, Z.; Yao, X.; Guo, L.; Chen, X.; Wang, Y. Surface-Active Isoporous Membranes Nondestructively Derived from Perpendicularly Aligned Block Copolymers for Size-Selective Separation. *J. Memb. Sci.* **2014**, *466*, 229–237, DOI: 10.1016/j.memsci.2014.04.055.
(104) Cho, H.; Park, H.; Russell, T. P.; Park, S. Precise Placements of Metal Nanoparticles from Reversible Block Copolymer Nanostructures. *J. Mater. Chem.* **2010**, *20* (24), 5047–5051, DOI: 10.1039/c0jm00651c.
(105) Meiners, J. C.; Quintel-Ritzi, A.; Mlynek, J.; Elbs, H.; Krausch, G. Adsorption of Block-Copolymer Micelles from a Selective Solvent. *Macromolecules* **1997**, *30* (17), 4945–4951, DOI: 10.1021/ma970327t.
(106) Roland, S. B.; Prud'homme, R. E.; Bazuin, C. G. Morphology, Thickness, and Composition Evolution in Supramolecular Block Copolymer Films over a Wide Range of Dip-Coating Rates. *ACS Macro Lett.* **2012**, *1* (8), 973–976, DOI: 10.1021/mz3003165.
(107) Balazs, A. C.; Emrick, T.; Russell, T. P. Nanoparticle Polymer Composites: Where Two Small Worlds Meet. *Science*. November 17, 2006, pp 1107–1110.
(108) Lee, J. Y.; Thompson, R. B.; Jasnow, D.; Balazs, A. C. Effect of Nanoscopic

Particles on the Mesophase Structure of Diblock Copolymers. *Macromolecules*. American Chemical Society June 18, 2002, pp 4855–4858.
(109) Yeh, S. W.; Wei, K. H.; Sun, Y. Sen; Jeng, U. S.; Liang, K. S. CdS Nanoparticles Induce a Morphological Transformation of Poly(Styrene-b-4-Vinylpyridine) from Hexagonally Packed Cylinders to a Lamellar Structure. *Macromolecules* **2005**, *38* (15), 6559–6565, DOI: 10.1021/ma047653a.
(110) Kim, B. J.; Chiu, J. J.; Yi, G. R.; Pine, D. J.; Kramer, E. J. Nanoparticle-Induced Phase Transitions in Diblock-Copolymer Films. *Adv. Mater.* **2005**, *17* (21), 2618–2622, DOI: 10.1002/adma.200500502.
(111) Chiu, J. J.; Kim, B. J.; Kramer, E. J.; Pine, D. J. Control of Nanoparticle Location in Block Copolymers. *J. Am. Chem. Soc.* **2005**, *127* (14), 5036–5037, DOI: 10.1021/ja050376i.
(112) Dong, R.; Yan, J.; Ma, H.; Fang, Y.; Hao, J. Dimensional Architecture of Ferrocenyl-Based Oligomer Honeycomb-Patterned Films: From Monolayer to Multilayer. *Langmuir* **2011**, *27* (14), 9052–9056, DOI: 10.1021/la201264u.
(113) Aw, J. E.; Goh, G. T. W.; Huang, S.; Reithofer, M. R.; Thong, A. Z.; Chin, J. M. Non-Close-Packed Breath Figures via Ion-Partitioning-Mediated Self-Assembly. *Langmuir* **2015**, *31* (24), 6688–6694, DOI: 10.1021/la504656j.
(114) Bormashenko, E.; Malkin, A.; Musin, A.; Bormashenko, Y.; Whyman, G.; Litvak, N.; Barkay, Z.; Machavariani, V. Mesoscopic Patterning in Evaporated Polymer Solutions: Poly(Ethylene Glycol) and Room-Temperature-Vulcanized Polyorganosilanes/-Siloxanes Promote Formation of Honeycomb Structures. *Macromol. Chem. Phys.* **2008**, *209* (6), 567–576, DOI: 10.1002/macp.200700552.
(115) Maruyama, N.; Koito, T.; Nishida, J.; Sawadaishi, T.; Cieren, X.; Ijiro, K.; Karthaus, O.; Shimomura, M. Mesoscopic Patterns of Molecular Aggregates on Solid Substrates. *Thin Solid Films* **1998**, *327–329* (1–2), 854–856, DOI: 10.1016/S0040-6090(98)00777-9.
(116) Scriven, L. E.; Sternling, C. V. The Marangoni Effects. *Nature* **1960**, *187* (4733), 186–188.
(117) Dou, Y.; Jin, M.; Zhou, G.; Shui, L. Breath Figure Method for Construction of Honeycomb Films. *Membranes (Basel).* **2015**, *5* (3), 399–424, DOI: 10.3390/membranes5030399.
(118) Bormashenko, E.; Pogreb, R.; Stanevsky, O.; Bormashenko, Y.; Stein, T.; Gaisin, V.-Z.; Cohen, R.; Gendelman, O. V. Mesoscopic Patterning in Thin Polymer Films Formed under the Fast Dip-Coating Process. *Macromol. Mater. Eng.* **2005**, *290* (2), 114–121, DOI: 10.1002/mame.200400217.
(119) Bormashenko, E.; Pogreb, R.; Stanevsky, O.; Bormashenko, Y.; Socol, Y.; Gendelman, O. Self-Assembled Honeycomb Polycarbonate Films Deposited on Polymer Piezoelectric Substrates and Their Applications. *Polym. Adv. Technol.* **2005**, *16* (4), 299–304, DOI: 10.1002/pat.585.
(120) Roszol, L.; Lawson, T.; Koncz, V.; Noszticzius, Z.; Wittmann, M.; Sarkadi, T.; Koppa, P. Micropatterned Polyvinyl Butyral Membrane for Acid−Base Diodes. *J. Phys. Chem. B* **2010**, *114* (43), 13718–13725, DOI: 10.1021/jp106773y.

(121) Mansouri, J.; Yapit, E.; Chen, V. Polysulfone Filtration Membranes with Isoporous Structures Prepared by a Combination of Dip-Coating and Breath Figure Approach. *J. Memb. Sci.* **2013**, *444*, 237–251, DOI: 10.1016/j.memsci.2013.05.022.
(122) Ferrari, E.; Fabbri, P.; Pilati, F. Solvent and Substrate Contributions to the Formation of Breath Figure Patterns in Polystyrene Films. *Langmuir* **2011**, *27* (5), 1874–1881, DOI: 10.1021/la104500j.
(123) Ferrari, E.; Fabbri, P.; Pilati, F. Solvent and Substrate Contributions to the Formation of Breath Figure Patterns in Polystyrene Films. *Langmuir* **2011**, *27* (5), 1874–1881, DOI: 10.1021/la104500j.
(124) Wong, K. H.; Hernández-Guerrero, M.; Granville, A. M.; Davis, T. P.; Barner-Kowollik, C.; Stenzel, M. H. Water-Assisted Formation of Honeycomb Structured Porous Films. *J. Porous Mater.* **2006**, *13* (3), 213–223, DOI: 10.1007/s10934-006-8007-4.
(125) Bolognesi, A.; Mercogliano, C.; Yunus, S.; Civardi, M.; Comoretto, D.; Turturro, A. Self-Organization of Polystyrenes into Ordered Microstructured Films and Their Replication by Soft Lithography. *Langmuir* **2005**, *21* (8), 3480–3485, DOI: 10.1021/la047427u.
(126) Böker, A.; Lin, Y.; Chiapperini, K.; Horowitz, R.; Thompson, M.; Carreon, V.; Xu, T.; Abetz, C.; Skaff, H.; Dinsmore, A. D.; et al. Hierarchical Nanoparticle Assemblies Formed by Decorating Breath Figures. *Nat. Mater.* **2004**, *3* (5), 302–306, DOI: 10.1038/nmat1110.
(127) Male, U.; Shin, B. K.; Huh, D. S. Coupling of Breath Figure Method with Interfacial Polymerization: Bottom-Surface Functionalized Honeycomb-Patterned Porous Films. *Polymer (Guildf).* **2017**, *119*, 206–211, DOI: 10.1016/j.polymer.2017.05.038.
(128) Tian, D.; He, L.; Zhang, N.; Zheng, X.; Dou, Y.; Zhang, X.; Guo, Z.; Jiang, L. Electric Field and Gradient Microstructure for Cooperative Driving of Directional Motion of Underwater Oil Droplets. *Adv. Funct. Mater.* **2016**, *26* (44), 7986–7992, DOI: 10.1002/adfm.201601843.
(129) Hiwatari, K. I.; Serizawa, T.; Seto, F.; Kishida, A.; Muraoka, Y.; Akashi, M. Graft Copolymers Having Hydrophobic Backbone and Hydrophilic Branches XXXIV. Fabrication and Control of Honeycomb Structure Prepared from Amphiphilic Graft Copolymers. *Polym. J.* **2001**, *33* (9), 669–675, DOI: 10.1295/polymj.33.669.
(130) Kasai, W.; Kondo, T. Fabrication of Honeycomb-Patterned Cellulose Films. *Macromol. Biosci.* **2004**, *4* (1), 17–21, DOI: 10.1002/mabi.200300054.
(131) Wang, Y.; Liu, Z.; Huang, Y.; Han, B.; Yang, G. Micropatterned Polymer Surfaces Induced by Nonsolvent. *Langmuir* **2006**, *22* (4), 1928–1931, DOI: 10.1021/la051646d.
(132) de León, A. S.; Muñoz-Bonilla, A.; Fernández-García, M.; Rodríguez-Hernández, J. Breath Figures Method to Control the Topography and the Functionality of Polymeric Surfaces in Porous Films and Microspheres. *J. Polym. Sci. Part A Polym. Chem.* **2012**, *50* (5), 851–859, DOI: 10.1002/pola.25826.

(133) Samuel, A. Z.; Umapathy, S.; Ramakrishnan, S. Functionalized and Postfunctionalizable Porous Polymeric Films through Evaporation-Induced Phase Separation Using Mixed Solvents. *ACS Appl. Mater. Interfaces* **2011**, *3* (9), 3293–3299, DOI: 10.1021/am200735t.
(134) Park, M. S.; Kim, J. K. Breath Figure Patterns Prepared by Spin Coating in a Dry Environment. *Langmuir* **2004**, *20* (13), 5347–5352, DOI: 10.1021/la035915g.
(135) Ma, Y.; Liang, J.; Sun, H.; Wu, L.; Dang, Y.; Wu, Y. Honeycomb Micropatterning of Proteins on Polymer Films through the Inverse Microemulsion Approach. *Chem. - A Eur. J.* **2012**, *18* (2), 526–531, DOI: 10.1002/chem.201102337.
(136) Bubník, Z.; Kadlec, P. Sucrose Solubility. In *Sucrose*; Springer US, 1995; pp 101–125.
(137) Wong, K. H.; Hernández-Guerrero, M.; Granville, A. M.; Davis, T. P.; Barner-Kowollik, C.; Stenzel, M. H. Water-Assisted Formation of Honeycomb Structured Porous Films. *J. Porous Mater.* **2006**, *13* (3), 213–223, DOI: 10.1007/s10934-006-8007-4.
(138) Kasai, W.; Kondo, T. Fabrication of Honeycomb-Patterned Cellulose Films. *Macromol. Biosci.* **2004**, *4* (1), 17–21, DOI: 10.1002/mabi.200300054.
(139) Imhof, A.; Pine, D. J. Ordered Macroporous Materials by Emulsion Templating. *Nature* **1997**, *389* (6654), 948–951, DOI: 10.1038/40105.
(140) Binks, B. P. Particles as Surfactants - Similarities and Differences. *Curr. Opin. Colloid Interface Sci.* **2002**, *7* (1–2), 21–41, DOI: 10.1016/S1359-0294(02)00008-0.
(141) Böker, A.; He, J.; Emrick, T.; Russell, T. P. Self-Assembly of Nanoparticles at Interfaces. *Soft Matter* **2007**, *3* (10), 1231–1248, DOI: 10.1039/b706609k.
(142) Lin, Y.; Skaff, H.; Emrick, T.; Dinsmore, A. D.; Russell, T. P. Nanoparticle Assembly and Transport at Liquid-Liquid Interfaces. *Science* **2003**, *299* (5604), 226–229, DOI: 10.1126/science.1078616.
(143) Vohra, V.; Bolognesi, A.; Calzaferri, G.; Botta, C. Multilevel Organization in Hybrid Thin Films for Optoelectronic Applications. *Langmuir* **2009**, *25* (20), 12019–12023, DOI: 10.1021/la9032089.
(144) Li, X.; Zhang, L.; Wang, Y.; Yang, X.; Zhao, N.; Zhang, X.; Xu, J. A Bottom-up Approach to Fabricate Patterned Surfaces with Asymmetrical TiO2 Microparticles Trapped in the Holes of Honeycomblike Polymer Film. *J. Am. Chem. Soc.* **2011**, *133* (11), 3736–3739, DOI: 10.1021/ja1106767.
(145) Gong, J.; Xu, B.; Tao, X. Three-Dimensionally Conformal Porous Microstructured Fabrics via Breath Figures: A Nature-Inspired Approach for Novel Surface Modification of Textiles. *Sci. Rep.* **2017**, *7* (1), 1–9, DOI: 10.1038/s41598-017-02615-1.
(146) Murray, C. B.; Kagan, C. R.; Bawendi, M. G. Synthesis and Characterization of Monodisperse Nanocrystals and Close-Packed Nanocrystal Assemblies. *Annu. Rev. Mater. Sci.* **2000**, *30* (1), 545–610, DOI: 10.1146/annurev.matsci.30.1.545.
(147) Brust, M.; Walker, M.; Bethell, D.; Schiffrin, D. J.; Whyman, R. Synthesis of Thiol-Derivatised Gold Nanoparticles in a Two-Phase Liquid-Liquid System. *J. Chem. Soc. Chem. Commun.* **1994**, No. 7, 801–802, DOI:

10.1039/C39940000801.
(148) Acharya, H.; Sung, J.; Bae, I.; Kim, T.; Kim, D. H.; Park, C. Coassembly of Metal and Titanium Dioxide Nanocrystals Directed by Monolayered Block Copolymer Inverse Micelles for Enhanced Photocatalytic Performance. *Chem. - A Eur. J.* **2012**, *18* (46), 14695–14701, DOI: 10.1002/chem.201200934.
(149) Weng, C. C.; Hsu, K. F.; Wei, K. H. Synthesis of Arrayed, TiO<sub>2<sub> Needlelike Nanostructures via a Polystyrene-Block-Poly(4-Vinylpyridine) Diblock Copolymer Template. *Chem. Mater.* **2004**, *16* (21), 4080–4086, DOI: 10.1021/cm049367j.
(150) Bezrodna, T.; Puchkovska, G.; Shimanovska, V.; Chashechnikova, I.; Khalyavka, T.; Baran, J. Pyridine-TiO_2 Surface Interaction as a Probe for Surface Active Centers Analysis. *Appl. Surf. Sci.* **2003**, *214* (1–4), 222–231, DOI: 10.1016/S0169-4332(03)00346-5.
(151) Williams, R.; Goodman, A. M. Wetting of Thin Layers of SiO_2 by Water. *Appl. Phys. Lett.* **1974**, *25* (10), 531–532, DOI: 10.1063/1.1655297.
(152) Yang, X. M.; Zhong, Z. W.; Diallo, E. M.; Wang, Z. H.; Yue, W. S. Silicon Wafer Wettability and Aging Behaviors: Impact on Gold Thin-Film Morphology. *Mater. Sci. Semicond. Process.* **2014**, *26* (1), 25–32, DOI: 10.1016/j.mssp.2014.03.044.
(153) Hermansson, K.; Lindberg, U.; Hok, B.; Palmskog, G. Wetting Properties of Silicon Surfaces. In *Transducers '91*; Publ by IEEE, 1991; pp 193–196.
(154) Grundner, M.; Jacob, H. Investigations on Hydrophilic and Hydrophobic Silicon (100) Wafer Surfaces by X-Ray Photoelectron and High-Resolution Electron Energy Loss-Spectroscopy. *Appl. Phys. A Solids Surfaces* **1986**, *39* (2), 73–82, DOI: 10.1007/BF00616822.
(155) Deligiannis, D.; Alivizatos, S.; Ingenito, A.; Zhang, D.; Van Sebille, M.; Van Swaaij, R. A. C. M. M.; Zeman, M. Wet-Chemical Treatment for Improved Surface Passivation of Textured Silicon Heterojunction Solar Cells. In *Energy Procedia*; Elsevier Ltd, 2014; Vol. 55, pp 197–202.
(156) Seago, A. E.; Brady, P.; Vigneron, J.-P.; Schultz, T. D. Gold Bugs and beyond: A Review of Iridescence and Structural Colour Mechanisms in Beetles (Coleoptera). *J. R. Soc. Interface* **2009**, *6* (suppl_2), DOI: 10.1098/rsif.2008.0354.focus.
(157) Finnish Meteorological Institute. Climate elements https://en.ilmatieteenlaitos.fi/climate-elements (accessed Jun 21, 2020).
(158) Roland, S.; Gamys, C. G.; Grosrenaud, J.; Boissé, S.; Pellerin, C.; Prud'Homme, R. E.; Bazuin, C. G. Solvent Influence on Thickness, Composition, and Morphology Variation with Dip-Coating Rate in Supramolecular PS- b -P4VP Thin Films. *Macromolecules* **2015**, *48* (14), 4823–4834, DOI: 10.1021/acs.macromol.5b00847.
(159) Roland, S.; Prud'Homme, R. E.; Bazuin, C. G. Supramolecular PS-P4VP Diblock Copolymer Thin Films Slowly Dip-Coated from Chloroform Solutions. In *Science China Chemistry*; Springer, 2013; Vol. 56, pp 33–39.
(160) O'Driscoll, S.; Demirel, G.; Farrell, R. A.; Fitzgerald, T. G.; O'Mahony, C.; Holmes,

J. D.; Morris, M. A. The Morphology and Structure of PS-b-P4VP Block Copolymer Films by Solvent Annealing: Effect of the Solvent Parameter. *Polym. Adv. Technol.* **2011**, *22* (6), 915–923, DOI: 10.1002/pat.1596.